LEVEL

AFWAL-TR-81-4033

SATELLITE CHARGING CONTROL MATERIALS

L. LEVY, A. PAILLOUS, D. SARRAIL

ONERA
CENTRE D'ETUDES ET DE RECHERCHES DE TOULOUSE
2 AVENUE EDOUARD BELIN 31055   TOULOUSE CEDEX
FRANCE

JUNÉ 1981

FINAL REPORT FOR PERIOD MAY 1980 - DECEMBER 1980.

APPROVED FOR PUBLIC RELEASE; DISTRIBUTION UNLIMITED

AD A101939

DTIC
ELECTE
S JUL 24 1981
D
C

DTIC FILE COPY

81 7   24 011

THOMAS J. THORNTON, CAPTAIN, USAF
Project Engineer

WILLIAM C. KESSLER, Chief
Coatings & Thermal Protective
 Materials Branch
Nonmetallic Materials Division

FOR THE COMMANDER

FRANKLIN D. CHERRY, Chief
Nonmetallic Materials Division

REPORT DOCUMENTATION PAGE		READ INSTRUCTIONS BEFORE COMPLETING FORM
1. REPORT NUMBER AFWAL-TR-81-4033	2. GOVT ACCESSION NO. AD-A101 939	3. RECIPIENT'S CATALOG NUMBER
4. TITLE *(and Subtitle)* SATELLITE CHARGING CONTROL MATERIALS		5. TYPE OF REPORT & PERIOD COVERED FINAL SCIENTIFIC REPORT. 1 May - 31 Dec 80.
		6. PERFORMING ORG. REPORT NUMBER ONERA/CERT/DERTS —CR—AF—07
7. AUTHOR(s) L. LEVY , A. PAILLOUS ; D. SARRAIL		8. CONTRACT OR GRANT NUMBER(s) AFOSR-80-0183
9. PERFORMING ORGANIZATION NAME AND ADDRESS ONERA/CERT- Dept. of studies and research in Space Technology. 2 av. E. Belin 31055 TOULOUSE CEDEX; France		10. PROGRAM ELEMENT, PROJECT, TASK AREA & WORK UNIT NUMBERS 61101F ILIR 0104 04
11. CONTROLLING OFFICE NAME AND ADDRESS AFWAL/MLBE WRIGHT-PATTERSON AFB, OH 45433		12. REPORT DATE APRIL 1981
		13. NUMBER OF PAGES 152
14. MONITORING AGENCY NAME & ADDRESS *(if different from Controlling Office)* EUROPEAN OFFICE OF AEROSPACE RESEARCH AND DEVELOPMENT Box 14 FPO; New York, NY 09510		15. SECURITY CLASS. *(of this report)* UNCLASSIFIED
		15a. DECLASSIFICATION/DOWNGRADING SCHEDULE

16. DISTRIBUTION STATEMENT *(of this Report)*

Approved for public release; distribution unlimited.

17. DISTRIBUTION STATEMENT *(of the abstract entered in Block 20, if different from Report)*

Same as Block 16.

18. SUPPLEMENTARY NOTES

19. KEY WORDS *(Continue on reverse side if necessary and identify by block number)*
SPACECRAFT CHARGING, THERMAL CONTROL COATINGS, CONDUCTIVE ADHESIVE, CONDUCTIVE COATINGS, ELECTRON IRRADIATION, GEOSYNCHRONOUS ORBITS.

20. ABSTRACT *(Continue on reverse side if necessary and identify by block number)*
     The secondary emission conductivity of silica fabrics and silica fabric/FEP/Aluminum composites under low energy electron irradiation has been studied. The dependence on electrical field of the conductivity across the samples has been shown. The surface potentials depend on the flux rate; the presence of low energy electrons acting together with medium energy electrons decrease the potential values; the potential values increase with the time of exposure to vacuum and/or irradiation, as well as with contamination build up.
     Teflon based conductive SSM with ITO coatings proved to be extremely

DD $_{1\ JAN\ 73}^{FORM}$ 1473   EDITION OF 1 NOV 65 IS OBSOLETE

Unclassified

vulnerable to thermal cycling and water absorption. A grounding technique based on a filled silicone adhesive proved to be applicable to this teflon based material and was stable during prequalification tests. The degradation of the samples was due to failure in the ITO coating rather than to a failure in the bonding/grounding technique.

PREFACE

CONTENTS

viii

TABLE OF FIGURES

TABLES

1. INTRODUCTION

1 - 1 BACKGROUND

Anomalous spacecraft operation due to spacecraft charging and subsequent arcing and discharging is a problem experienced by satellites operating at synchronous orbit. The disruptions, anomalies or even catastrophic damage to electronic subsystems and components caused by these discharges as well as the satellite thermal control materials degradation and contamination which may result are of special concern to those systems which are expected to perform for long periods of time, seven to ten years in synchronous orbit.

A variety of new non charging satellite thermal control materials as well as electrical grounding techniques have been developped in the laboratory and applied to various charge prone satellite materials such as for instance thin film materials either metallized or coated with conductive transparent layers and quartz fabrics.

A study supported by the grant AFOSR 78-3304 has shown (Ref. 1, 2, 3) that it is possible to achieve electrical interconnection of conductive coatings by means of conductive adhesive bonding techniques. A new heat probe for silver loaded silicone adhesives was developped in order to realize joints under controlled temperature and controlled pressure. The feasability of the techniques was proved for thin aluminum and ITO layers deposited on Kapton. An electrostatic discharge test and a prequalification program were carried out on a representative "component". After

---

Ref. 1   L. LEVY, A. PAILLOUS - Satellite Spacecraft Charging
         Control Materials - Grant AFOSR 78-3704 - Progress Report
         n° 1 (1978 - Sept. 01 - 1978 Nov. 30)

Ref. 2   L. LEVY, A. PAILLOUS, D. SARRAIL - Satellite Spacecraft
         charging Control Materials - Grant AFOSR 78- 3704 -
         Progress Report n° 2 (1978 Dec. 01 - 1979 Feb. 28)

Ref. 3   B. BENAISSA, L. LEVY, A. PAILLOUS, D. SARRAIL - Satellite
         Spacecraft Charging Control Materials - Interim Scientific
         Report 78 Sept. 01 79 - April 30 Grant AFOSR 78-3704
         AFWAL-TR 80-4029

completion of this test, the conductive adhesive bonding technique can be considered as prequalified for ITO coated Kapton.

On the other hand, an investigation about the electrostatic behaviour of silica fabrics and silica fabric/FEP Teflon/ Aluminum composites has been started at DERTS. In a first phase (Ref. 3) various sample configurations using silica fabrics have been tested in identical conditions under electron beam. The composite behaves like a fabric alone. It must be grounded by its aluminum back face in order to ensure good electrostatic properties. However it has been shown that rather high surface potential value can be measured for electron energies higher than 10 keV. Arcing phenomena have been observed at 20 keV/0.5 nA cm^{-2}.

The work done in a second phase that we describe below deals with some additional tests on silica fabrics and composites, the effect of contaminants on the electrostatic behaviour of some thermal control surfaces, and the prequalification of conductive FEP second surfaces mirrors.

This work has been supported by grants AFOSR 78-3704 (Ref. 4) and 80-0183.

1 - 2   APPROACH

The purpose of this research is:

(i)   to complete the study of the quartz fabrics behaviour under an electron beam simulating the geosynchronous environment during geomagnetic substorms. It was decided to evaluate possible damages of the composite's aluminum layer, the influence of the irradiation density, the dependence on electrical field of conduction mechanisms and the effect of low energy electrons acting together with medium energy electrons,

---

(Ref. 4) L. LEVY, A. PAILLOUS, D. SARRAIL - Satellite Spacecraft charging control materials - Grant AFOSR 78-3704 - Interim Scientific Report n° 2 (79 MAY 01 - 80 JAN 31).

(ii)   to obtain some data concerning the contamination effect on the charge control performance for conductive coatings and namely silica fabrics,

(iii)   to perform a prequalification work on conductive flexible second surface mirrors (metallized FEP whose the top surface has been made conductive by deposition of a layer of Indium oxide).These materials have been tested in combination with a grounding method using conductive adhesives.

2. <u>ELECTROSTATIC BEHAVIOR OF QUARTZ FABRICS AND COMPOSITES.</u>

2 - 1 <u>LONG DURATION AGEING TEST OF COMPOSITES</u>

2-1-1 <u>Purpose</u>

During the first phase of the study (see Ref. 3, Section 3.5.2.4-2) it had been observed that a composite sample the aluminum back face of which was in direct contact with a grounded sample holder, clearly exhibited defects in its aluminum layer after irradiation with low energy electrons (5 to 20 keV). However the whole irradiation history of this sample had been rather intricate and the damage origin was not certain. Consequently it was necessary to check if any degradation of a composite grounded by its back face was likely to occur, because such a degradation could have been correlated for instance with optical variations.

2-1-2 <u>Experimental set up</u>

2121 facility

The test facility has been described in Section 3-2 of Ref. 3. In the present experiment the collecting hemispheric electrode is removed in order to allow photographs to be taken.

Two composite samples were exposed. One of them (sample A, FIGURE 1A) had all its aluminum back face in intimate contact with a grounded holder. The second one (sample B, FIGURE 1 B) had its aluminum conductive back face electrically insulated from the grounded holder except in 4 small selected grounding areas (less than 10 mm^2). One edge of each sample was covered with a grounded aluminum part in direct contact with the composite fabric.

4

ELECTRON BEAM

COMPOSITE SAMPLE

$I_L + I_C$

METALLIC HOLDER

COMPOSITE ALUMINUM BACK FACE
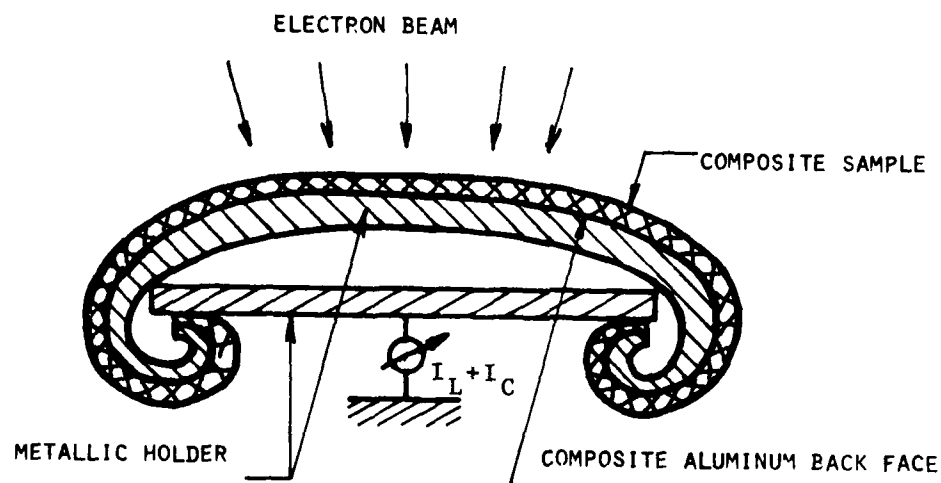
FIGURE 1A – THE ALUMINUM BACK FACE IS GROUNDED THROUGH
ITS ENTIRE SURFACE

ELECTRON BEAM

ALUMINUM BACK
FACE

INSULATOR
(FEP)

COMPOSITE
SAMPLE

METALLIC HOLDER

$I_L + I_C$

4 METALLIC SCREWS IN ELECTRIC
CONTACT WITH THE ALUMINUM BACK
FACE AND WITH THE METALLIC HOLDER
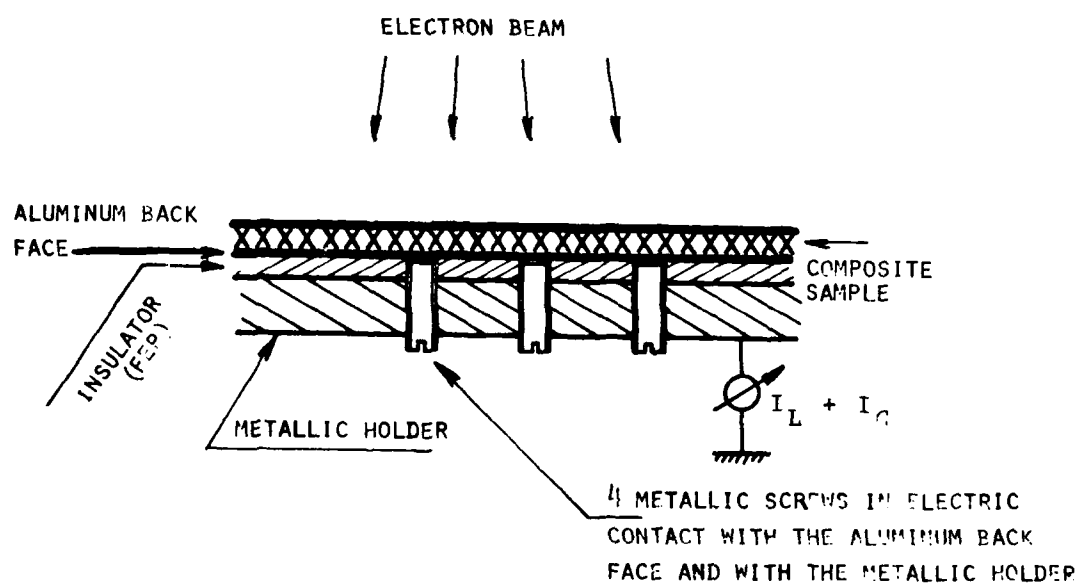
FIGURE 1B – THE GROUNDING OF THE ALUMINUM BACK FACE IS DONE
THROUGH ONLY 4 SMALL AREAS

5

2122   *material*

The composite we have used was sent by AFML/MBE. The 581 Astroquartz lot 98269 was heat cleaned in air at 800°C for 3 hours and then laminated at 280°C to 1 mil aluminum foil with 1 mil type A FEP Teflon film. The 581 Astroquartz is from the same lot as the specimens used in the first phase of the study (Ref. 3). However the composite supplied earlier by AFML/MBE and used in the first phase was backed with 0.5 mil rather than 1 mil aluminum foil.

2123   *test procedure*

The electrostatic behaviour of the two samples was evaluated before and after the ageing test: the surface potential kinetics was determined at 10, 15 and 20 keV under 0.5 nA cm^{-2} electron irradiation (the composite sample being discharged by a 5 keV 1 nA cm^{-2} irradiation between each energy step).

For the ageing test the two composite samples were exposed for 16 hours to 20 keV electrons with a 3 nA cm^{-2} beam density. These conditions were selected in order to enhance the test severity. During the ageing test, the $I_L + I_C$ current (that is to say sample-to-holder leakage current, see Ref.3 Section 3.2) was monitored.

2-1-3   Results

During the long duration irradiation test, the $I_L + I_C$ record showed a large number of pulses (about 50 per hour) for the sample B that was grounded by the 4 discrete areas (see FIGURE 2B). This behaviour was not observed at the other sample position (A) for which about one or two pulses per hour were recorded (FIGURE 2A) under the 20 keV/3 nA cm^{-2} beam.

FARADAY CUP MONITORING CURRENT

6 MIN →

3 NA

350 NA

6 MIN →

LEAKAGE CURRENT
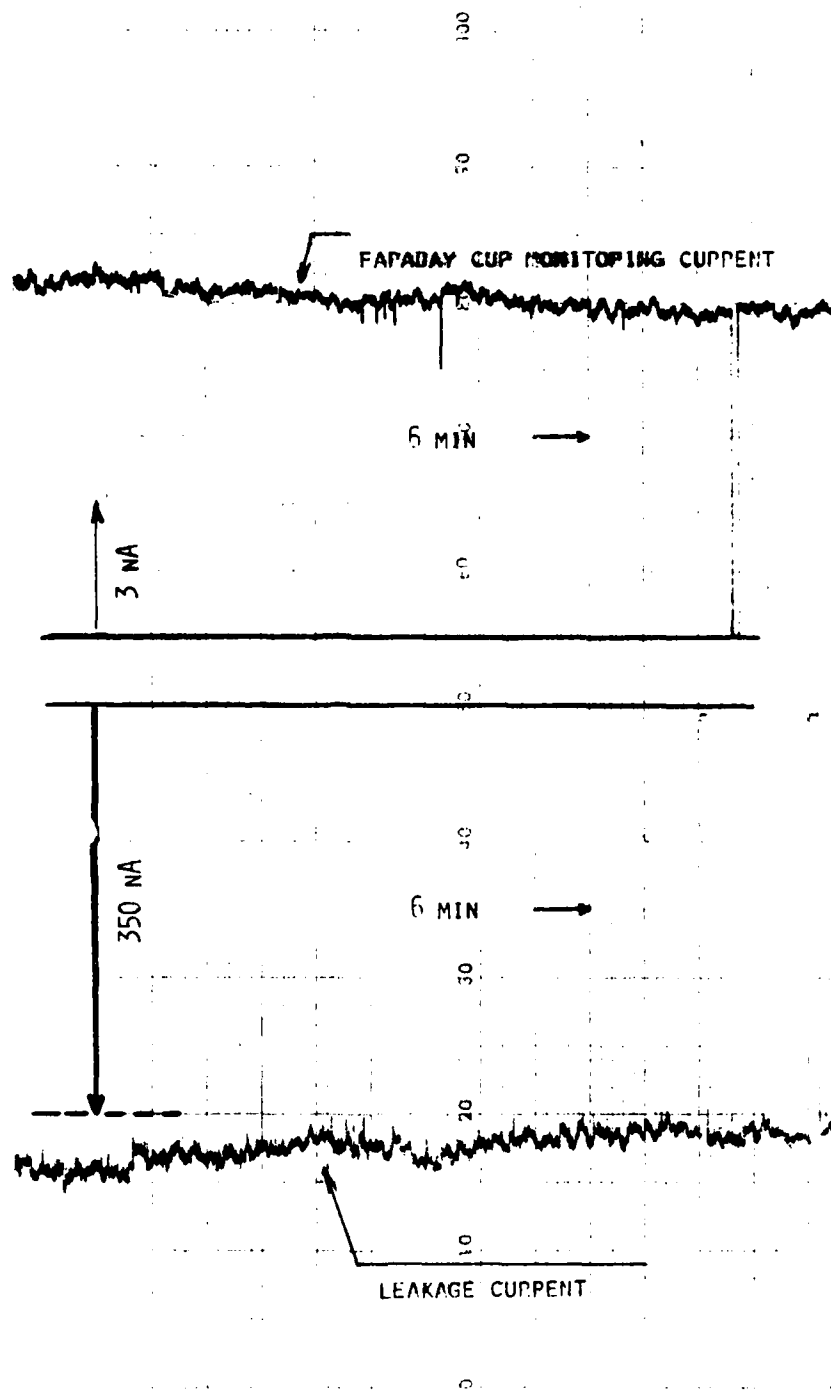
FIGURE 2A

CURRENT RECORD FOR THE LONG TERM IRRADIATION OF SAMPLE "A"

7

FARADAY CUP MONITORING CURRENT

3 NA

350 NA

LEAKAGE CURRENT
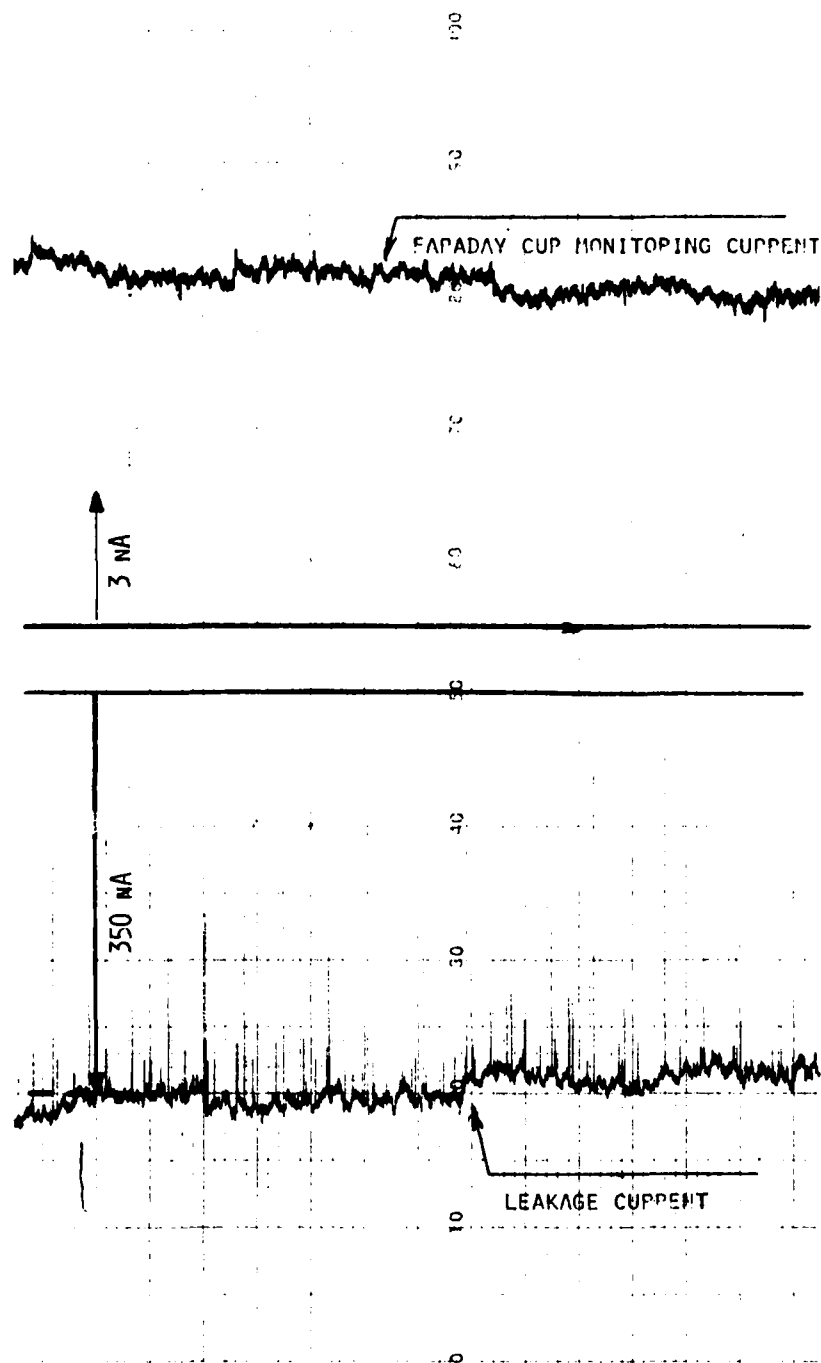
2θ KEV/3 NA CM^{-2}

FIGURE 2B

CURRENT RECORD FOR THE LONG TERM IRRADIATION OF SAMPLE "B"

FIGURE 3A - SAMPLE A DURING ELECTRON IRRADIATION
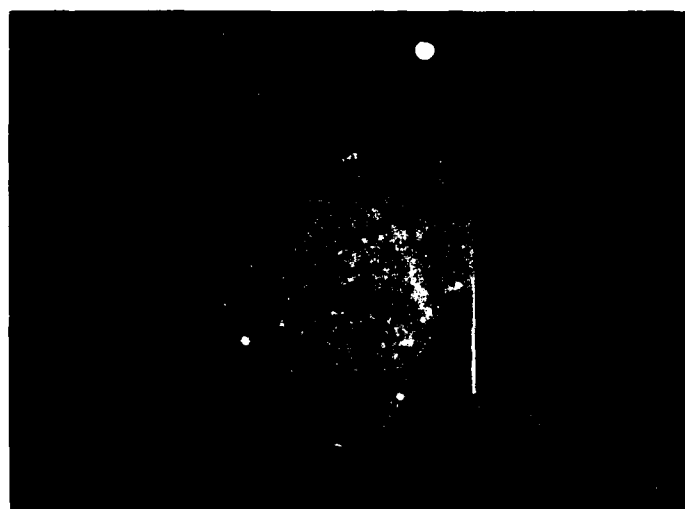
FIGURE 3B - SAMPLE B DURING ELECTRON IRRADIATION

Photographs taken during the long duration irradiation revealed that the sample grounded by discrete areas (FIGURE 3b) exhibited a rather bright edge that corresponded to an overflowing of the underlaying insulating PET film. We suppose that this direct exposure of the PET film to electrons is responsible of the large number of pulses observed for sample B.

Besides this rather bright edge, sample B appeared to have a rather uniform luminescence that is slightly more reinforced in some small zones. That was also the case for sample A (FIGURE 3a). It was not possible to correlate these zones with any visible damage nor with sample heterogeneities. The edge of the fabric that was not covered by the aluminum part (see Section 2121) appeared to behave exactly like the uncovered edge for both samples A and B.

Surface potentials measured for various beam energies before and after the long duration 20 keV irradiation, are given in FIGURES 4,5,6[(*)].In all cases,for a same sample,steady state values of the surface potential, that are measured after the 16 hours 20 keV irradiation, are higher than the ones observed before irradiation. Moreover surface potential kinetics are different before and after the long duration irradiation, especially during the first minutes of exposure. Whether this is due to a non-controlled chamber contamination effect or only to irradiation cannot be known. Results obtained in the first phase of study (Ref. 3, FIGURES 30, 31, 32) are also reported in FIGURES 4, 5, 6. Therefore earlier results show a rather good concordance with the present ones.

Visual and microscopic inspection of the samples after the ageing test did not reveal any trace of degradation of the composite aluminum back layer.

(*)   the surface potential is very near to zero (less than 15 Volts under a 5 keV electron beam)
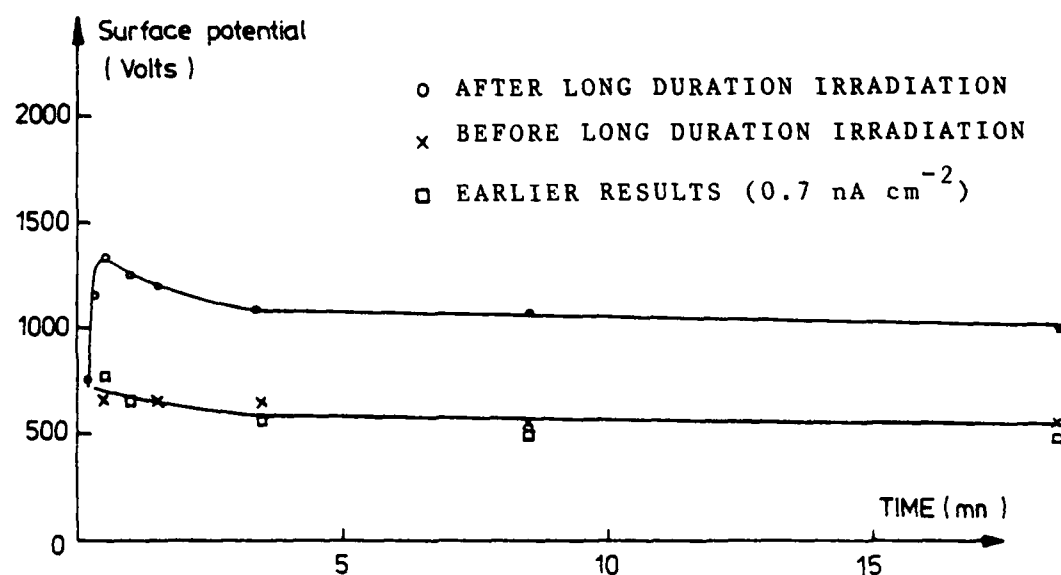
FIGURE 4A – SURFACE POTENTIAL VERSUS TIME FOR SAMPLE A AT
10 KEV 0.5 NA CM^{-2}
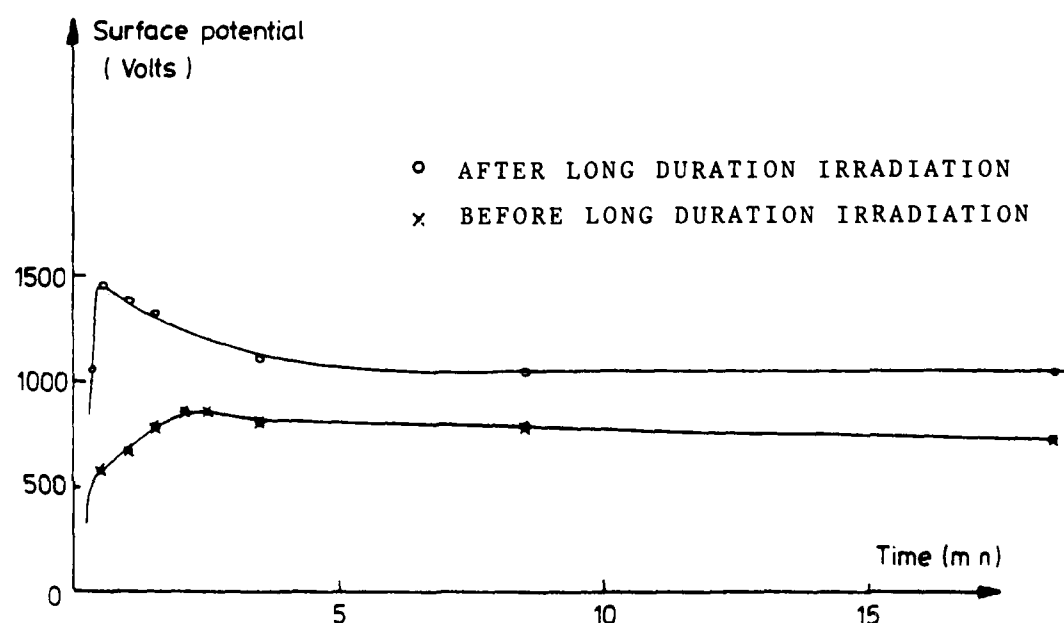
FIGURE 4B – SURFACE POTENTIAL VERSUS TIME FOR SAMPLE B AT
10 KEV 0.5 NA CM^{-2}
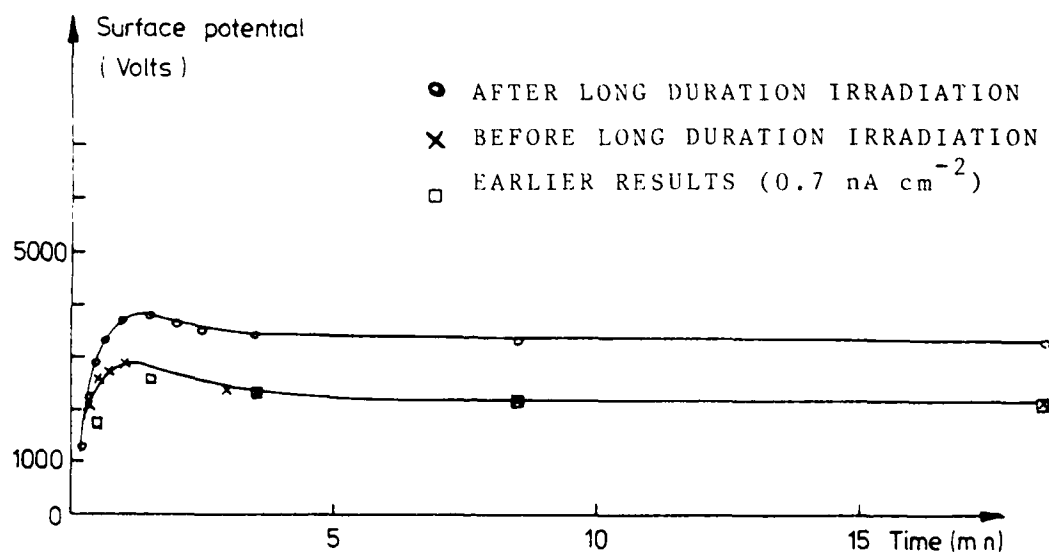
FIGURE 5A - SURFACE POTENTIAL VERSUS TIME FOR SAMPLE A
AT 15 KEV 0.5 NA CM^{-2}
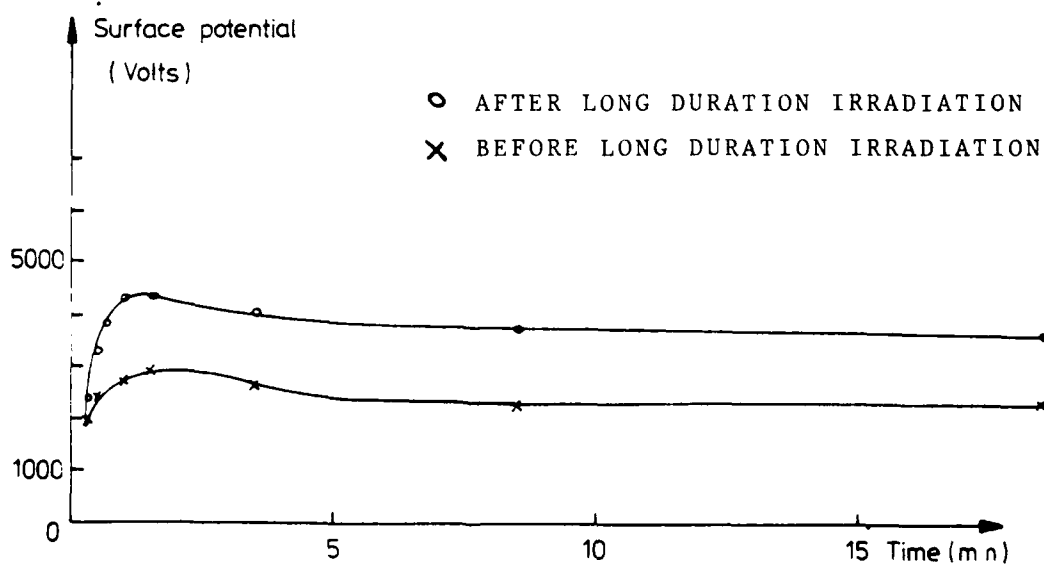
FIGURE 5B - SURFACE POTENTIAL VERSUS TIME FOR SAMPLE B
AT 15 KEV 0.5 NA CM^{-2}
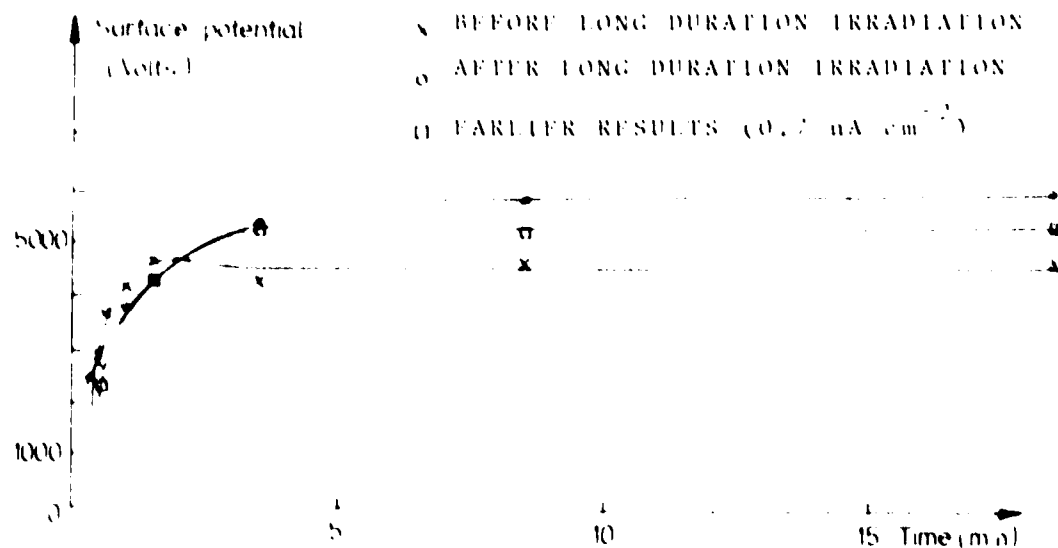
FIGURE 6A — SURFACE POTENTIAL VERSUS TIME FOR SAMPLE A
AT 20 keV 0.5 nA cm⁻²
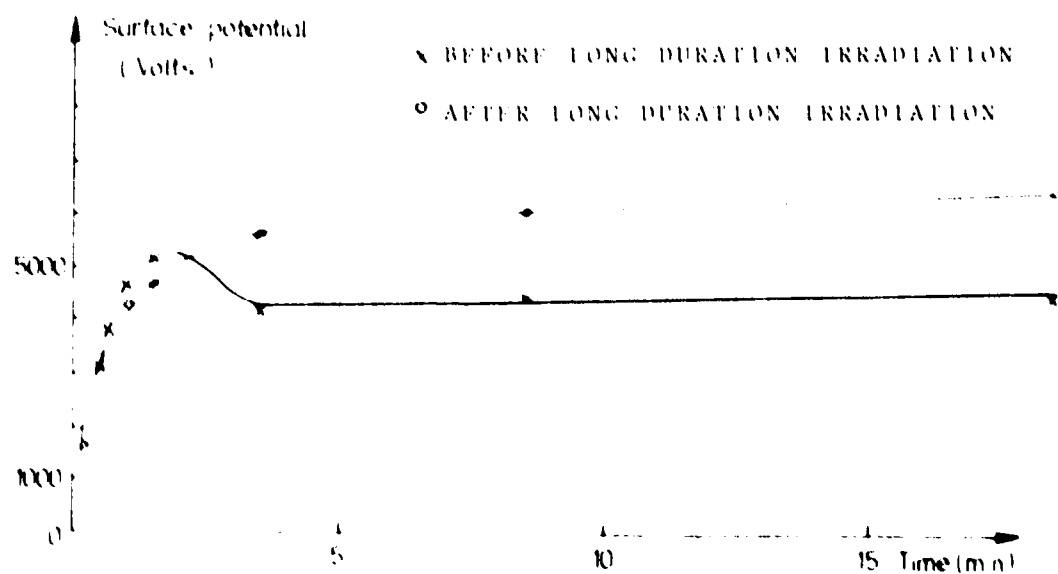
FIGURE 6B — SURFACE POTENTIAL VERSUS TIME FOR SAMPLE B
AT 20 keV 0.5 nA cm⁻²

2-1-4   Conclusion

The aluminum rear face of the composite is not affected
by a long duration exposure to low energy electrons (20 keV,
3 nA cm^{-2}) even if this aluminum layer is grounded only by some
small areas. Moreover there is no visible damage of the quartz
fabric side of the composite.

However the electric performance of the composite has
been shown to be slightly decreased by the long duration exposure.
This could be either due to a parasitic contamination inside the
chamber or a true irradiation effect.

2 - 2   FIELD DEPENDENT CONDUCTIVITY OF THE COMPOSITE

2-2-1   Purpose

The experiment we describe below was performed in order to obtain a better understanding of the good performance of silica fabrics and composites under low energy electrons simulating geo-synchronous substorm conditions.

The silica fabric behaviour had been attributed by EAGLES and BELANGER (Ref. 5) to a secondary emission conductivity. Such a conductivity could explain the results we have observed in a previous study phase (Ref. 3, section 3.5.2): a peak value in the curve expressing the surface potential in terms of time was in evidence for irradiations of silica fabric and composite at 10, 15 and 20 keV. However this peak value occured at rather high values of the surface potential (about 1000 Volts). Consequently it appeared useful to evaluate the conductivity in quartz fabrics for similar electrical fields. So it was decided to apply to a composite sample such electrical fields corresponding to potential in the 0-1 kV range and to evaluate the electrical conductivity through the sample under electron beam. The experiments were performed in a facility similar to the one described in Ref. 5 by BELANGER and EAGLES, but with far lower current densities, higher surface potential and higher beam energies.

2-2-2   Experimental test set up

Composites were irradiated by an electron beam (5 to 20 keV) with a fixed electric field imposed across the cross section of the composite. The composite sample was mounted with its back face directly on a grounded sample holder. The outer fabric surface was in intimate contact with a brass grid. The grid potential with respect to the sample holder was held below 2000 Volts

Ref. 5   V.J. BELANGER, A.E. EAGLE - Secondary emission conductivity of high purity silica fabrics - Proceedings 1st Spacecraft charging technology conference. Colorado Springs October 1976

biased grid

I secondary

Ø 70

Ø 62

composite

alluminium back face

Conductive holder

I supply

V₀

I leakage

INSULATOR
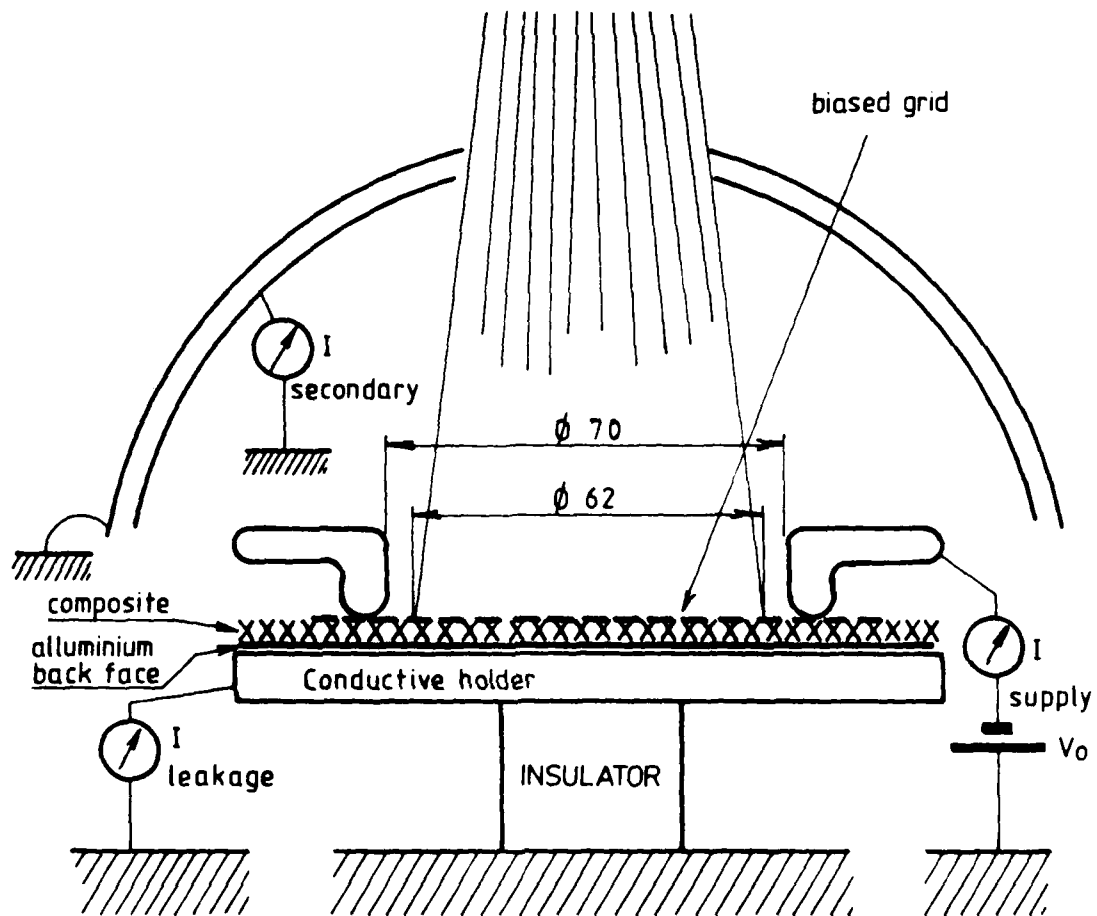
FIGURE 7 - EXPERIMENT SET UP

owing to breakdowns detected for that value in the absence of incident electron beam. In fact this potential V_0 was used in the range 0 - 1500 Volts which was, in the presence of incident electrons, the threshold value for breakdown to occur. The transmission coefficient of the wire screen was experimentally determined and found to be 50 per cent. The principle of the experiment set up is shown in FIGURE 7. The facility has been described in every detail in Section 3-2-3 of Ref. 3. The potential V_0 was fixed at a given level and the three currents $I_{leakage}$, $I_{secondary}$ and I_{supply} were simultaneously measured at steady state. Most significant is $I_{leakage}$ since it is directly related to the fabric conductivity. The beam conditions were the following: 5 keV/ 1.25 nA cm^{-2} (at sample level, after grid), 10 keV/1 nA cm^{-2}, 15 keV/1 nA cm^{-2}, 20 keV/1 nA cm^{-2}.

The material tested has been described earlier (see Section 2122). All experiments have been performed with the same sample.

2-2-3   Results

FIGURES 8a, 9a, 10a and 11a are plots of the leakage current against the grid potential.

These data suggest that there is an increase in the leakage current with the applied voltage V_0 (for V_0 greater than two or three hundred volts). That is to say that the resistance across the cross section of the composite decreases for surface potentials values beyond a certain threshold.

The large dependence of the conductivity on the electric field is particularly shown in FIGURE 9a for a 10 keV electron beam irradiation of the sample. In FIGURE 9b is plotted the surface potential induced by the same electron beam irradiation in terms of time (see also FIGURE 30 of Ref. 3). FIGURES 9a and 9b do match together since an increase of conductivity explains quite well the potential decrease after a very short irradiation time. FIGURES 10

17
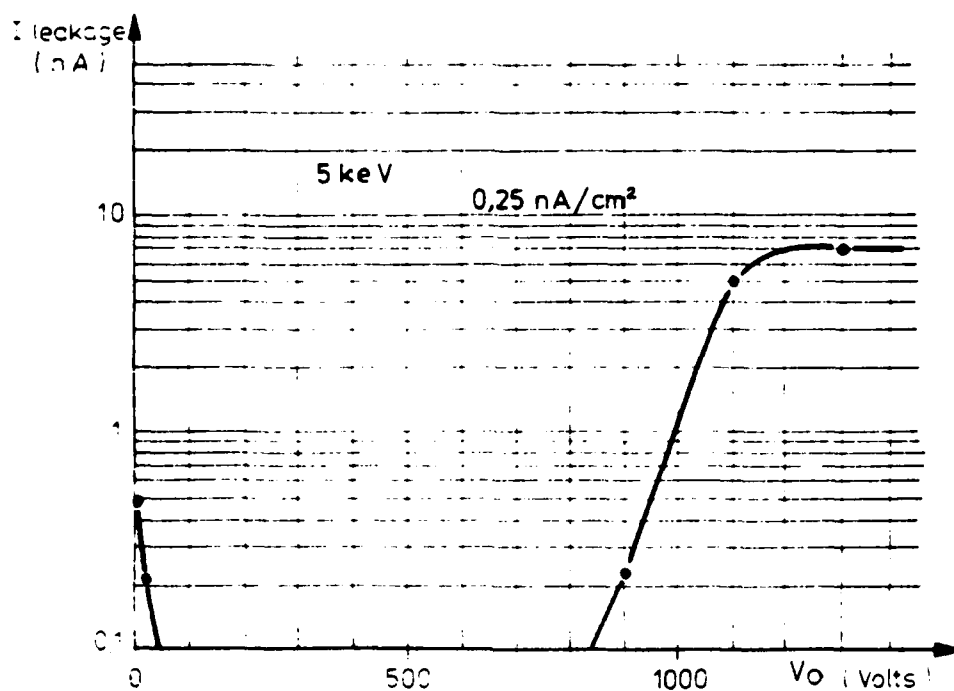
FIGURE 8A - LEAKAGE CURRENT VERSUS TIME AT 5 KEV
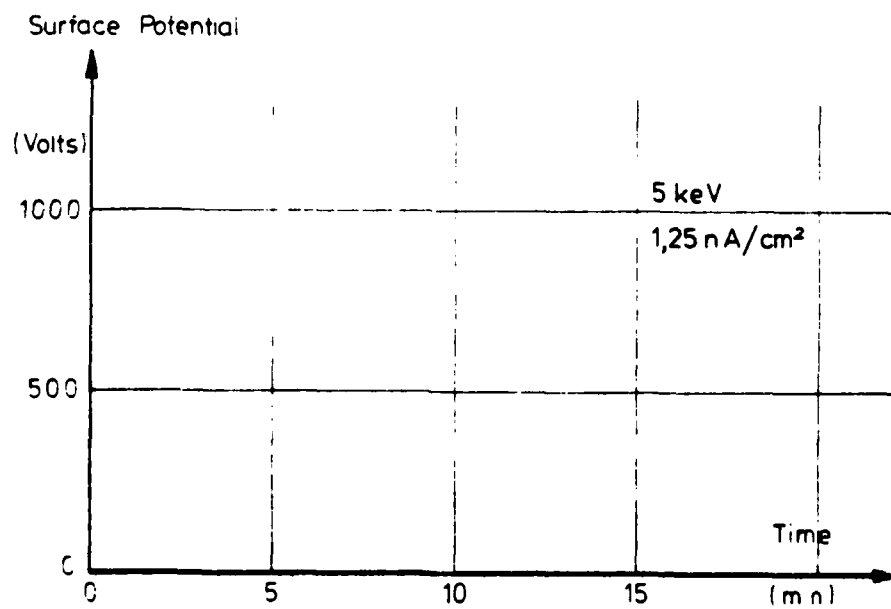
FIGURE 8B - SURFACE VOLTAGE VERSUS TIME AT 5 KEV
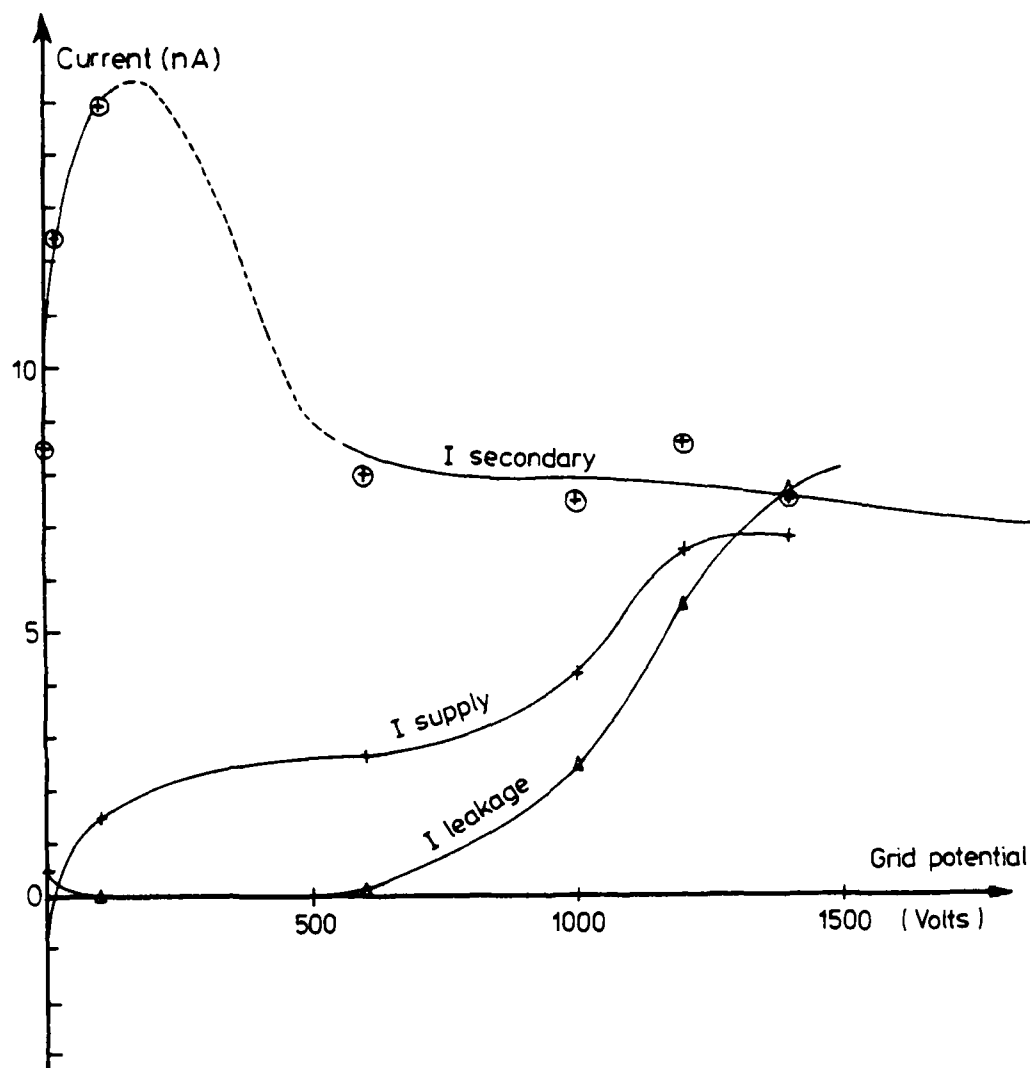
FIGURE 8 C – MEASURED CURRENTS VERSUS GRID
POTENTIAL AT 5 KEV
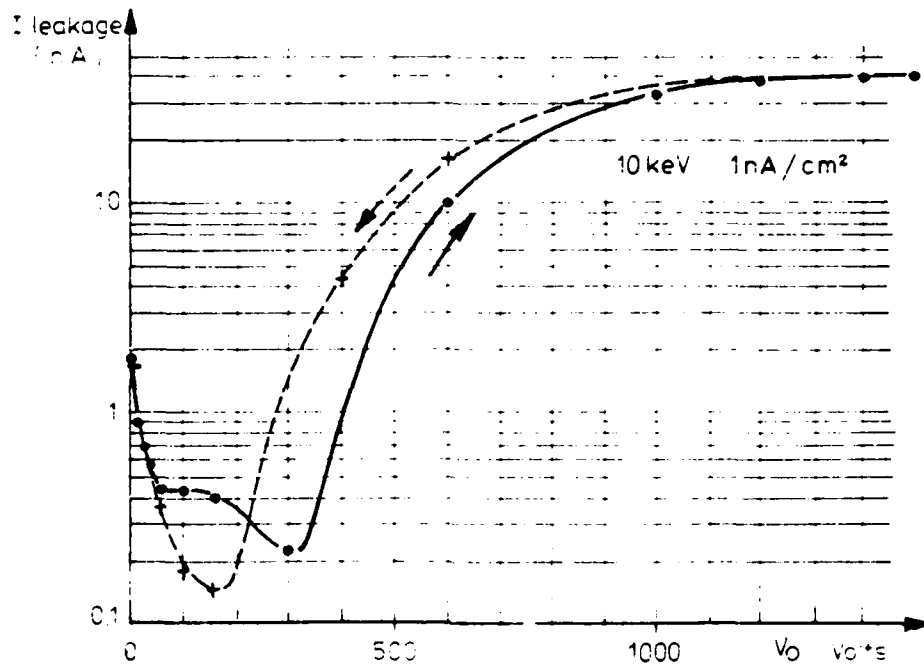
FIGURE 9A - LEAKAGE CURRENT VERSUS TIME AT 10 KEV
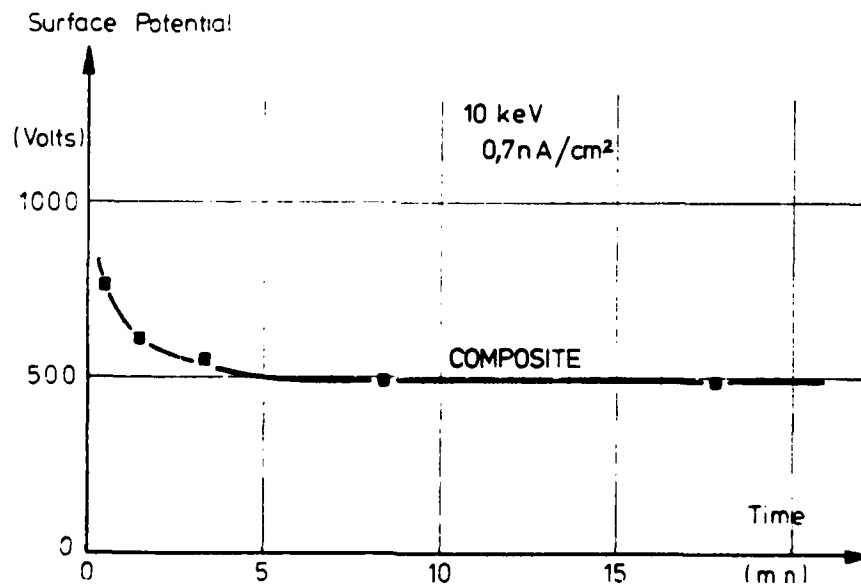
FIGURE 9B - SURFACE POTENTIAL VERSUS TIME AT 10 KEV

20
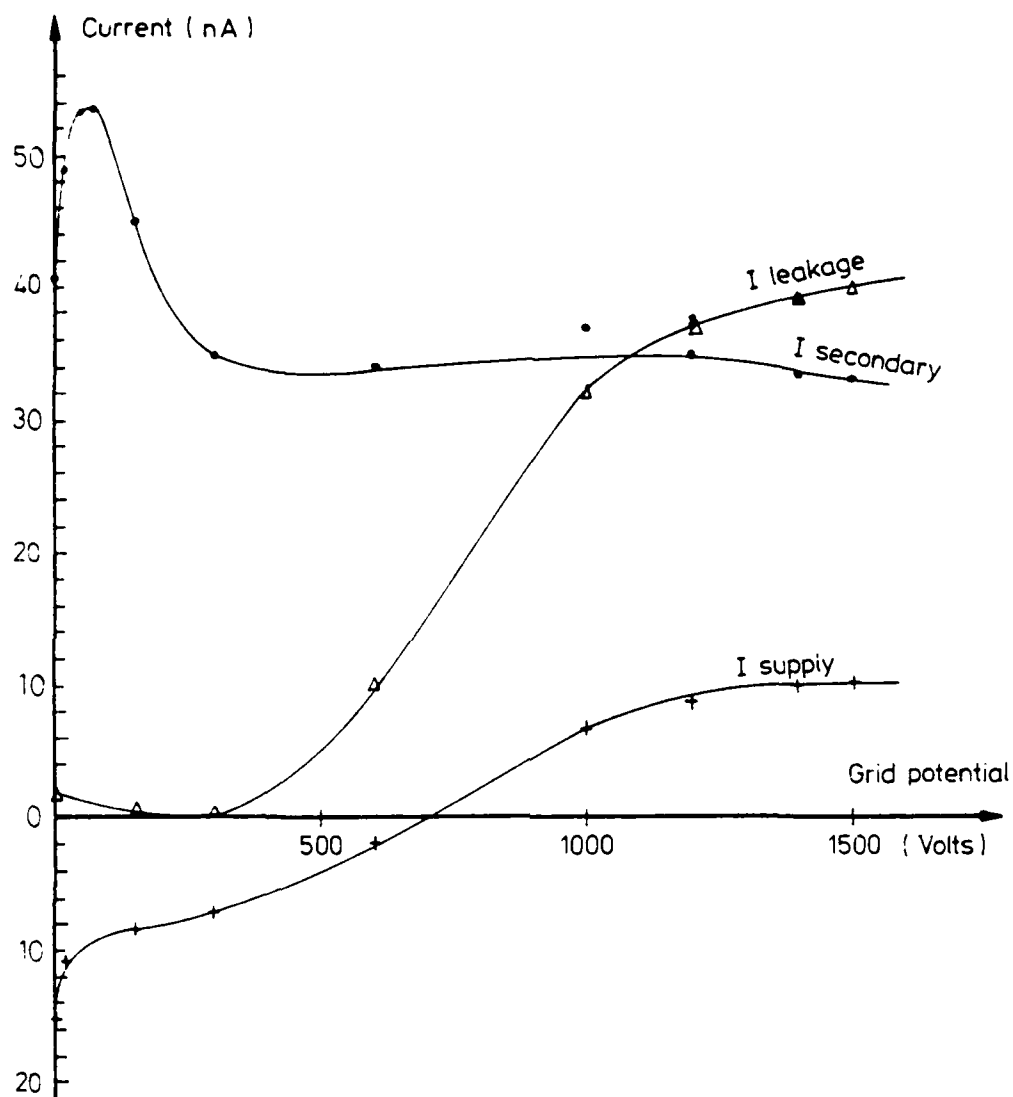
FIGURE 9c - MEASURED CURRENTS VERSUS GRID POTENTIAL
AT 10 KEV

21
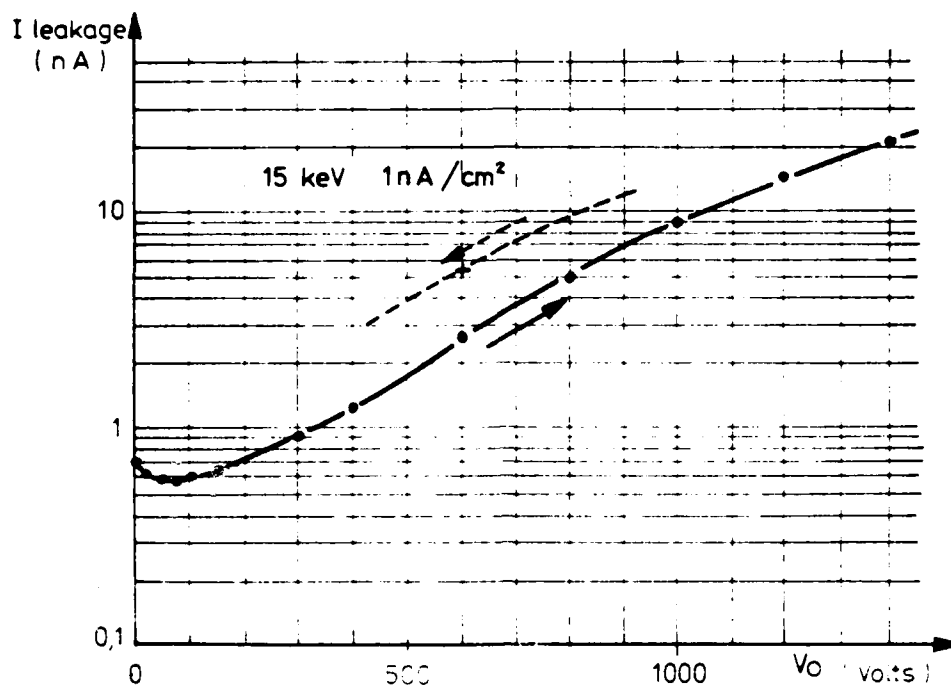
FIGURE 10A – LEAKAGE CURRENT VERSUS TIME AT 15 KEV
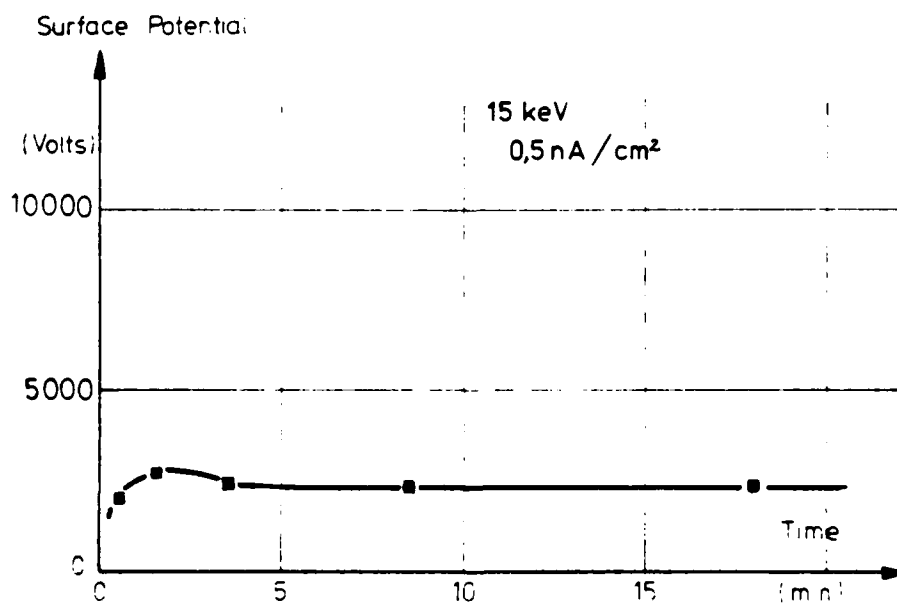
FIGURE 10B – SURFACE POTENTIAL VERSUS TIME AT 15 KEV
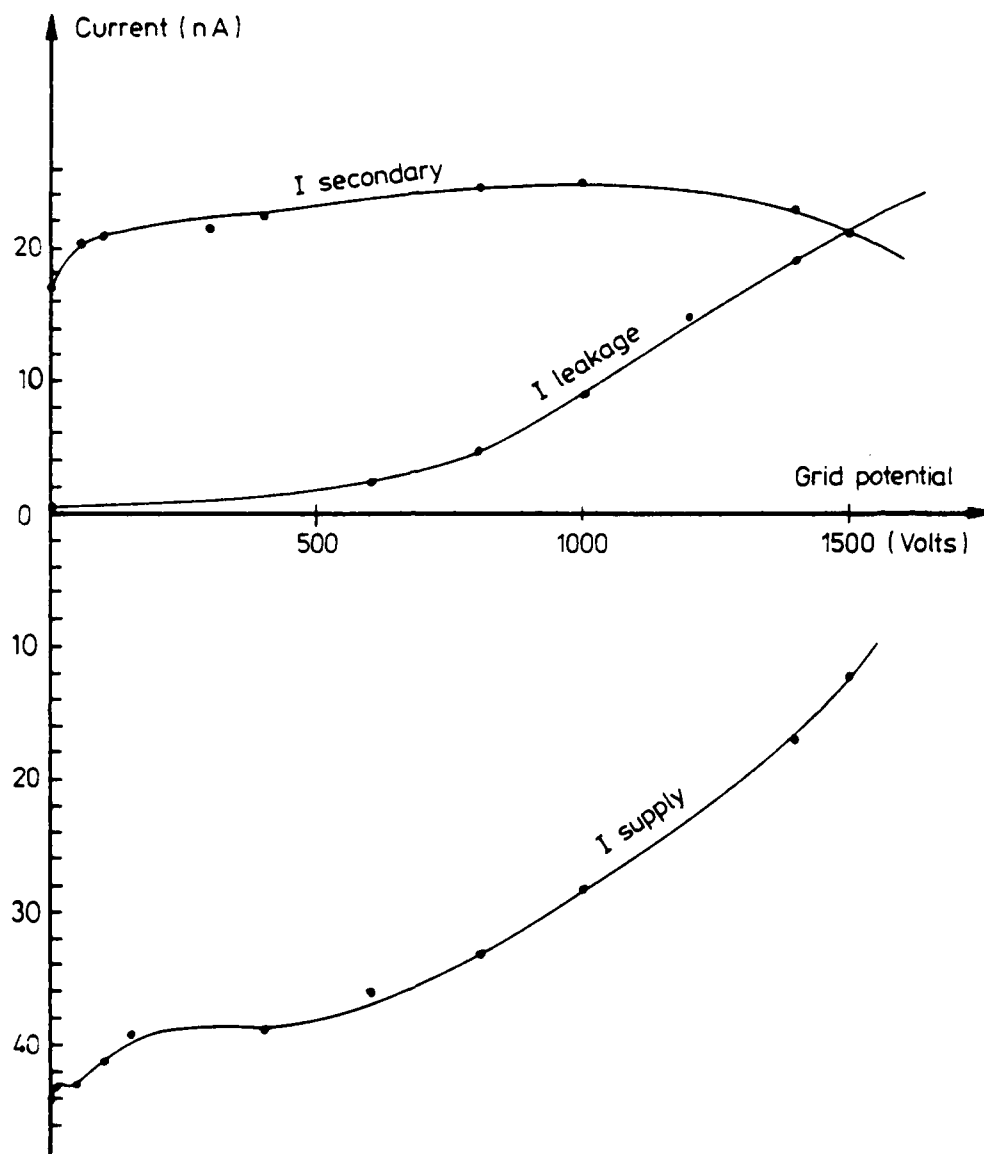
FIGURE 10c - MEASURED CURRENTS VERSUS TIME AT
15 keV 1 nA cm^{-2}
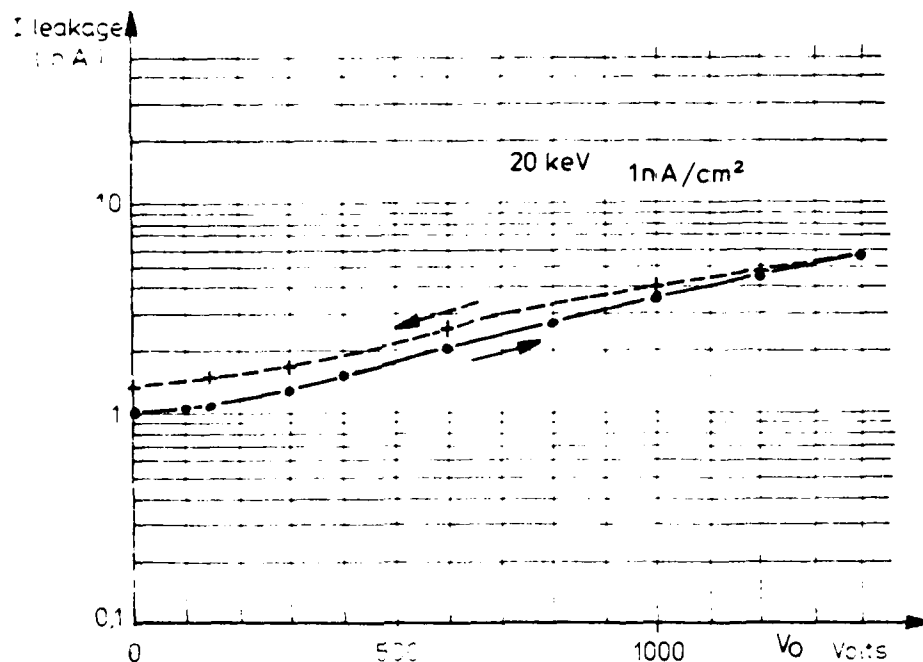
FIGURE 11A - LEAKAGE CURRENT VERSUS TIME AT 20 keV
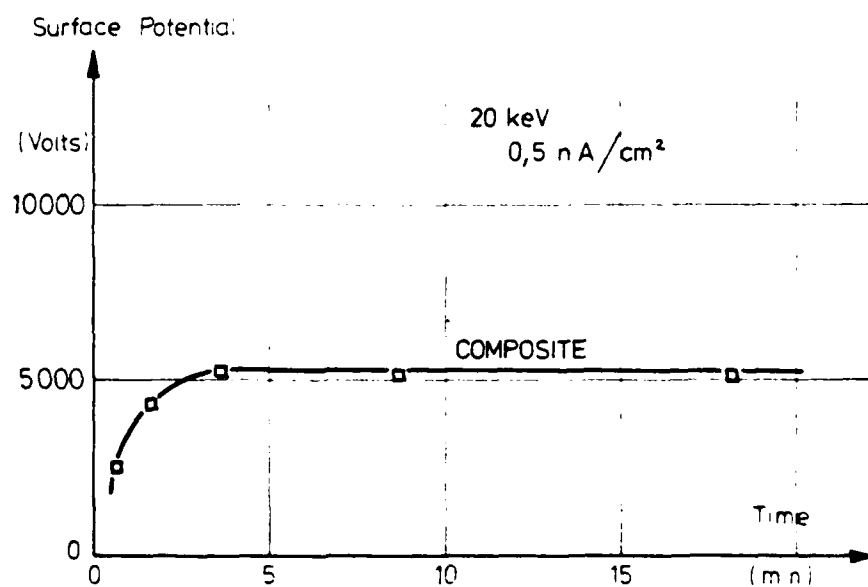
FIGURE 11B - SURFACE POTENTIAL VERSUS TIME AT 20 keV

24
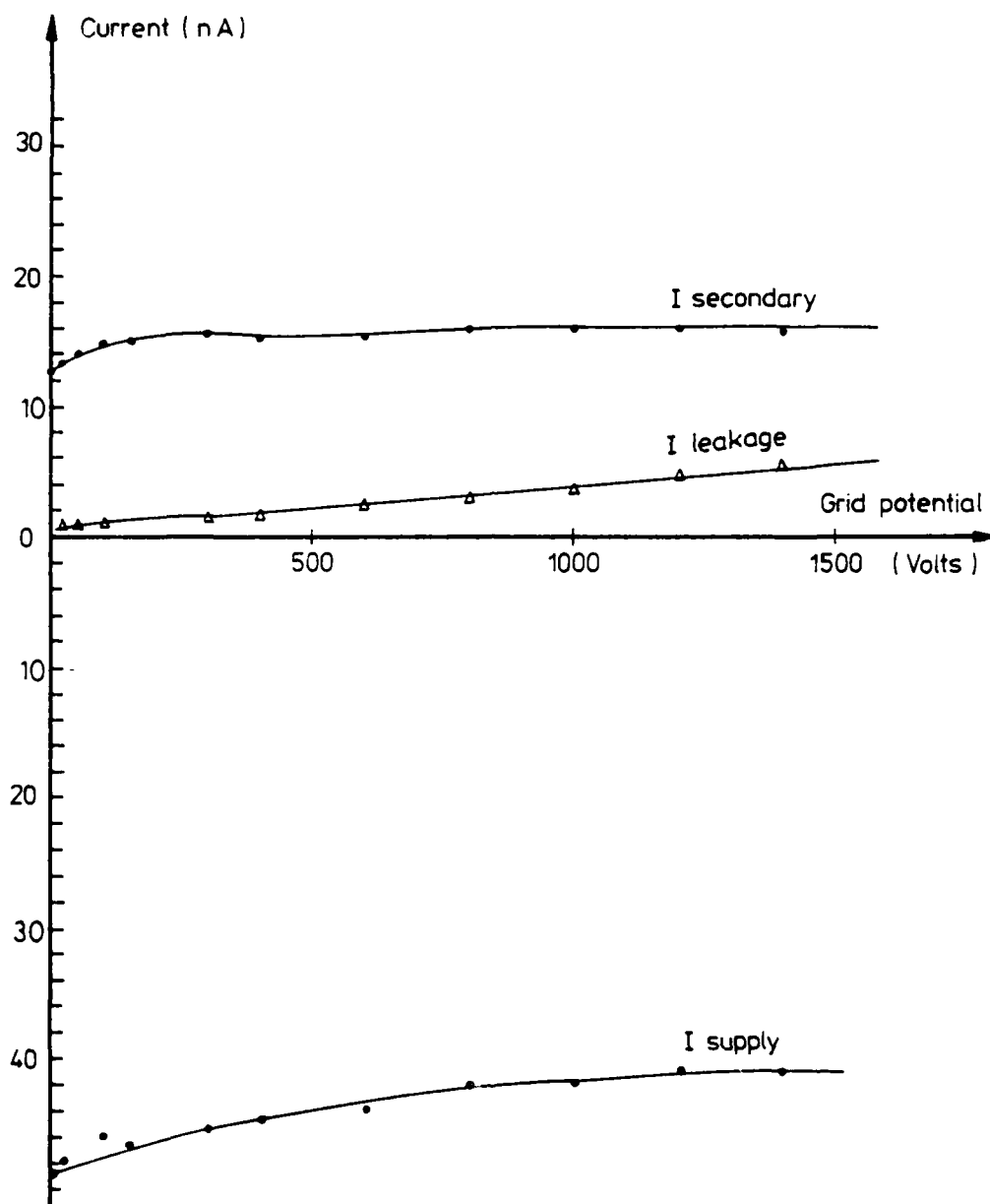
FIGURE 11c – MEASURED CURRENTS VERSUS TIME AT 20 KEV

and 11 with their corresponding induced potentials against time are equally suggestive of a surface potential in strong correlation with the field-dependent conductivity.

For the lowest electron beam energy (5 keV) the transmitted current $I_{leakage}$ (FIGURE 8a) is rather low for V_0 less than 1200 Volts; One should note that the surface potential observed under a 5 keV electron irradiation is zero due to a very high secondary emission that can be evidenced by the current collected on an hemispheric electrode (see for instance FIGURE 36 of Ref. 3). In FIGURE 8a the initial decrease of $I_{leakage}$ in terms of V_0 is correlated with an increase of the current collected on the hemispheric electrode $I_{secondary}$: see FIGURE 8c. The same trend is also obvious in FIGURE 9c for 10 keV.

2-2-4   Conclusion

The large dependence between the electrical field and the conductivity across the cross section of the composite has been confirmed. An increase in the leakage current is observed when the applied field is increased (beyond a certain threshold value). This fact substantiates the secondary emission conductivity mechanism proposed by BELANGER and EAGLES (Ref. 5).

2 - 3   INFLUENCE OF THE IRRADIATION DENSITY ON THE CHARGE DISSIPATION PERFORMANCE

2-3-1   Purpose of the study

The secondary emission conductivity that has been proposed (Ref. 5) in order to explain the behaviour of silica fabrics and composites under electron beam, supposes that a free electron population is created inside voids between silica fibers. This suggests a possible irradiation density influence on the charge dissipation performance. In the first phase of the study some sudden discharges of silica fabrics have been observed. Such discharges had not been reported by others at 30 keV/30 nA cm^{-2} and at 20 keV/1 nA cm^{-2} (Ref.6).

Ref. 6   A.E. EAGLES and coworkers : Fabric coatings - AIAA Thermophysics Conf. Denver Colorado May 1975 (AIAA Paper 65-668)

Accordingly it was decided to perform several electron irradiations at various beam densities.

2-3-2   Experimental set up

The experimental set up has been described in an earlier report (Ref. 3).

Two series of tests were run on the same sample.

The first one at 10 keV with one specimen that was irradiated in the following successive conditions:

(a) 10 pA cm^{-2} for 16 000 s
(b) 30 pA cm^{-2} for 5 300 s
(c) 100 pA cm^{-2} for 2 800 s
(d) 300 pA cm^{-2} for 1 900 s
(e)   1 nA cm^{-2} for 1 000 s
(f)   3 nA cm^{-2} for 1 000 s
(g) 10 pA cm^{-2} for 20 000 s

Between these various irradiations the sample was totally discharged with electrons at 5 keV 1 nA cm^{-2}. The same sample was used for a second series of tests at 15 keV in the following conditions:

(h) 10 pA cm^{-2} for 27 000 s
(i) 30 pA cm^{-2} for 13 000 s
(j) 100 pA cm^{-2} for 4 000 s
(k) 300 pA cm^{-2} for 1 300 s
(l)   1 nA cm^{-2} for   400 s
(m)   3 nA cm^{-2} for   133 s
(n) 10 pA cm^{-2} for 27 000 s
(O) 100 pA cm^{-2} for 4 000 s

For the irradiations at 15 keV, the sample charge was also removed after each irradiation step with an electron beam at 5 keV 1 nAcm^{-2} or 5 keV 10 pA cm^{-2}.

The surface potential was measured at several exposure times for each irradiation step.

The composite we have tested has been described in Section 2122.
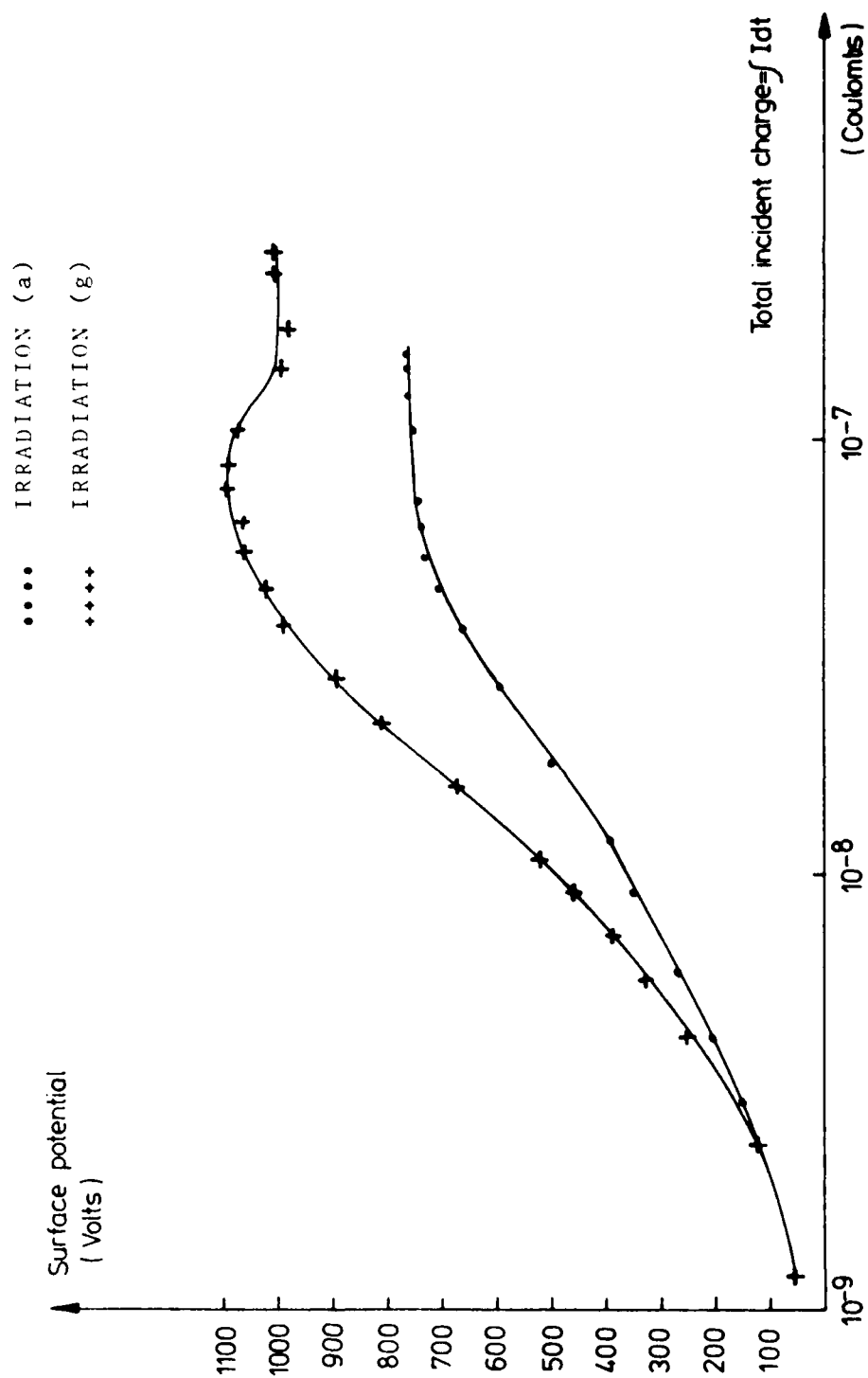
FIGURE 12 - EVOLUTION OF THE SURFACE POTENTIAL WITH TIME $(10 \text{ KEV}/10 \text{ PA CM}^{-2})$

2-3-3   Results

2331   Preliminary remark

In FIGURE 12 are reported results obtained for two irra-diations with 10 keV electrons with a flux rate equal to 10 pA cm^{-2} The labels (Section 2-3-2) for these two irradiations are (a) and (g). Irradiation (a) was performed on a fresh sample (never irra-diated before) after 10 hours under vacuum. Irradiation (g) was performed on the same sample after 2 days under vacuum and seve-ral irradiation steps.

FIGURE 12 shows that higher surface potentials are obtai-ned during the second irradiation (g). This observation corrobora-tes what was said earlier (Section 2.1.3). Here also it is diffi-cult to decide whether this fact is due to contamination or to ageing.

However it seems that the phenomenon importance decreases with time: irradiations (h) (j) and (n) (o) performed respec-tively after 4 and 8 days under vacuum with the same beam condi-tions, lead exactly to the same values of the surface potential see FIGURES 13 and 14.

2332   Surface potentials and flux rates

FIGURES 15 and 16 show the variation of the surface poten-tial in terms of total incident charge (flux rate multiplied by irradiation time). This allows normalization and unique presenta-tion for the various involved flux rates (0.01 to 3 nA/cm^2).

FIGURE 16 exhibits clearly that surface potential values at steady state depend on flux rate, while the intermediate values (for incident charge lower than $10^{-8}C$) depend only on electrical charge.

The flux rate dependency is illustrated in FIGURE 17 where steady state potential values are expressed in terms of flux rate. This dependency is particularly obvious at 15 keV between 0.01 and 0.1 nA/cm^2. At 10 keV the variations of the potential value

29
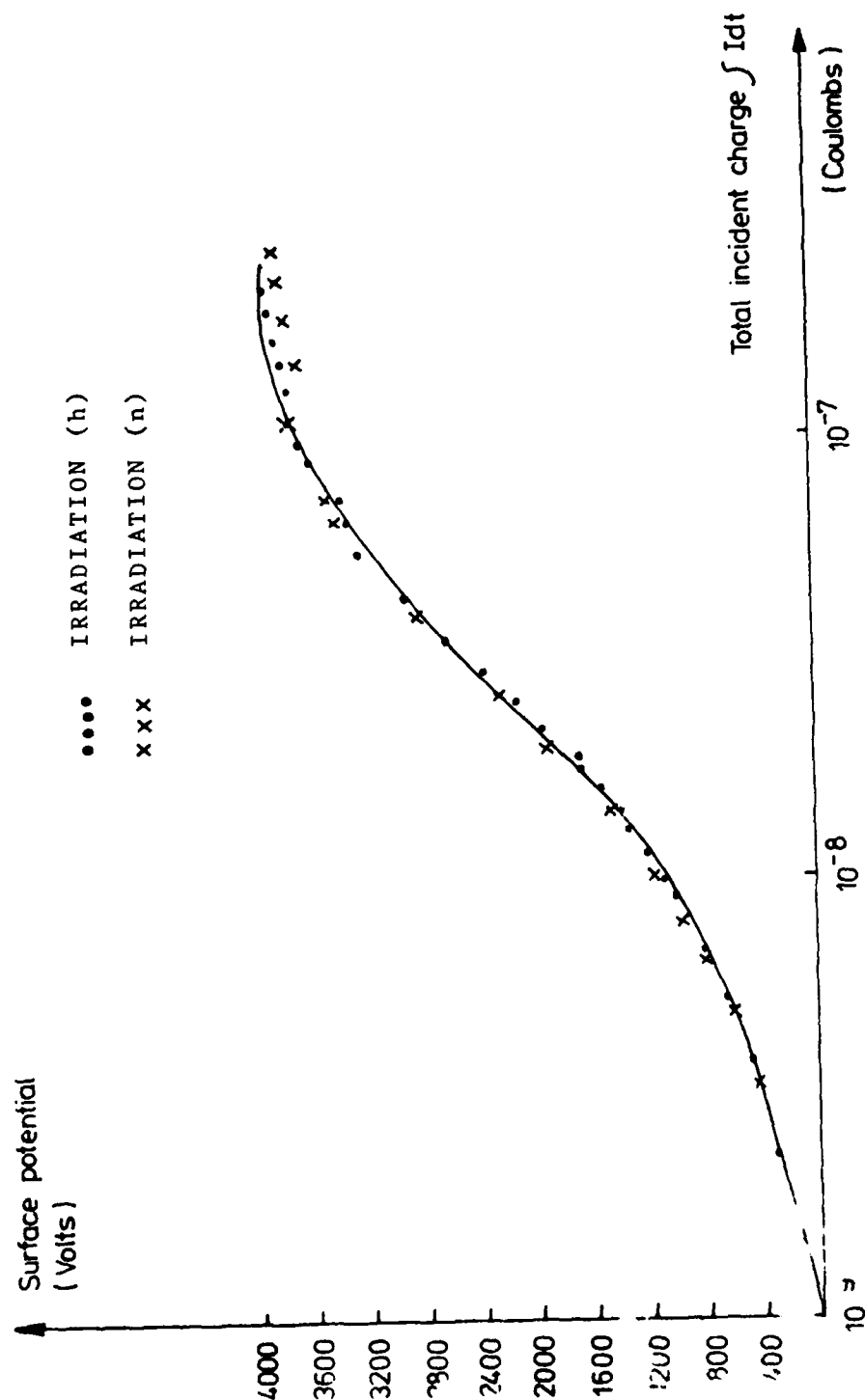
FIGURE 13 - EVOLUTION OF THE SURFACE POTENTIAL WITH TIME (15 KEV/10 pA. CM^{-2}.)

Surface potential
(Volts)

Total incident charge ∫ Idt

(Coulombs)

•••   IRRADIATION (j)

xxx   IRRADIATION (o)

4000

3000

2000

1000

10^{-9} 10^{-8} 10^{-7}
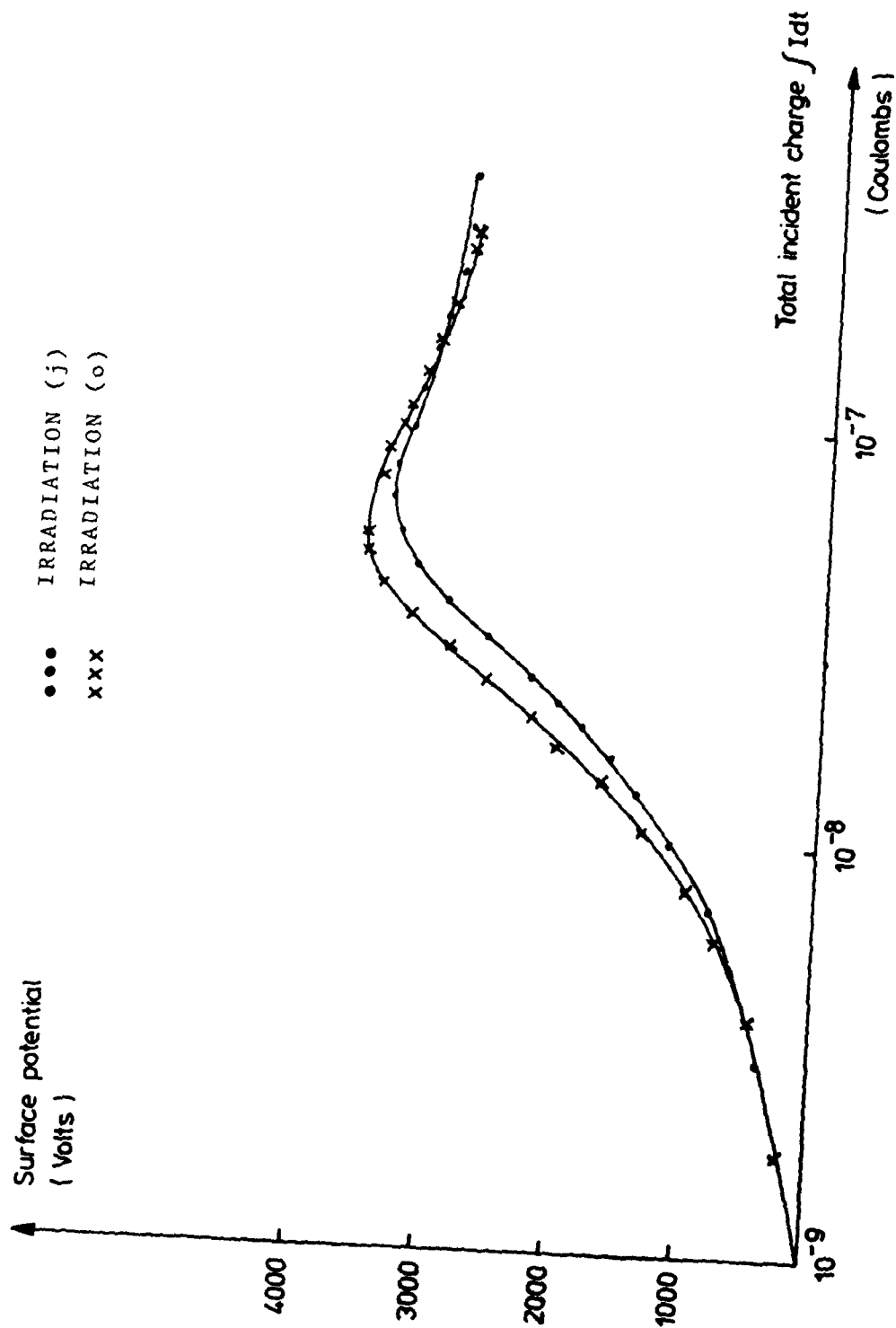
FIGURE 14 - EVOLUTION OF THE SURFACE POTENTIAL WITH TIME (15 KEV/100 PA CM^{-2})

31
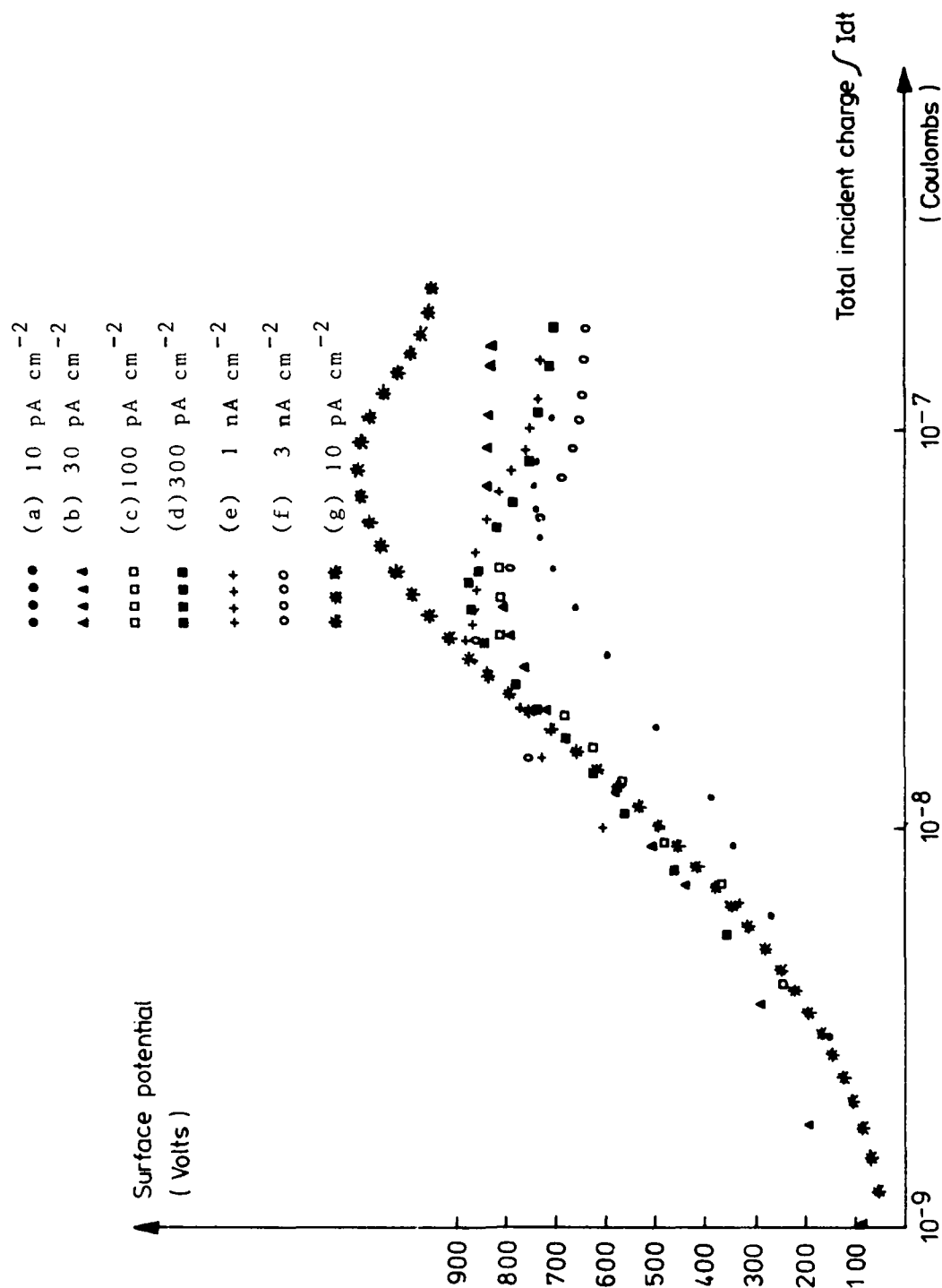
FIGURE 15 - CURRENT DENSITY EFFECT AT 10 keV

Total incident charge ∫ Idt (Coulombs)

Surface potential (Volts)

• • • •	(a)	10 pA	cm^{-2}
▲ ▲ ▲ ▲	(b)	30 pA	cm^{-2}
□ □ □ □	(c)	100 pA	cm^{-2}
■ ■ ■ ■	(d)	300 pA	cm^{-2}
+ + + +	(e)	1 nA	cm^{-2}
o o o o	(f)	3 nA	cm^{-2}
✳ ✳ ✳ ✳	(g)	10 pA	cm^{-2}

32
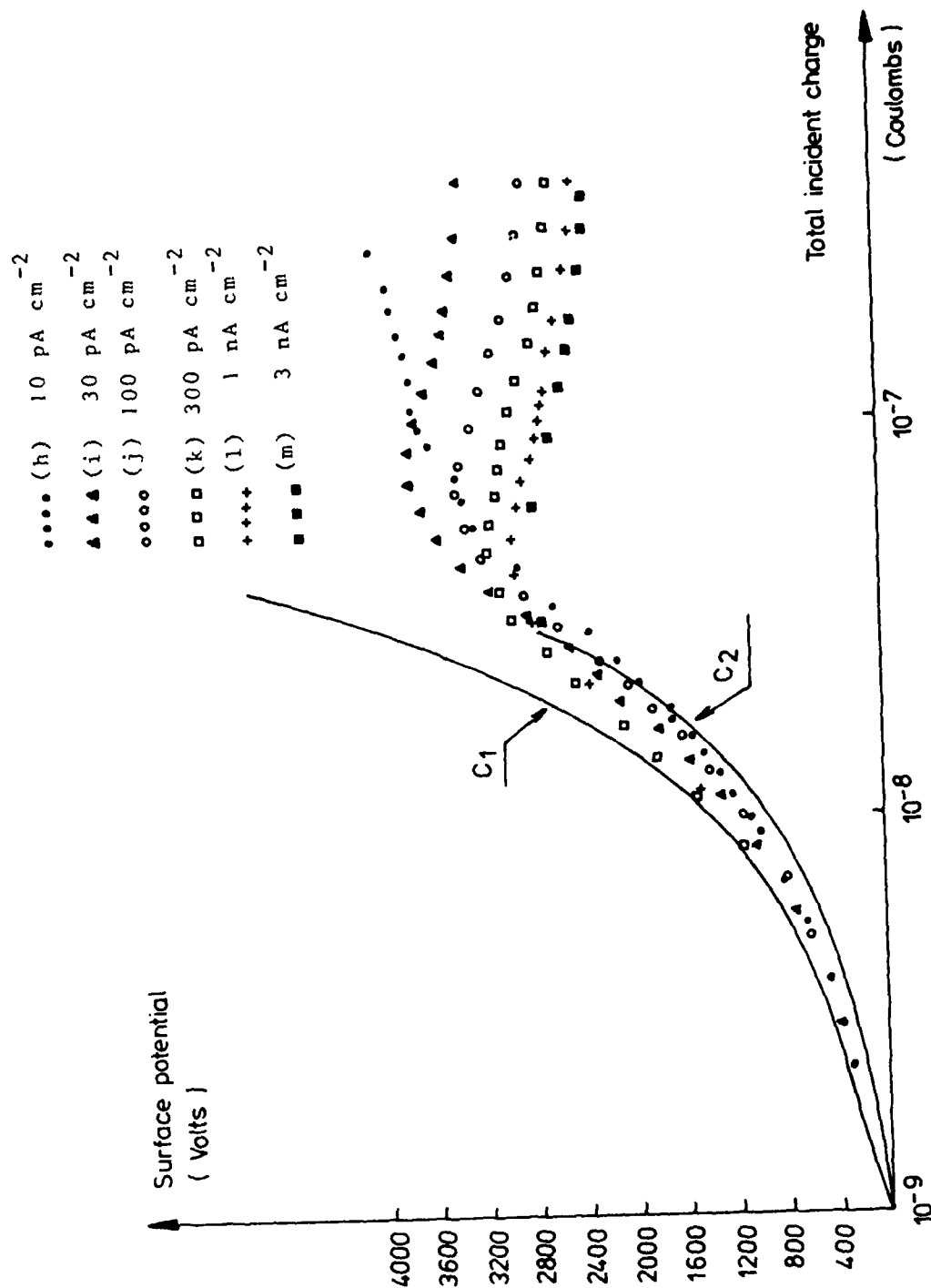
FIGURE 16 - CURRENT DENSITY EFFECT AT 15 KeV
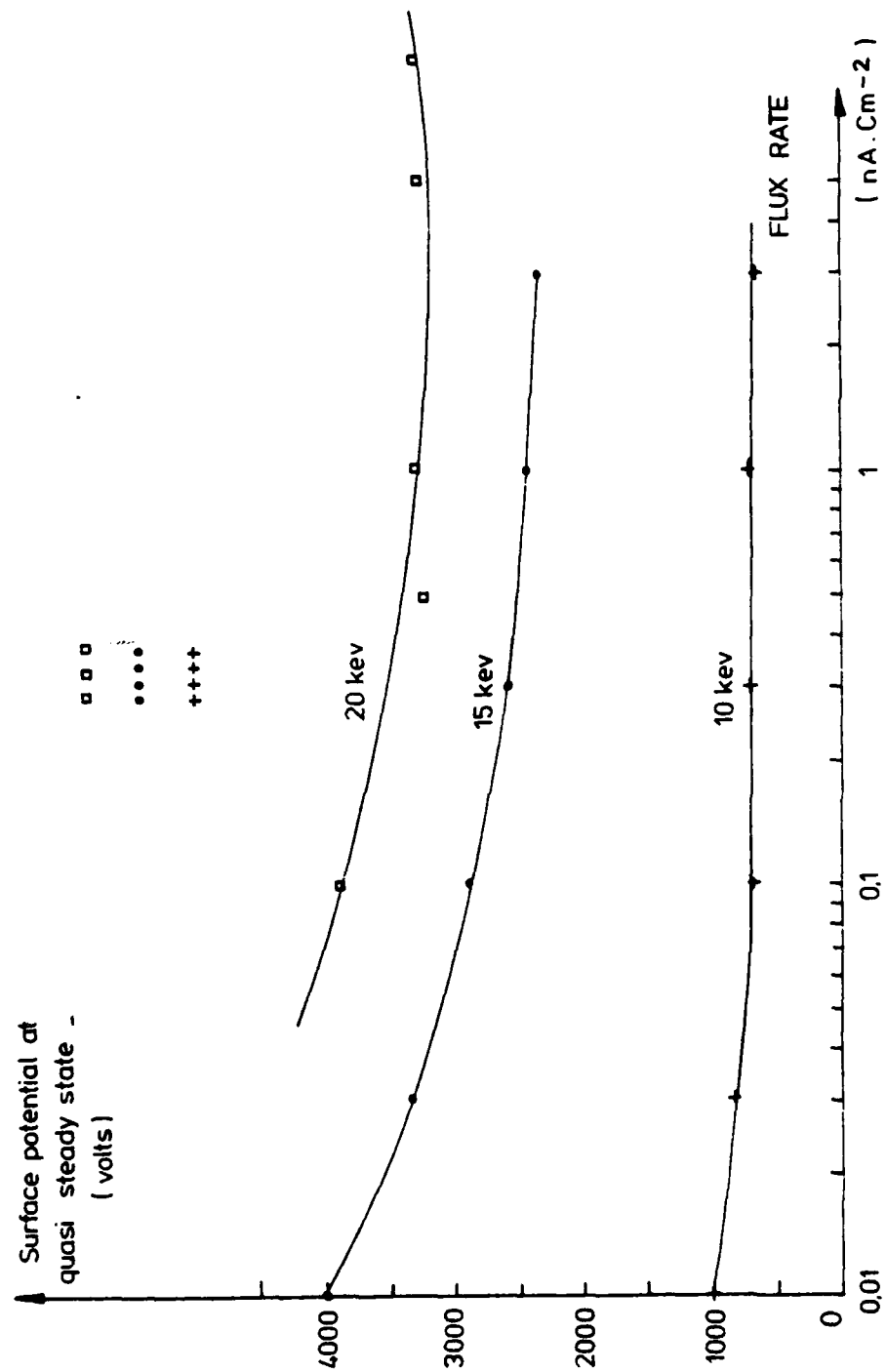
FIGURE 17 – SURFACE POTENTIAL (AT STEADY STATE) VERSUS FLUX RATE

at steady state are much less noticeable.

In FIGURE 16 the experimental values of the surface potential are compared to calculated potential values of pure capacitors submitted to the same irradiation. Assuming a secondary emission coefficient of 30 per cent, we find two capacitances values showing similar values of the induced surface potentials (estimated by calculation):see FIGURE 16, C_1 and C_2 . These values are 5 and 8 picoFarads per cm^2. This observation helps to elucidate the electrostatic behaviour of silica fabrics and composites under electron bombardment. At 15 keV, they behave like a capacitor (whose value is in the range of 5 to 8 picoFarads per cm^2) until a leakage current arises due to the secondary emission conductivity for potential values around 1000 Volts.

At 10 keV, the dependency on flux rate of the surface potential values is less obvious but there is the same trend for surface potentials to be lowered by greater flux rates (see FIGURES 15 and 17).

It must also be emphasized about FIGURE 15 that a possible contamination and/or ageing effect could have interfered with the flux rate effect. FIGURE 12 reveals an alteration of the silica fabric electric properties : FIGURE 12a gives the potentials values of the first irradiation for a fresh sample while FIGURE 12g was obtained after a series of irradiation (see preliminary remark Section 2331).

FIGURES 13 and 14 show that in the case of the 15 keV irradiation series, the contamination effect had not interfered, probably because the sample was not fresh from the beginning and that the contamination and/or ageing effect was stabilized.

Irradiations at 5 keV and 0.01 nA/cm^2 were also performed in the same sample that had been irradiated with 10 keV and 15 keV electrons. It was checked that no detectable potential appeared in these conditions. Moreover an irradiation at 5 keV and 0.01 nA cm^{-2} effectively discharged a sample that had been previously charged at 10 or 15 keV.

2-3-4 Conclusion

The results that have been observed on a composite silica fabric/FEP/Alu can be summarized as follows:

.   under a 5 keV electron beam, the surface potential is very near to zero (less than 15 Volts) whatever the flux rate may be.

.   The surface potentials that are induced by a 10 keV or a 15 keV electron irradiation, are dependent on the flux rate. They are the highest for the lowest flux rates.

The surface potentials are dependent on the sample history. They are increasing with the time of exposure to vacuum and/or irradiation. However after a certain time a stabilization seems to occur.

2 - 4   INFLUENCE OF THE PRESENCE OF LOW ENERGY
ELECTRONS (2 to 4 keV) TOGETHER WITH HIGH
ENERGY ELECTRONS (10 to 20 keV) ON THE ELEC-
TROSTATIC BEHAVIOUR OF SILICA FABRICS

2.4.1   Background

Secondary emission conductivity (SEC) has been proposed
by BELANGER and EAGLES (Ref. 5) as a mechanism to explain the
charge dissipation of silica fabrics under low energy electron
irradiation (see also Ref. 3). The secondary emission ratio δ has
the following characteristics numbers for normal incidence primaries
on silica :

$$\delta_{max} = 2.1 \text{ to } 2.9$$

$$E_{max} = 400 \text{ to } 440 \text{ eV}$$

$$E_1 = 30 \text{ to } 50 \text{ eV}$$

$$E_2 = 2.3 \text{ keV}$$
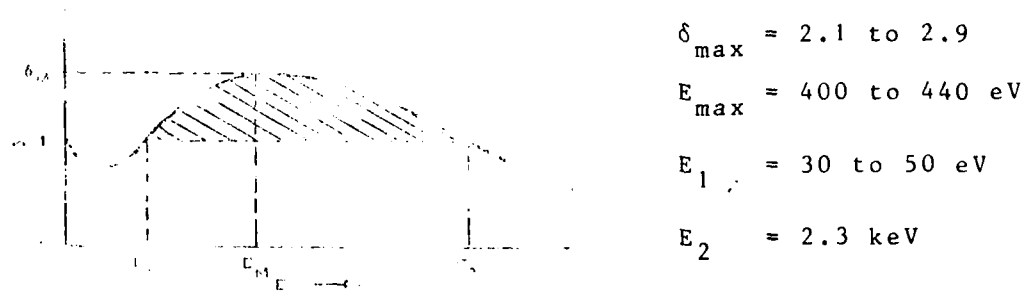
FIGURE 18 - SECONDARY EMISSION OF SILICA

The energy range E_1, E_2 for which δ is greater than 1.0
is extended when primaries have non normal incidences, as it is
the case for silica fabrics. Evidence has been given in Section
3-4 of Ref. 3 that a very high secondary emission can be measured
by an hemispheric collecting electrode for a 5 keV electron irra-
diation on silica fabrics with a surface potential equal to zero.
When the electron beam energy is increased to 10, 15, 20 keV, the
secondary emission is decreased and a leakage current that is due
to S.E.C. can be measured ; the surface potential becomes measu-
rable then increases up to reach some thousands volts for a 20 keV

Curved electrode

2-5 keV electron gun

5-20 keV electron gun

Scattering foil

Faraday cup

Potentiel probe

Sample 1 (under irradiation)

Rotating Sample holder

Sample 2

CEDRE CHAMBER
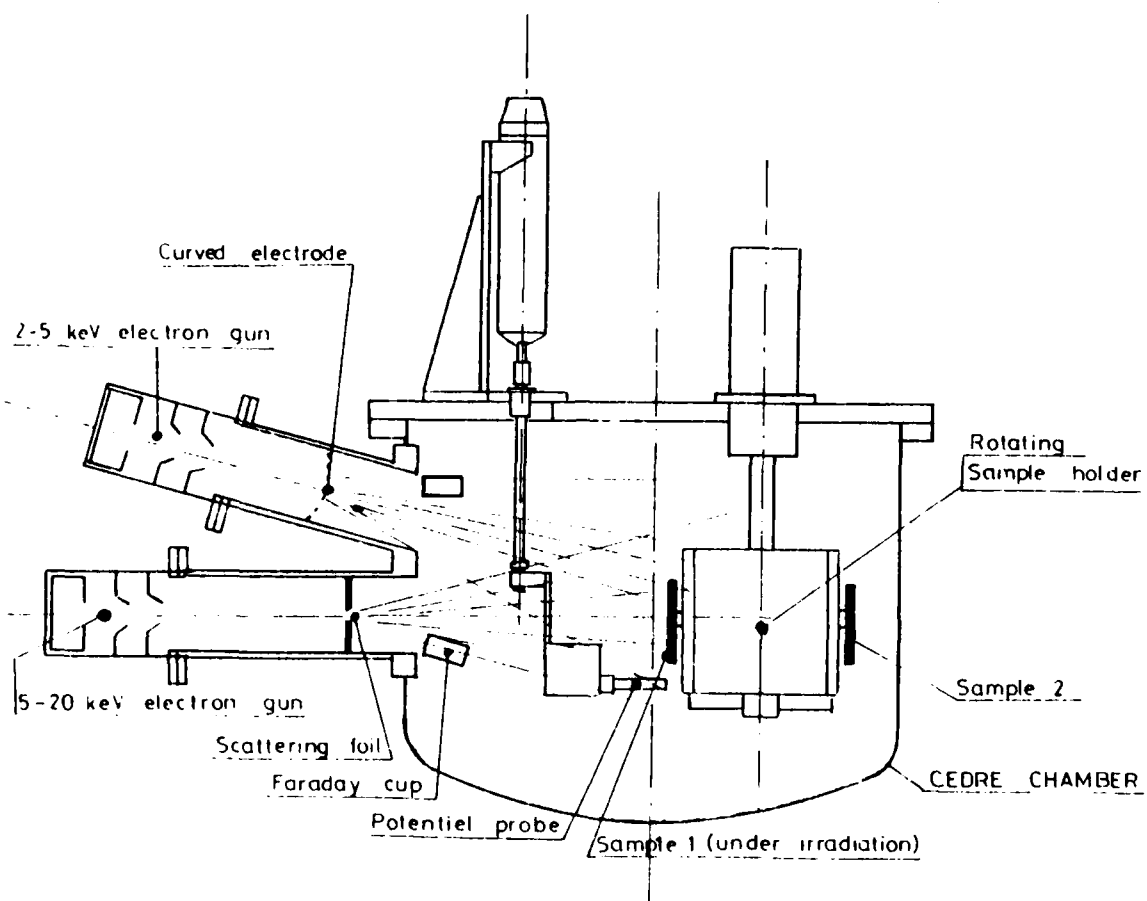
FIGURE 13 - IRRADIATIONS WITH TWO ELECTRON GUNS

38

beam. However the results that have been obtained with 10 to
20 keV electrons, have been measured only with quasi monoenergetic
electron beams. According to EAGLES, as the beam energy is increa-
sed above 5 keV, the incident electrons generate secondaries deeper
within the material where they are unavailable to act as charge
carriers towards the surface. In an actual substorm environment,
there is a continuous distribution of electron energies. Accor-
dingly it seems interesting to evaluate the silica fabric beha-
viour under irradiation either with a wide spectrum of electrons
or at least with two simultaneous beams of electrons giving two
quasi monoenergetic beams in two different energy ranges. The
second method is easier. It was decided to irradiate composite
samples with low energy electrons (2 to 4 keV) acting together
with medium energy electrons (10 to 20 keV).

2.4.2   EXPERIMENT SET UP AND PROCEDURE

2421   *Facility*

The facility was redesigned to allow a simultaneous irradia-
tion by low energy (2 to 4 keV) and medium energy (10 to 20 keV)
electrons.

The test chamber is the same as described in Section 3-2
of Ref. 3. However this chamber has been modified by addition of a
cryogenic shroud that surrounds the sample holder (see Section 3-2)
and a second electron gun (see FIGURE 19) giving particles in the
range 2 to 5 keV. Implantation of this second gun necessitates the
removal of the hemispheric electrode that is generally used to col-
lect secondary electrons.

The sample holder is cubic and made up of 4 plates 200 x
200 mm. A rotating shaft allows to present any of these four
plates in front of the guns. One of these plates carries five
Faraday cups used in order to measure the flux uniformity of both
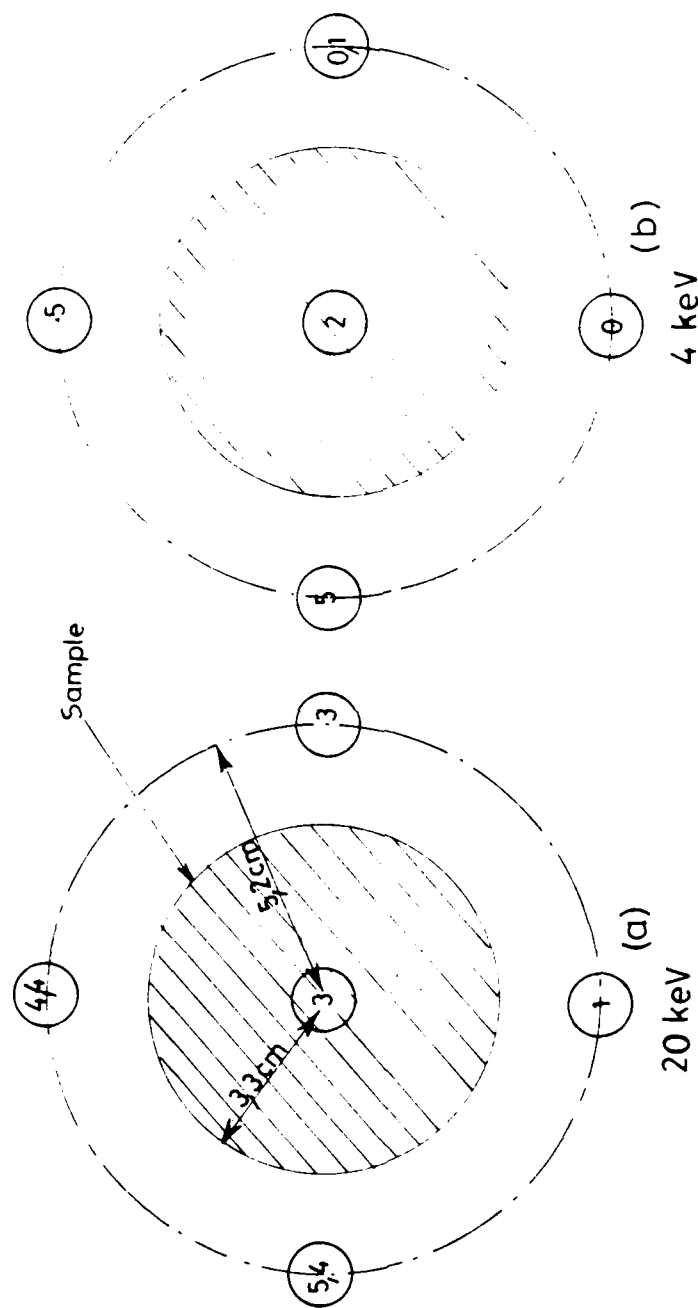
FIG:20 Irradiation uniformity with the low energy beam

electron beams. Two other plates carry the two samples to be irradiated. The last plate is used in the calibration procedure of the surface potential probe.

During the sample irradiations, two Faraday cups are used for beam monitoring. Two mechanical shutters can stop the electron beam for calibration purposes. Samples are receiving medium energy electrons with normal incidence and low energy electrons with a 15° incidence.

The irradiation uniformity with the low energy beam is not as good as the one for the medium energy beam, due to the very simple design of the gun. FIGURE 20 shows typical current values measured with the five calibration Faraday cups at 20 keV and 4 keV. At 10, 15 and 20 keV, the irradiation uniformity is better than $\pm$ 10 per cent, as measured by the same set of Faraday cups. The current value directly measured with the central Faraday cup is used in order to determine the irradiation flux rate at the sample.

The sample potential is measured by a continuous scan of a potential probe across the sample after end of the irradiation ; the "surface potential" value we give in TABLE 1 corresponds to the maximum value in this record.

2422   Samples

Two samples of the composites material (described at Section 2.1.2.2) have been irradiated:

One of them (B) is a specimen that has not been irradiated previously. The second (D) is the one that has been irradiated for 32 hours in the test described at Section 3-3-2 [*], this latter specimen has therefore a complicated history from both points of view of contamination and irradiation.

Each sample is mounted as sketched in FIGURE 21.

(*) this sample was called "C" at Section 3-3-2

ELECTRONS

GROUNDED RING

INSULATING FOIL

SAMPLE UNDER TEST (COMPOSITE or KAPTON with ITO LAYER)

Aluminium holder

$I_L + I_C$
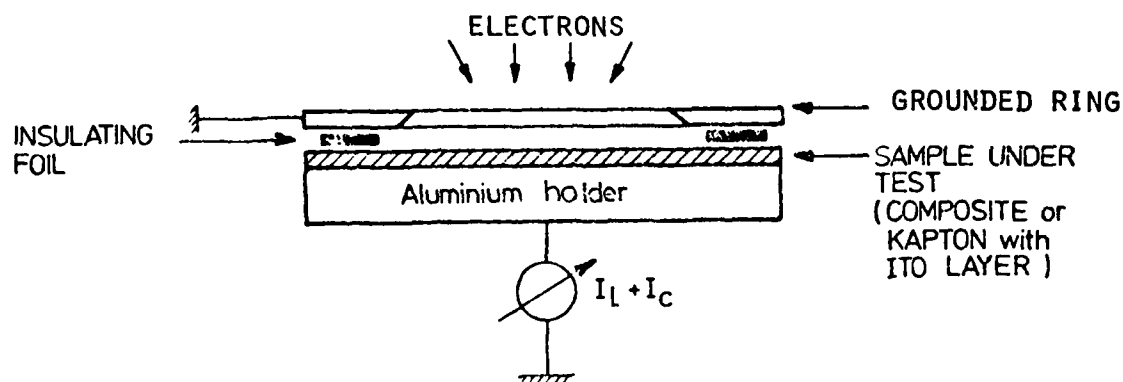
FIGURE 21 - SAMPLE SETTING

2423 Procedure

Both samples (B and D) have been irradiated with the same procedure. The energy of the low energy beam (beam # 1) was set at 2 or 4 keV ; the energy of the medium energy beam (beam # 2) was set at 10, 15 or 20 keV.

The procedure and irradiation times are described in FIGURE 22.

SAMPLE IRRADIA-TION

BEAM 1 (LOW ENERGY) FOR 1,5 MINUTE

BEAM 1 (LOW ENERGY) + BEAM 2 (MEDIUM ENERGY) FOR 20 MINUTES

BEAM 1 (LOW ENERGY) FOR 0,2 MINUTE

SURFACE POTENTIAL MEASUREMENT

CHANGE IN FLUX RATES OF THE BEAMS

SAMPLE DISCHARGE

BEAM 1 FOR 15 TO 30 MINUTES

CHANGE IN ENERGY OF BEAMS
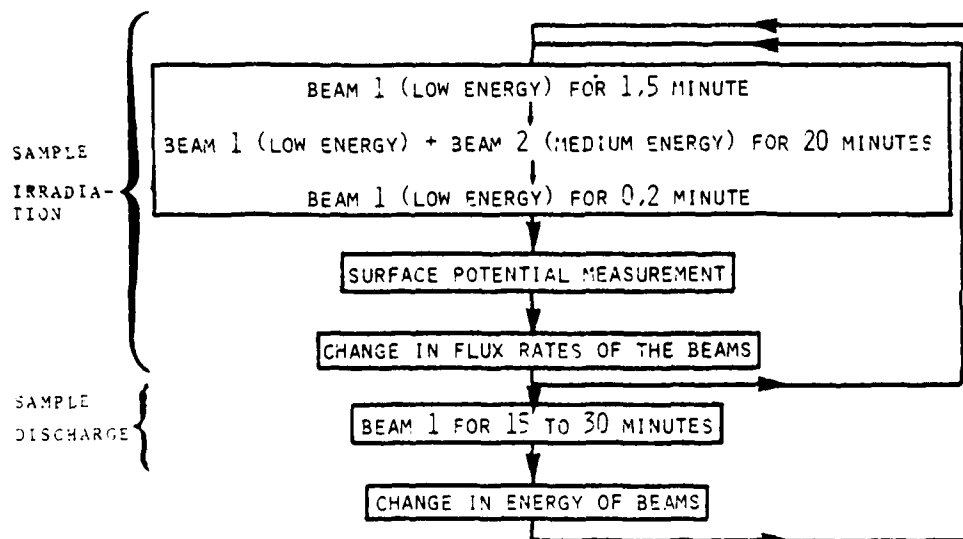
FIGURE 22 - TEST PROCEDURE

42

The following energy pairs have been successively achieved:

(a) 2 keV and 10 keV   (c)   4 keV and 15 keV
(b) 2 keV and 15 keV   (d)   4 keV and 20 keV

For each energy pair, several ratios of the two beams intensities have been selected. For each of these various ratios, the sum of the two beam intensities has been kept constant: 0.7 nA cm^{-2} for the energy pair (a), 0.5 nA cm^{-2} for the next pairs (b), (c), (d).

The leakage current is the only current that has been recorded during irradiation.

2 4.3.   RESULTS

TABLE 1 gives the potential surface values measured for various combinations of energies and beam intensities.

The occurrence of pulses in the leakage current of the samples is also reported in TABLE 1 as number of "arcing events". It is worth noting that four rather small breakdowns have been observed at 15 keV on the contaminated composite (Sample D). Many events are noticed at 20 keV for both samples.

2.4.4.   DISCUSSION

A substantial decrease in the surface potential of the sample is observed every time that an irradiation by low energy electrons (2 to 4 keV) is performed simultaneously with the irradiation by medium-energy electrons (10 to 20 keV) ; see TABLE 1. This can be explained by an enhancement of the secondary emission and the correlative secondary emission conductivity of the silica fabric for primaries in the 1 to 5 keV range.

Suprisingly ,   with the medium energy beam fixed at the 20 keV level, arcing events are still observed when the low energy beam is applied. However, as stated at section 2421 and in FIGURE 20 b

43

TABLE 1   RESULTS

EXPERIMENTS	BEAM 1		BEAM 2		SAMPLE A (*)		SAMPLE B(***)	
	Energy (keV)	Flux rate $(nAcm^{-2})$	Energy (keV)	Flux rate $(nAcm^{-2})$	Surface potential (V)	Arcing events (**)	Surface potential (V)	Arcing events (**)
1	2	0.7	-	-	0	-	0	-
2	2	0.6	10	0.1	<10		<10	
3	2	0.35	10	0.35	10to20		650	-
4	2	0.1	10	0.6	160	-	1260	-
5	-	-	10	0.7	740		1460	-
6	2	0.5	-	-	<10	-	<10	-
7	2	0.4	15	0.1	40to50	-	300	-
8	2	0.25	15	0.25	400	-	4410	-
9	2	0.1	15	0.4	1180	-	4500	-
10	-	-	15	0.5	1980		4500	4
11	4	0.5	-	-	<10	-	<10	-
12	4	0.25	15	0.25	1200		3960	
13	4	0.5	-	-	10	no	510	no
14	4	0.4	20	0.1	80	0	720	1
15	4	0.35	20	0.15	360	10	970	1
16	4	0.30	20	0.2	745	9	6600	12
17	4	0.25	20	0.25	1215	14	8190	78
18	4	0.20	20	0.30	1420	12	8100	119
19	4	0.15	20	0.35	3600	12	8200	60
20	4	-	20	0.5	4500	28	8370	150

(*)   experiments 1 to 12 have been successively performed with the same   specimen, that was replaced by a new one for the experiments 13 to 20

(**) for a 20 minutes period of time

(***) this sample has been previously irradiated and contaminated
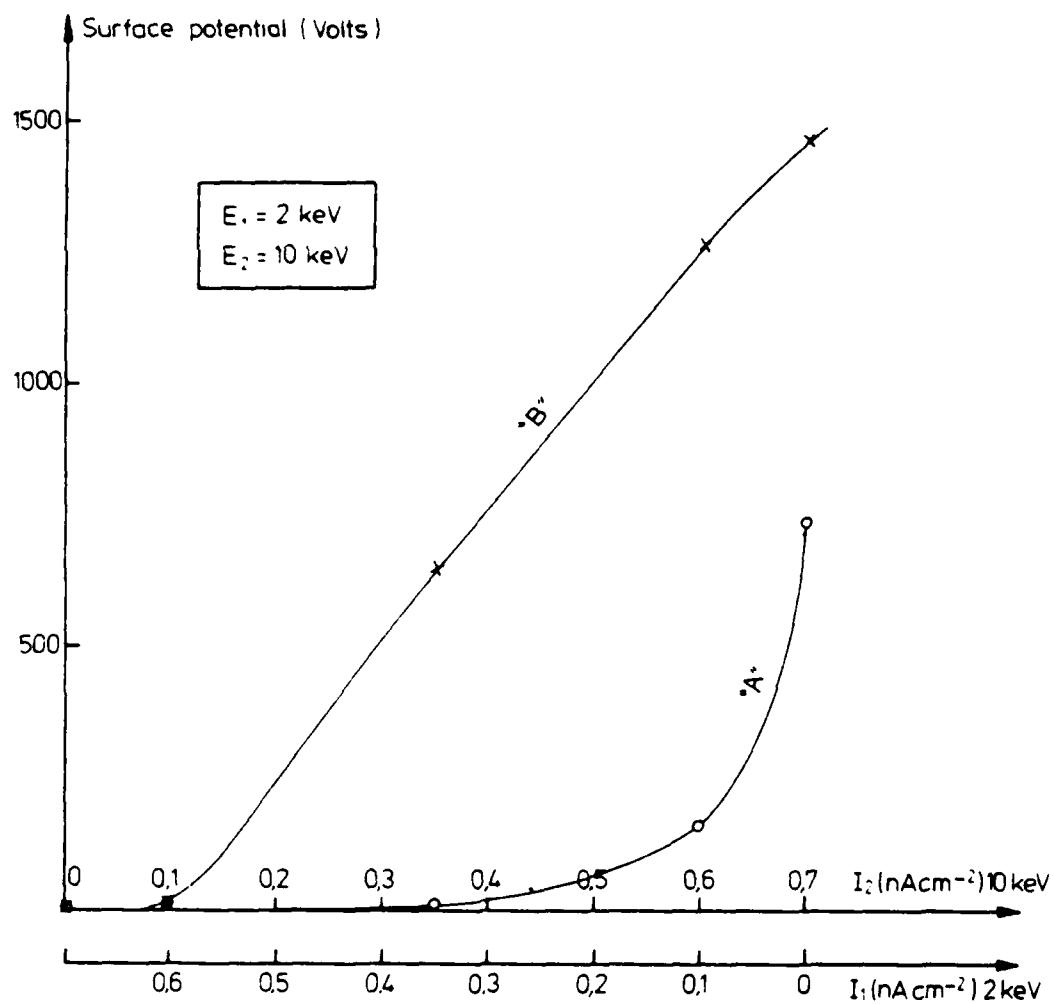
SAMPLE "B" = Aged / contaminated sample
Sample "A" = Fresh sample

FIGURE 23 – EFFECT OF CONTAMINATION AND/OR AGEING

45
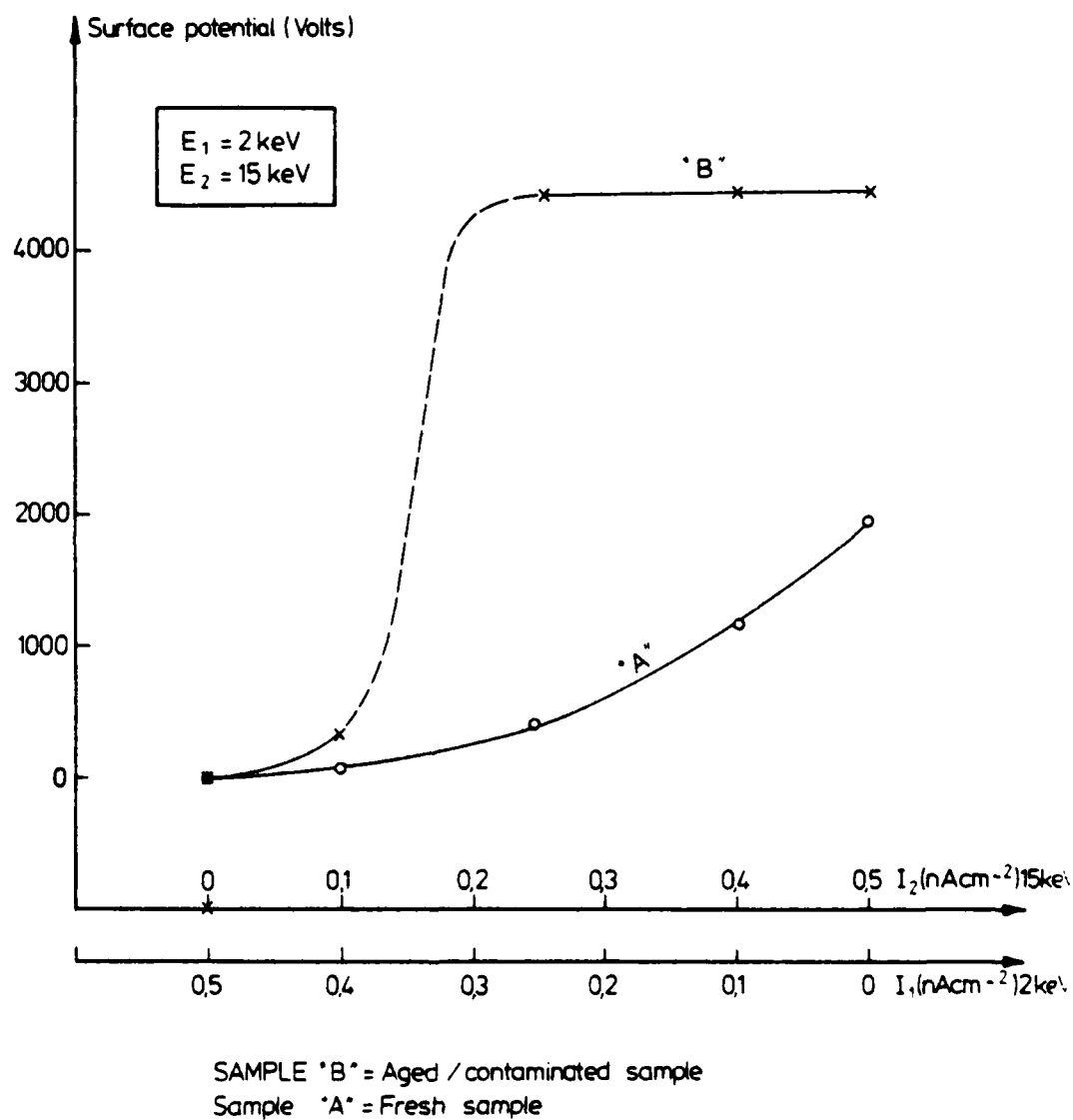
FIGURE 24 - EFFECT OF CONTAMINATION AND/OR AGEING
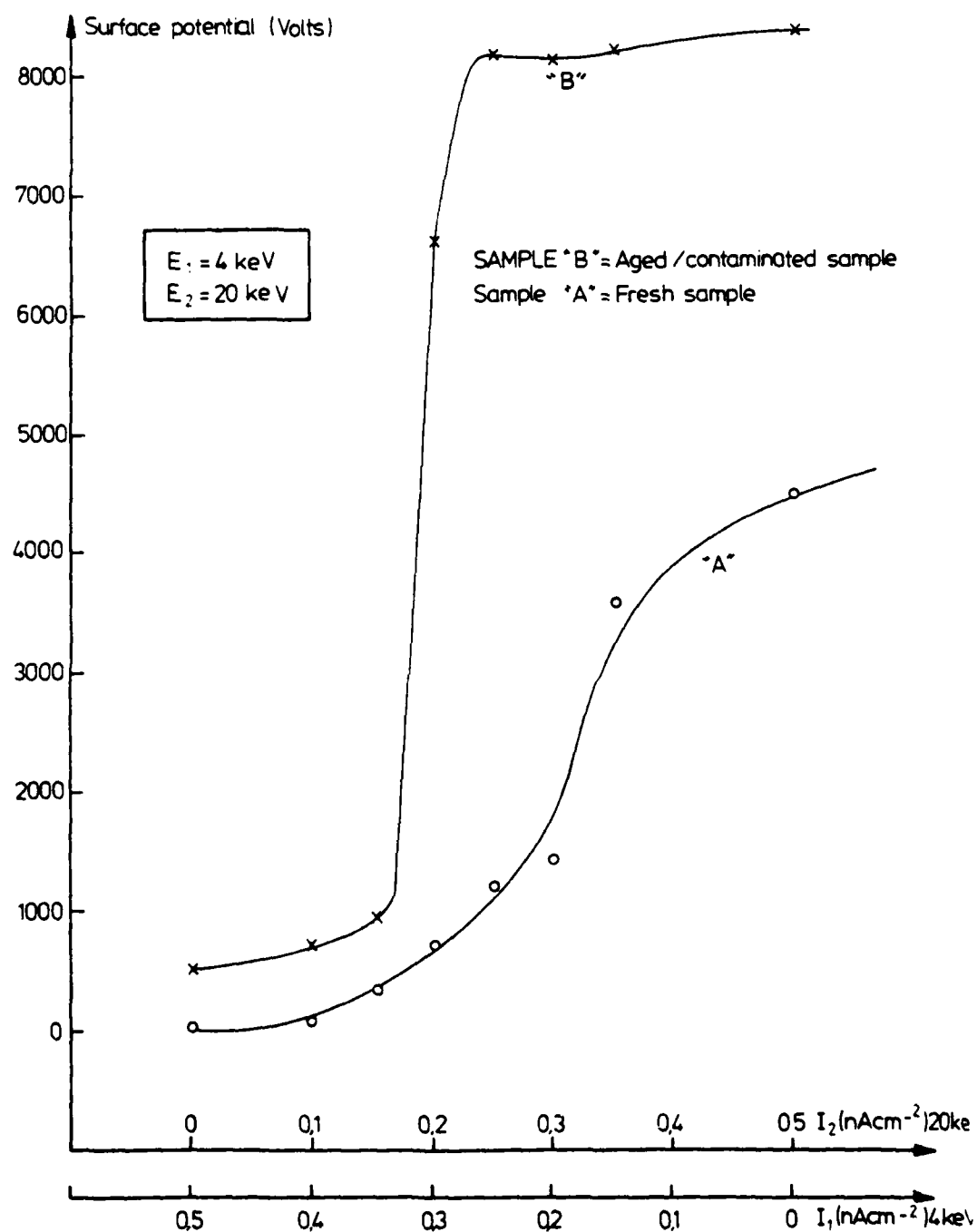
FIGURE 25 - EFFECT OF CONTAMINATION AND/OR AGEING

47

the uniformity of the 4 keV beam is bad. In its right part, the composite is receiving certainly a far less density of low energy electrons than in its left part. No scan can be made in the horizontal direction that could allow to determine whether the surface potential is higher in the right part and whether arcing can originate from this area.

The low energy component decreases also the electric charge of the contaminated sample (sample D) under electron beam but its efficiency is far less than with an uncontaminated sample (sample B) : see Fig. 23, 24, 25.

2.4.5   CONCLUSION

The electrostatic tests that are performed usually on silica fabrics and composites (Ref. 1, 2, 3) appear to be pessimistic when they are carried out with quasi-monoenergetic beams at rather high energies (10 to 20 keV). In space, wide distribution of energies including electrons in the range 1 to 5 keV are always observed. They tend to lessen the surface potentials that could be inferred from laboratory tests with monoenergetic beams on materials for which the secondary emission conductivity is the principal charge dissipation mechanism.

On the other hand, a degradation of the electrostatic properties of silica fabrics and composites is observed as consequence of contamination and/or long term irradiation.

3. EFFECT OF CONTAMINANT LAYERS ON CHARGING PERFORMANCE.

3 - 1   BACKGROUND

It has been reported in Ref. 3 (Section 3524-1) and in this very document (Sections 213 and 2331), that surface potentials are increasing when successive irradiations under vacuum are performed on quartz fabrics and composites. This behaviour could be a consequence of a contamination layer build-up on the sample surface, but it could be also a pure long term irradiation effect (ageing).

A detailed investigation was decided in order to assess the importance of contamination phenomena for the electrostatic behaviour.

As a first step, a contaminant layer was deposited ex-situ on the quartz fabric side of a composite and on the ITO layer of a conductive Kapton SSM. The electrostatic behaviour of these contaminated samples was compared to the one of clean samples.

In a second step, a comparative study has been performed *in identical conditions on a fabric sample receiving a long irra-*diation and also on a non irradiated sample in the same vacuum environment ; the test procedure was chosen to operate either in clean vacuum conditions or in controlled contamination conditions.

3 - 2   EX-SITU CONTAMINATION OF SAMPLES (SILICA FABRICS AND CONDUCTIVE SSM)

3.2.1   Facility

The test facility has been described in Section 3.2 of Ref. 3. However in order to allow a better control of experimental conditions a cryogenic shroud that fits the CEDRE chamber was designed and manufactured. This liquid nitrogen shroud surrounds the sample holder and all the functional equipments as sketched in FIGURE 26. It supresses the parasitic contamination by the turbomolecular pumping system used in the chamber.

49
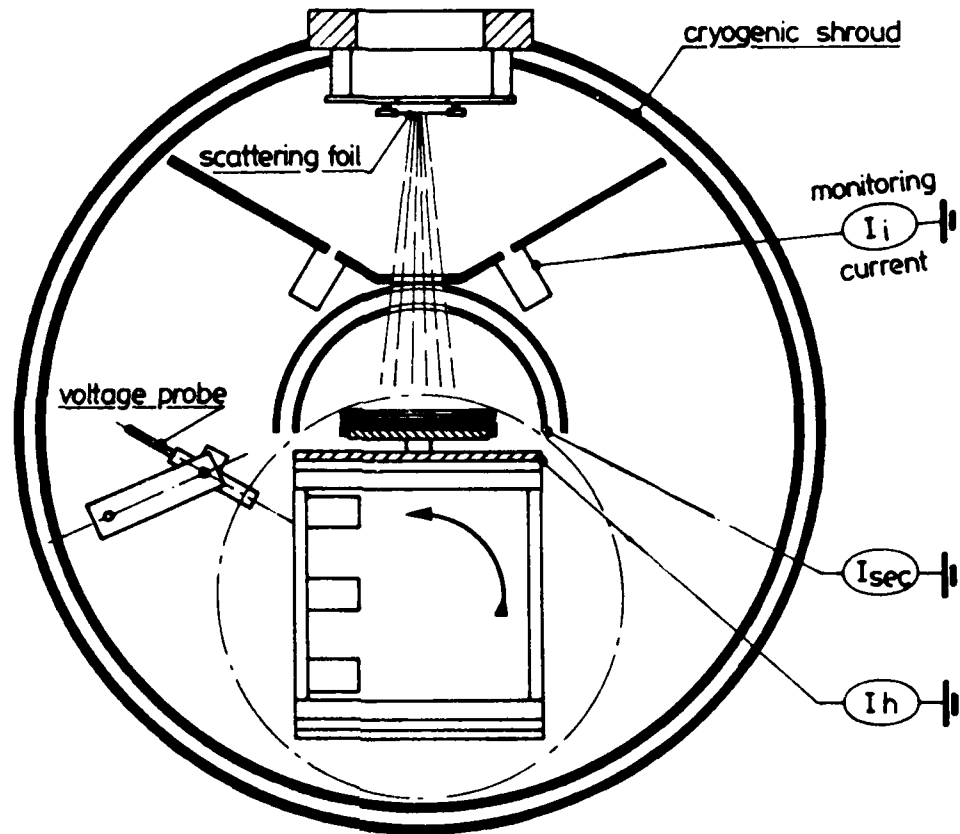
FIGURE 26 - CEDRE SUBSTORM SIMULATION FACILITY
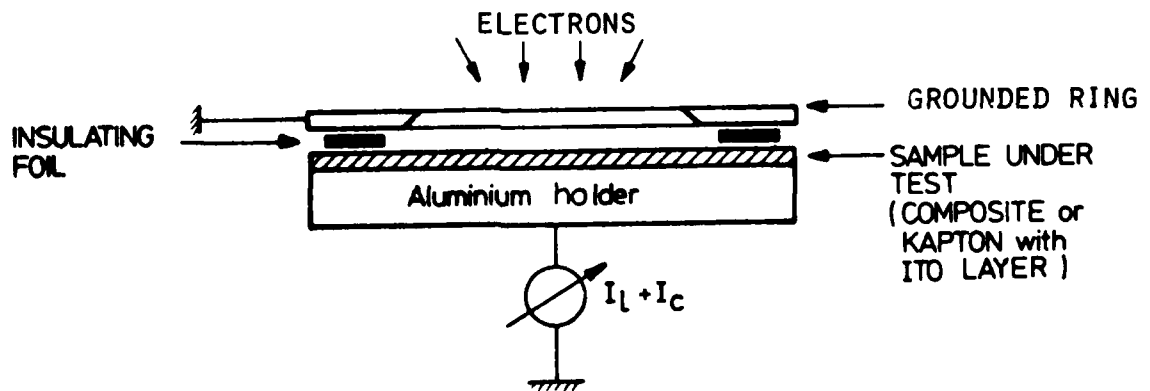
FIGURE 27 - SAMPLE SETTING

3.2.2   Samples

The samples under test are mounted on the sample holder as shown in FIGURE 27 [(*)].

Two types of samples were studies : (a) ITO/Kapton/Al. This ITO coated SSM was provided by AFML/MBE with label 838 K.3 (b) Silica fabric/FEP/Alu. This composite is the same as described at Section 2122.

These two materials were contaminated, ex-situ, with a mixture of three components that are thought to be representative of products outgassed in a large chamber for instance during thermal vacuum tests. The composition of this mixture is the following: 30% turbomolecular pump oil Leybold (ester) ; 30% turbomolecular pump oil Shell Z (hydrocarbon) ; 40% diffusion pump oil DC 705 Dow Corning (Silicone).

In order to contaminate the samples, 10 mg of the mixture were dissolved in ethylether and poured on the sample surface (30 cm^2). The deposit was not uniform as it was evidenced by visual inspection of the contaminated ITO/Kapton/Alu. If it were uniform, the contaminant thickness obtained by such a method would be 2μm.

3.2.3   Procedure

Two series of test were carried out:

(a)   In the first series the samples without contaminant layer were characterized under electron beam as described in Section 324 of Ref. 3. Four energy levels were used: 5, 10, 15, 20 keV with respective intensities 1.25, 0.7, 0.5 and 0.5 nA cm^{-2}. For each energy, the irradiation was stopped and the surface potential was measured after fixed times of irradiation: 0.5, 1, 2, 5 and 10 minutes. The sample-to- holder leakage + charging current (called $I_L + I_C$) and the secondary emission current (I_{sec}) were recorded versus time. For all the test, the cryogenic shroud inside the chamber was filled with liquid nitrogen. Accordingly the sample

---

(*) The ITO layer of the ITO/Kapton/Al was proved to be electrically connected to the rear aluminum layer after the sample was cutted out. Accordingly it was not useful to ground the ITO layer by an other means.

temperature varied with time and it was necessary to measure its value with a thermistor.

(b)   In the second series the contaminated samples were characterized in the same conditions.

3-2-4 Results

FIGURES 28 to 31 (for the ITO/Kapton/Alu sample) and 32 to 35 (for the quartz fabric/FEP/Alu sample) show the variation of the surface potential (if not equal to zero), of the sample-to-holder leakage current $I_L + I_C$, and of the secondary current, I_{sec}, in terms of irradiation time, and for the respective energy levels : 5, 10, 15 and 20 keV. (*)

For the ITO Kapton/Alu sample, FIGURES 28 to 31 a and b show that the presence of a 2 μm thick contaminant layer over the conductive ITO increases the leakage current $I_L + I_C$, and decreases the secondary current, I_{sec}. However, the surface potentials (not shown because continuously equal to zero) are not affected by contamination.

This is not the case for the contaminated composite: FIGURES 32a to 35a clearly exhibit an increase, (even if moderate), of the surface potential values (as a consequence of the contamination). This is correlated with an increase in the leakage current $I_L + I_C$ (FIGURES 32b to 35b), and with a decrease in the secondary current I_{sec} (FIGURES 32c to 35c).

As a general remark (for the ITO coated SSM as well as for the composite), it is worth noting that the $I_L + I_C$ increase seems to be larger than the correlated decrease in I_{sec} that is measured as a consequence of contamination (**).

(*) In these figures the measured sample temperature is reported

(**) However the constancy in the sum of the various currents cannot be verified since all the other current components (for instance I_g, I_{surf}, I_f, as described at Section 3.2.3 of Ref. 3) are not recorded in the experiments we are reporting here.

These variations of the recorded currents are particularly important for the 5 keV irradiations reported in FIGURES 28 and 32, for which the secondary emission yield is strongly lowered in consequence of contamination.

However the moderate increase of the surface potentials of the contaminated composite must be emphasized with regard to the relatively higher surface potential variations exhibited after the long lasting irradiation tests that have been reported earlier (Sections 213 and 2331).

TABLE 2 gives the surface potential measurement in Volts after 15 minutes irradiation time that is to say at quasi steady state after the ageing test and the contamination test that have been carried out with the composite sample.

In TABLE 2, the contamination effect (5 keV excepted) seems to be less important than the surface potential variations observed after the ageing test.

It is worth noting that, at 5 keV, the surface potential is zero due to a quasi-total reemission of the incident irradiation current (see FIGURE 29 and Section 3521-1 a of Ref. 3). So, at 5 keV, secondary emission as measured by an hemispheric collecting electrode. is the only way by which the composite evacuates the incident incoming electrons (see FIGURE 29 of Ref. 3). A decrease in the secondary emission yield at 5 keV is consistent with the occurrence of a low detectable potential on a contaminated composite (see FIGURE 24a). At 10, 15 and 20 keV, the recorded contamination effects can very well be explained as a consequence of the lowering of the secondary emission yield, leading to higher surface potentials and higher sample-to-holder leakage currents $I_L + I_C$.
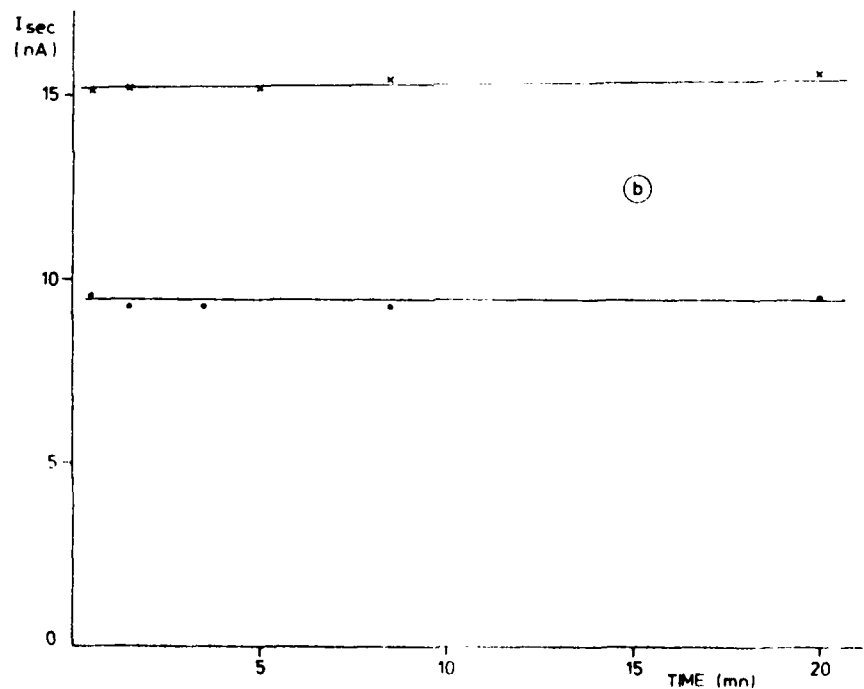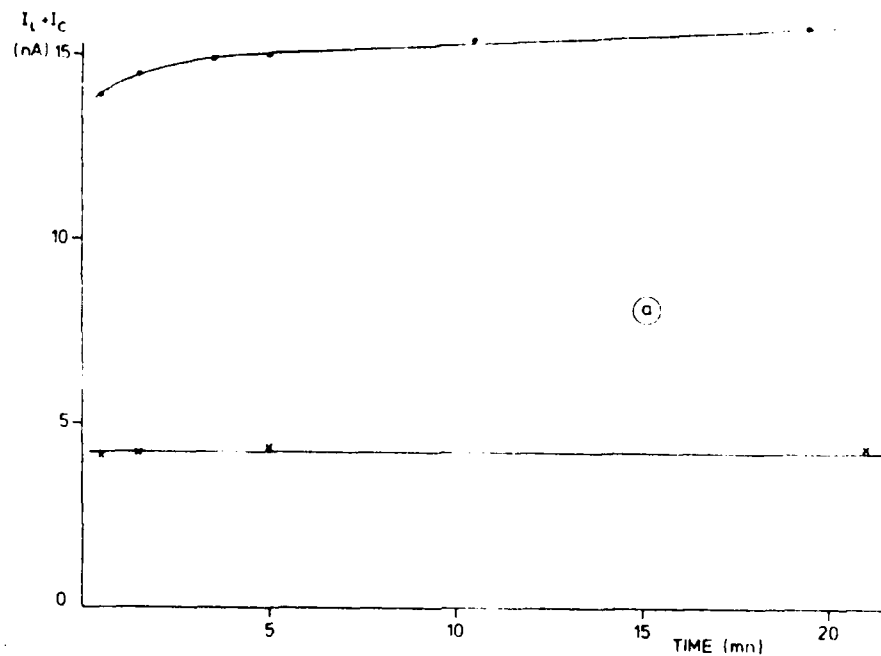
• CONTAMINATED

x NON CONTAMINATED

$4 < T(°C) < 7$

FIGURE 28 - CONTAMINATION EFFECT ON ITO-COATED KAPTON SSM BEHAVIOUR AT 5 keV/1.25 NA CM^{-2}
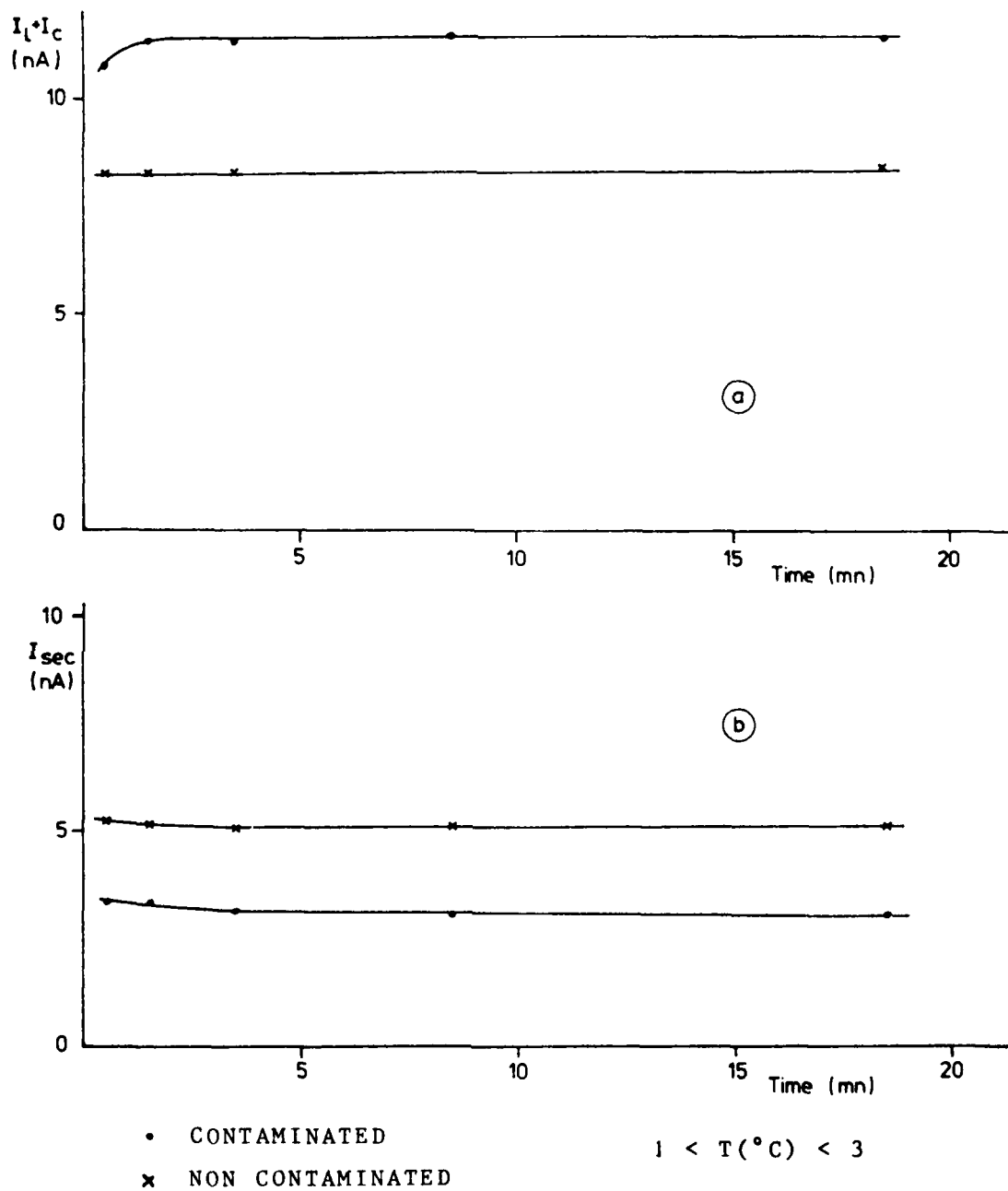
FIGURE 29 - CONTAMINATION EFFECT ON ITO COATED KAPTON
SSM BEHAVIOUR AT 10 keV/0,7 nA cm^{-2}
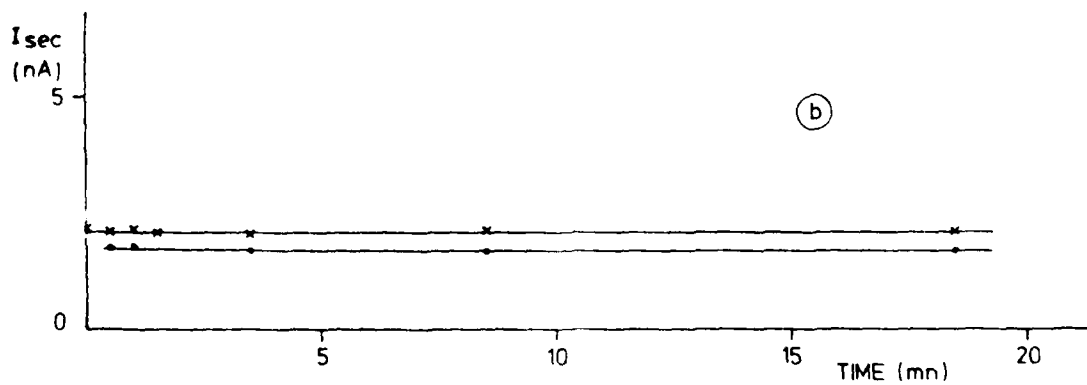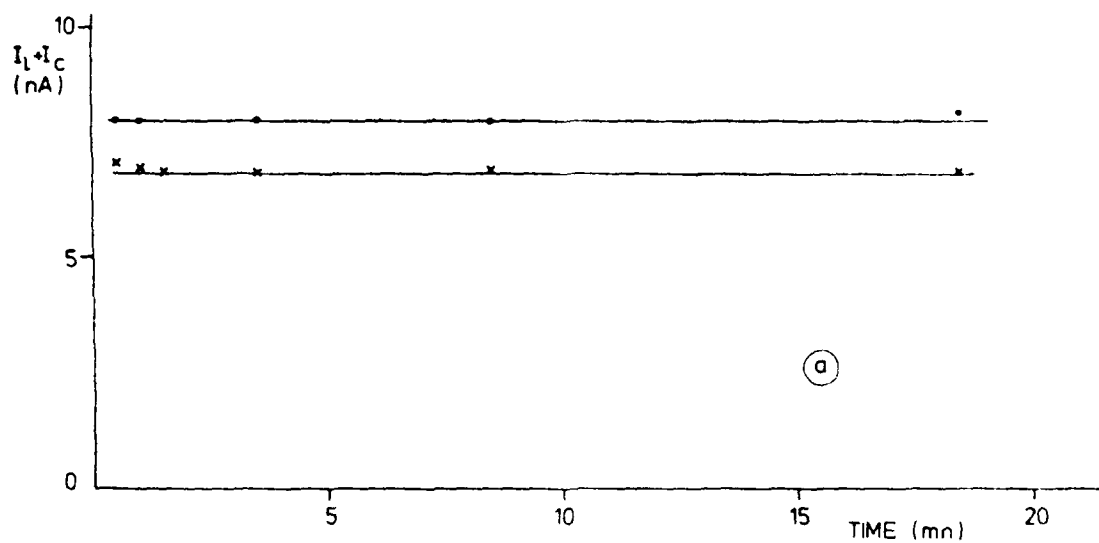
FIGURE 30 – CONTAMINATION EFFECT ON ITO-COATED KAPTON
SSM BEHAVIOUR AT 15 KEV/0.5 NA CM^{-2}
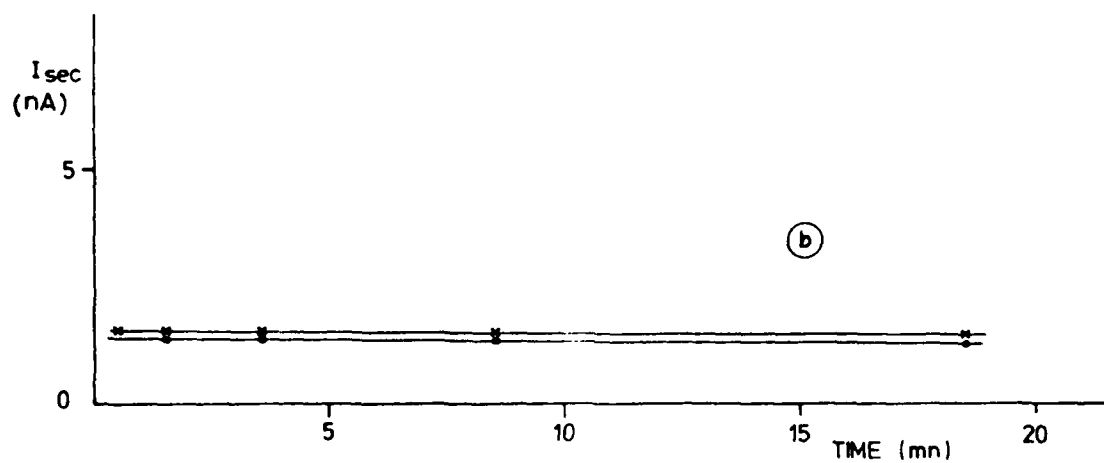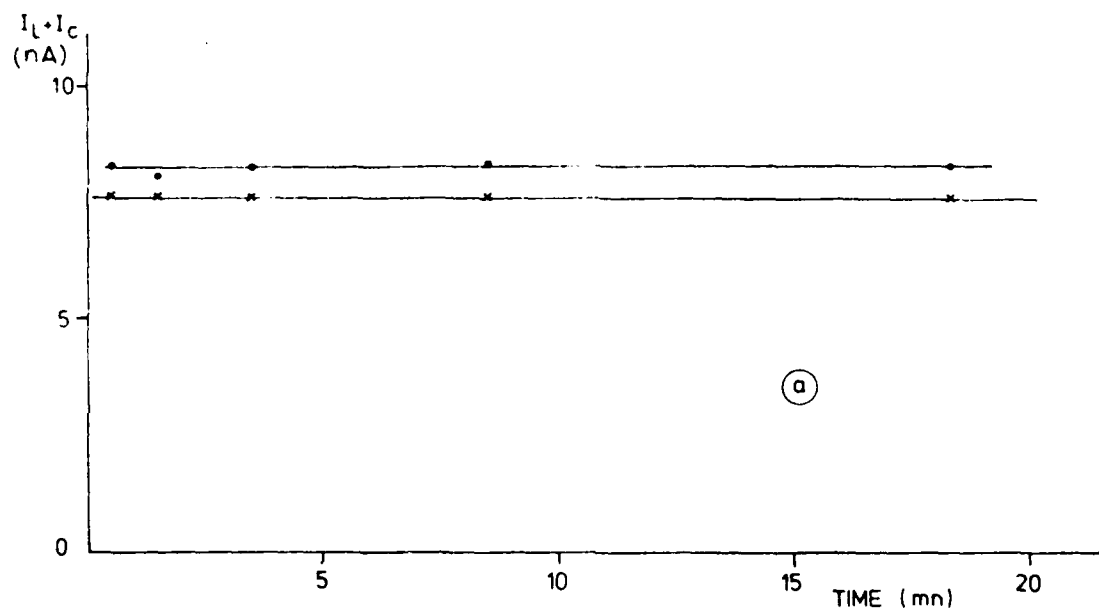
CONTAMINATED
NON CONTAMINATED

$- 10 < T(°C) < - 8$

FIGURE 31 - CONTAMINATION EFFECT ON ITO-COATED KAPTON SSM BEHAVIOUR AT 20 KEV/0,5 NA CM^{-2}
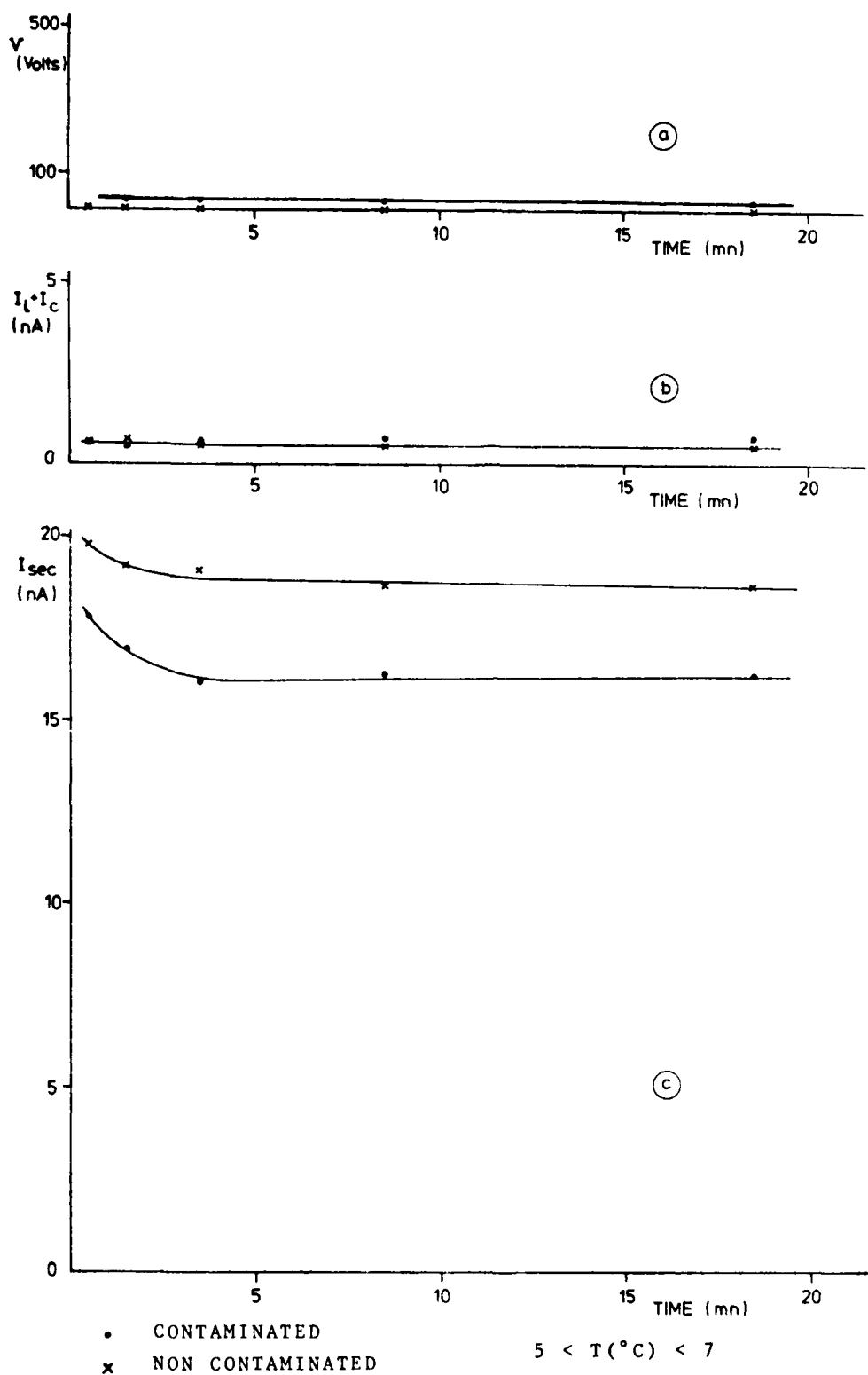
FIGURE 32 -- CONTAMINATION EFFECT ON ELECTROSTATIC BEHAVIOUR OF COMPOSITE AT 5 KEV/1.25 NA CM^{-2}
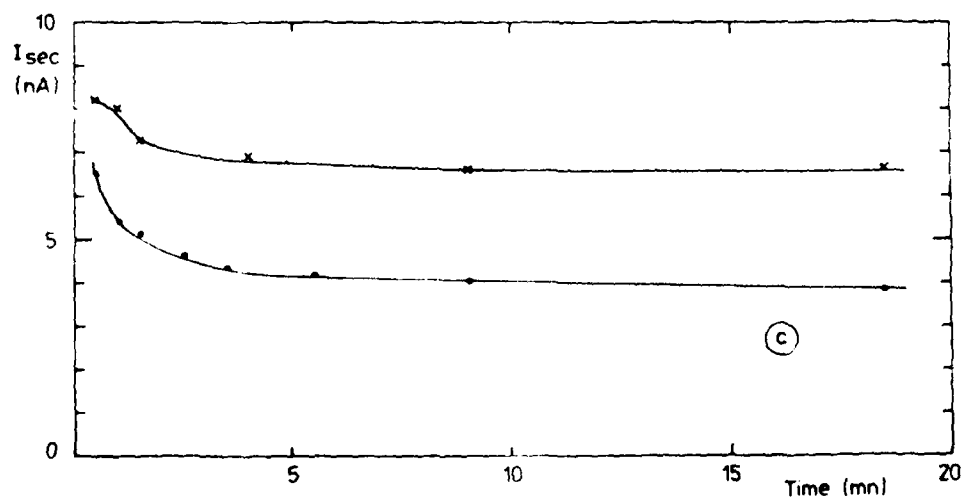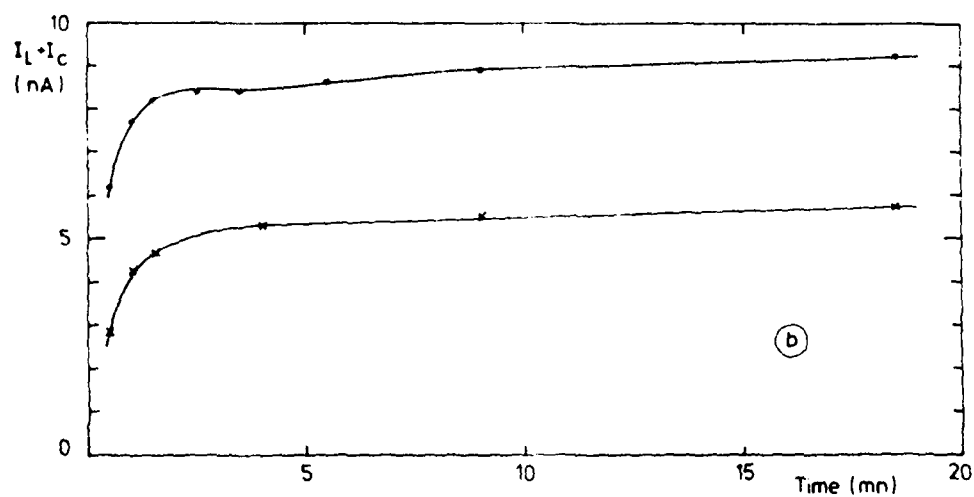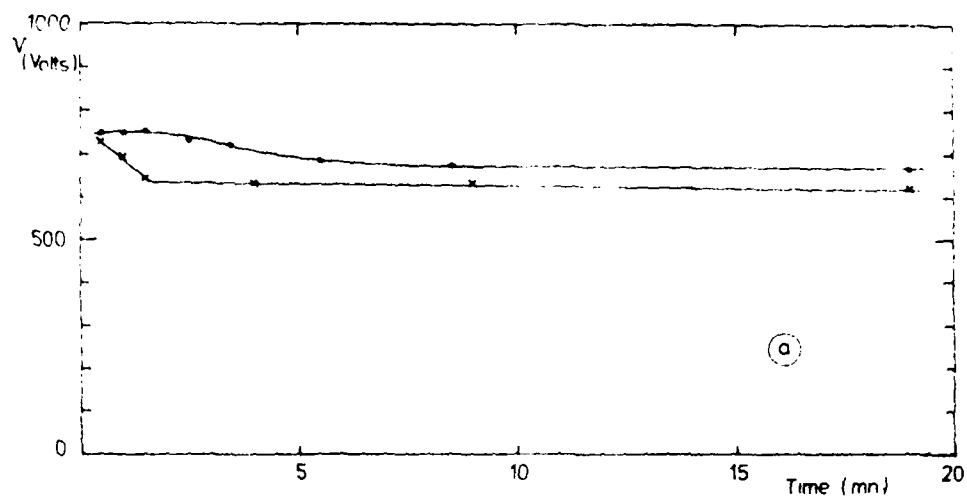
• CONTAMINATED $0 < T(°C) < 2$

× NON CONTAMINATED

FIGURE 33 – CONTAMINATION EFFECT ON ELECTROSTATIC BEHAVIOUR OF COMPOSITE AT 10 KEV/0.5 NA CM^{-2}
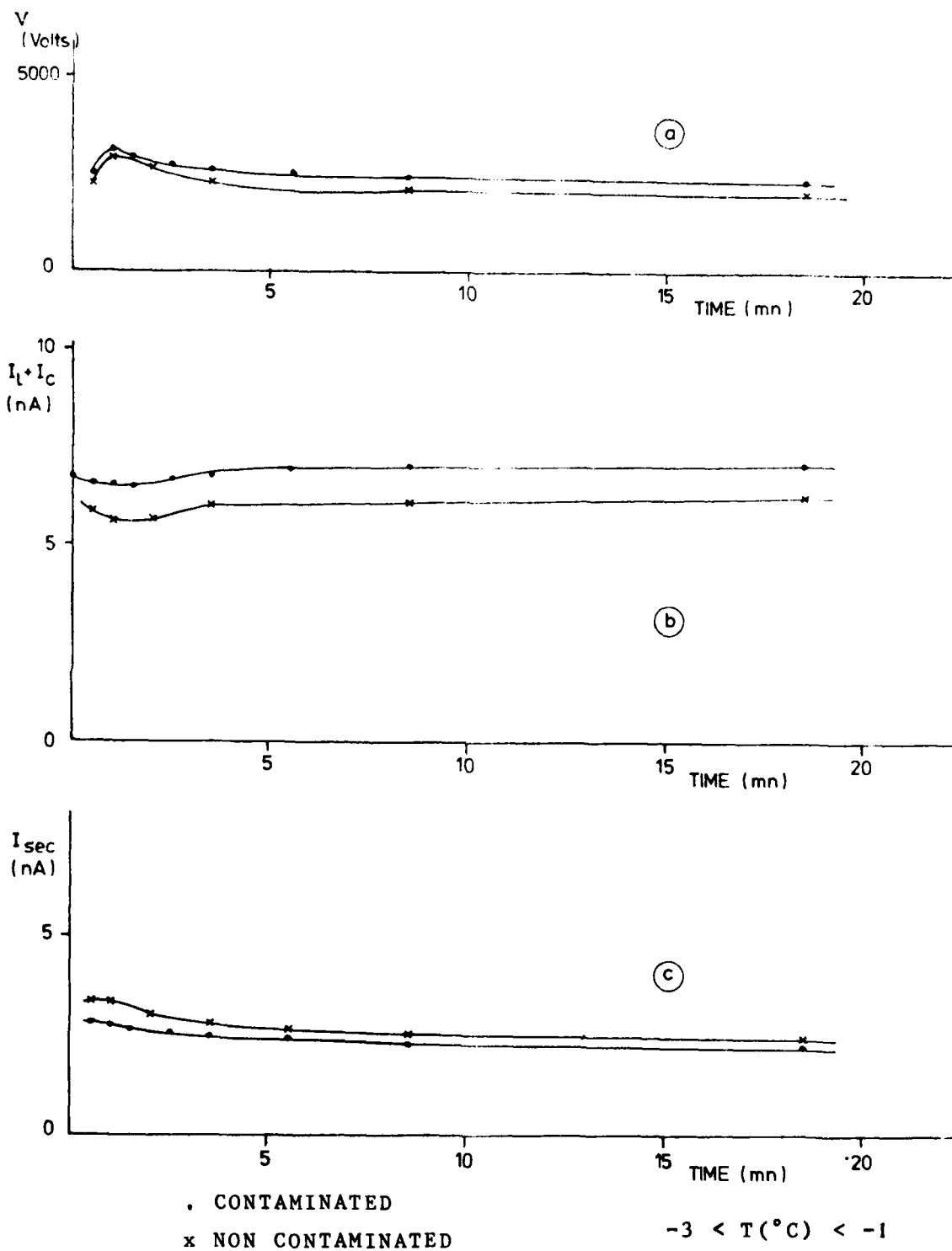
FIGURE 34 - CONTAMINATION EFFECT ON THE ELECTROSTATIC
BEHAVIOUR OF COMPOSITE AT 15 KEV/0.5 NA CM^{-2}

. CONTAMINATED

x NON CONTAMINATED

$-3 < T(°C) < -1$
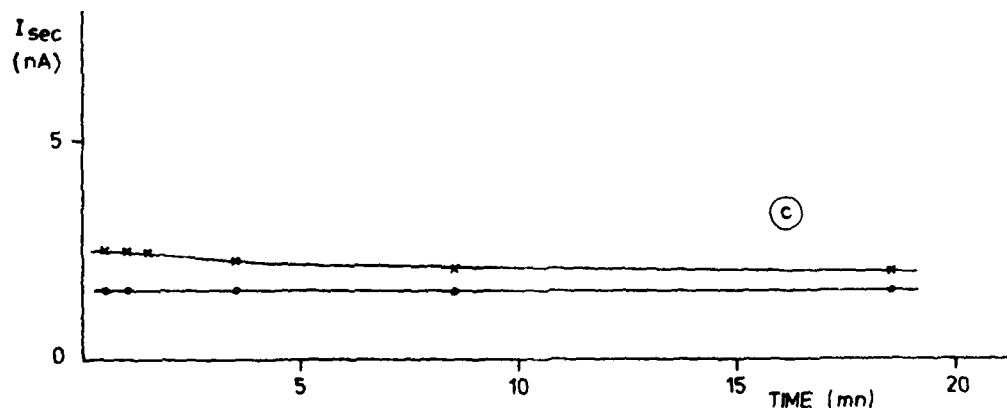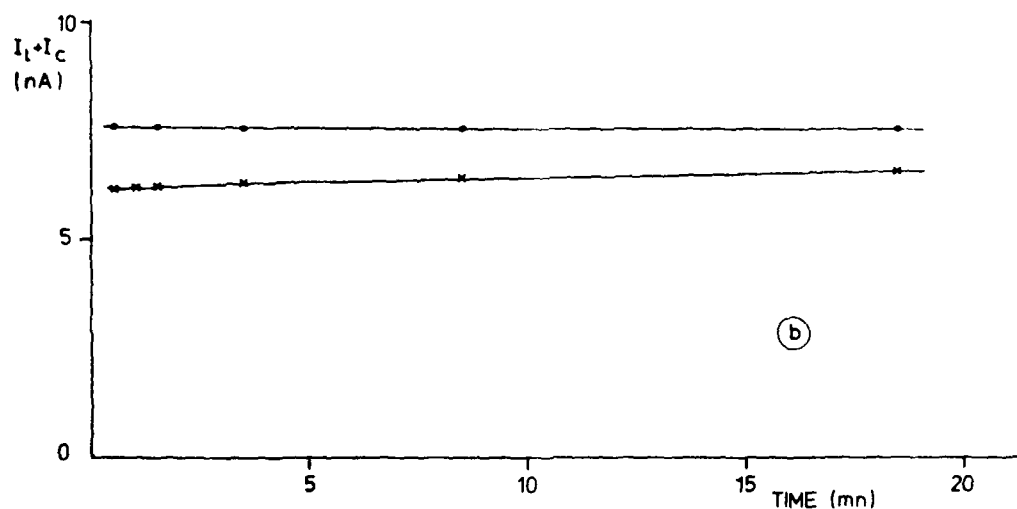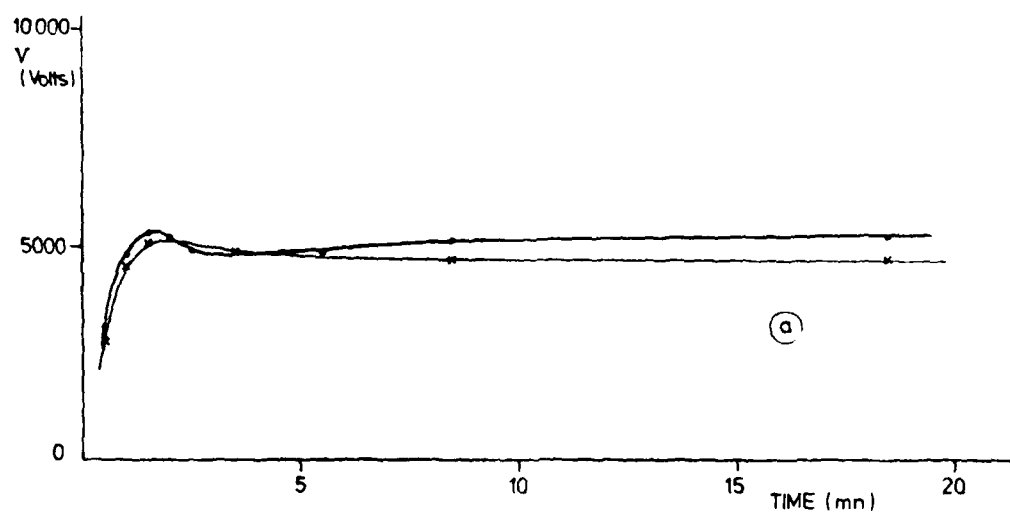
FIGURE 35 – CONTAMINATION EFFECT ON ELECTROSTATIC BEHAVIOUR
COMPOSITE AT 20 keV/0,5 nA cm^{-2}

TABLE 2 SURFACE POTENTIAL AT STEADY STATE UNDER ELECTRON IRRADIATION FOR
THE COMPOSITE SAMPLE.

TEST NATURE	ELECTRON ENERGY (keV)	FLUX RATE ($nA\ cm^{-2}$)	SURFACE POTENTIAL (VOLTS)		SURFACE POTENTIAL VARIATION (VOLTS)
			BEFORE TEST	AFTER TEST	
AGEING TEST	5	0.5	$\simeq 0$	$\simeq 0$	$\simeq 0$
	10	0.5	550	1025	475
	15	0.5	2200	3300	1100
	20	0.5	4700	6000	1300
CONTAMINA-TION TEST	5	1.25	$\simeq 0$	20 to 30	20 to 30
	10	0.7	620	670	50
	15	0.5	2050	2400	350
	20	0.5	4650	5200	550

62

3.2.5.   Conclusions

Results that have been obtained for samples the surface
of which had been contaminated with a 2 μm thick layer can be
summarized as follows:

- for the ITO/Kapton/Al SSM as well as for the composite, a
  lowering of the secondary emission yield and an increase
  in the sample-to-holder leakage current are observed for
  the contaminated samples, in every case

- for the ITO/Kapton/Al SSM, no measurable surface potential
  variation can be correlated with this decrease in the
  secondary emission

- for the composite, a systematic increase in the steady state
  surface potential value is measured as a consequence of the
  contamination.

  This increase of the steady state surface potential value
  is lower (excepted at 5 keV) than the one induced by the
  long lasting irradiation tests that have been mentioned
  earlier (Sections 2.1.3 and 2.3.3).

3 - 3   CONTAMINATION AND/OR AGEING OF SILICA FABRICS

3.3.1   Purpose of the experiments

After the experiment we have reported just above, a question remained that necessitated further studies: is there a pure long irradiation ageing effect   or did we induce a combined contamination/ageing effect when performing the ageing test without cryogenic shroud.

The experiments we are going to describe below were undertaken in order to distinguish the contamination effect from this possible pure radiation effect. For these experiments a comparative study has been performed, in identical conditions, on a sample receiving a long irradiation and also on a non irradiated sample, in the same vacuum environment. The test procedure was chosen to operate, in a first step, with very clean vacuum conditions, and in a second step with controlled contamination conditions.

3.3.2   Experimental set up and procedure

3321   *facility*

The test facility is the same as the one used in the experiments described at Section 3.2.1

3322   *samples*

Two identical composite specimen (A and C) were set onto two opposite sides of the sample holder. Each was mounted as sketched in FIGURE 27. The composite material silica fabric/FEP/aluminum has been described at Section 2122. Samples A and C had never been irradiated nor exposed to vacuum before the test.

The procedure is described in FIGURE 36.

- In a first phase, sample A, the temperature of which was approximateley - 30°C, has been irradiated in "clean" vacuum conditions (that is to say with the cryogenic shroud filled with liquid nitrogen) for 16 hours with 20 keV electrons at 3 nA cm^{-2}, while sample C has been maintained without irradiation $^{(*)}$ in identical vacuum conditions. The electrostatic behaviour of samples A and C (surface potential and current components under electron beam $^{(**)}$) after this irradiation has been compared with the one before irradiation.

- In a second phase, the liquid nitrogen has been removed from the cryogenic shroud. Accordingly, the products that had been cryocondensed on the shroud, have reevaporated and have been spread every where in the chamber. A sample contamination is expected as a consequence of this dissemination.

- In a third phase, after another electrostatic characterisation for both samples A and C, sample A the temperature of which was about +15°C has received a second irradiation with 20 keV electrons at 3 nA cm^{-2} for 16 hours while sample C has been maintained

---

(*)   except for the electrostatic characterization, see below

(**)   For the electrostatic characterization under electron beam, see Section 324 of Ref. 3. Four energy levels were used: 5, 10, 15, 20 keV with respective intensities 1.25, 0.7, 0.5 and 0.5 nA cm^{-2}. For each energy step the surface potential was measured contactless with a voltage probe after fixed irradiation times 0.5, 1, 2, 5 and 10 minutes. The sample-to-holder current $I_L + I_C$ and the secondary emission current (I_{sec}) were recorded versus time. The sample temperature was monitored during the measurements.

The sample charge after irradiation at high energy is removed (or decreased at a value less than some ten volts) by irradiation with a 5 keV beam, before the electrostatic characterization is made.
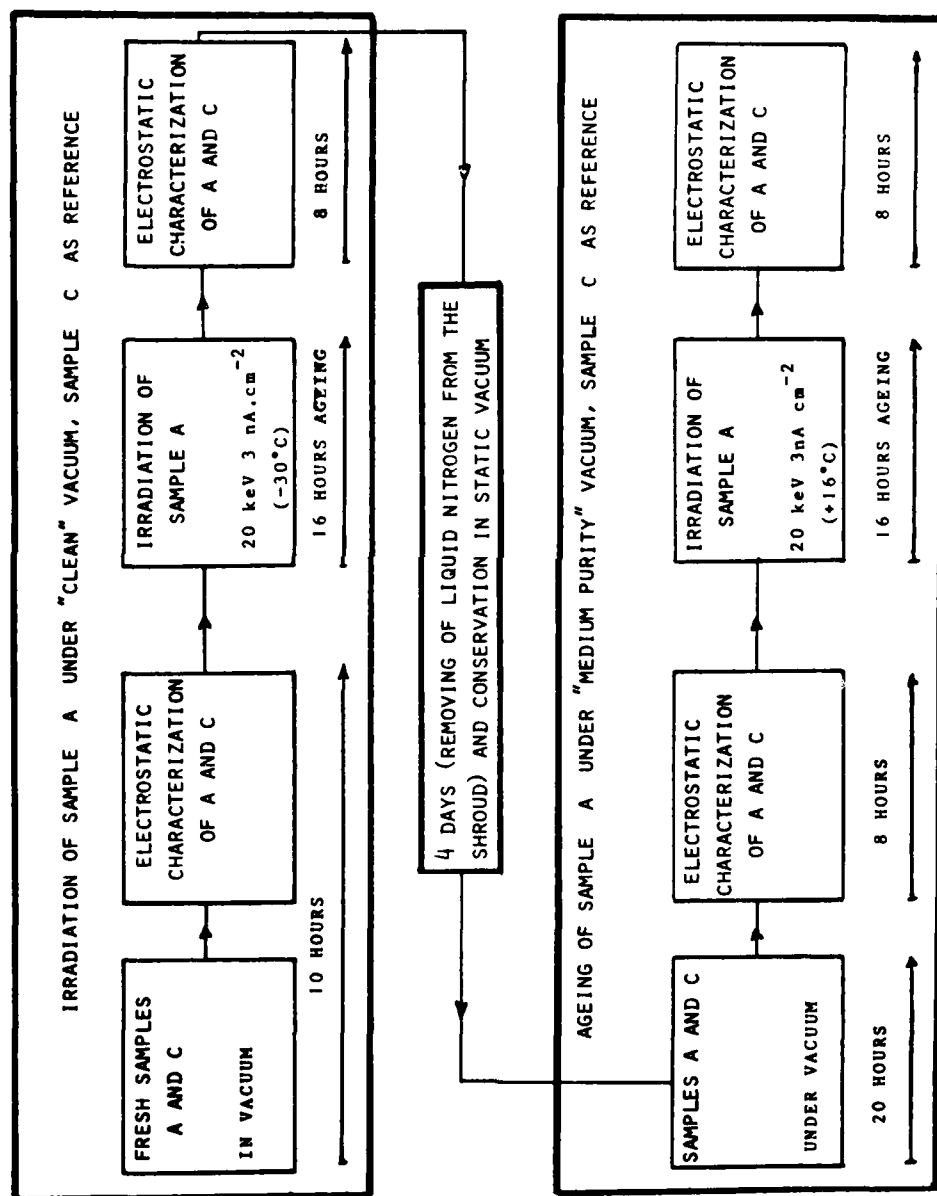
FIGURE 36 - TEST PROCEDURE

in identical vacuum conditions, that is to say turbomolecular pumping without cryogenic shroud. At the end of this latter irradiation, an electrostatic characterization has been performed again for both samples A and C.

For the irradiation period,as well as for the electrostatic characterisation, the sample-to-holder current $(I_L + I_C)$ and the secondary emission current (I_{sec}) have been recorded simultaneously, together with the irradiation monitoring current. This monitoring current is used to eliminate parasitic effects in I_L and I_{sec} of the beam instabilities.

TABLE 3 - ELECTROSTATIC BEHAVIOUR AFTER BOTH TESTS

BEAM ENERGY (keV)	TEST CONDITIONS	SAMPLE C (NO LONG IRRADIATION)					SAMPLE A IRRADIATED				
		BEFORE TEST		AFTER TEST		SURFACE POTENTIAL INCREASE (V)	BEFORE TEST		AFTER TEST		SURFACE POTENTIAL VARIATION (V)
		TEMPERATURE (°C)	SURFACE POTENTIAL (V)	TEMPERATURE (°C)	SURFACE POTENTIAL (V)		TEMPERATURE (°C)	SURFACE POTENTIAL (V)	TEMPERATURE (°C)	SURFACE POTENTIAL (V)	
5keV	with cryogenic shroud	7	0	-33	120*	120*	3,5	0	-33	430*	430*
	without cryogenic shroud	16	50*	16	100*	50*	15	30	16	350*	320*
10keV	with cryogenic shroud	1	880	-33	1110	230	0	660	-33	990	330
	without cryogenic shroud	16	940	16	1380	440	16	850	16	1400	550
15keV	with cryogenic shroud	-4	2587	-33	2887	300	-6	1690	-33	2340	650
	without cryogenic shroud	16	3100	16	3140	40	16	3030	16	4950	1920
20keV	with cryogenic shroud	-10	5775	-33	5890	115	-10,5	3740	-33	4240	500
	without cryogenic shroud	16	7200**	16	7200**	0	16	6260**	16	7600**	1380

* large measurement incertainty due to an incomplete discharge of the sample after a previous 20 keV irradiation

** unstable measurement due to breakdowns

3.3.3 Results

Although all the current components have been measured during the various electrostatic characterization periods, only the surface potential values at steady state are reported here (TABLE 3) for the sake of simplification.

There is a rather large uncertainty in the potential values that have been measured under a 5 keV electron beam. This is due to the fact that this electrostatic characterization at 5 keV is usually performed after a 20 keV irradiation which leads to very high surface potentials ; the next 5 keV electron irradiation largely decreases this potential ; however it is very difficult to ascertain whether the steady state value of the potential (value given in TABLE 3) is obtained because the discharge by 5 keV electrons can last some tens of minutes, depending on the specimen.

It is worth noting that the electrostatic properties have not been recorded at the same temperature, because the sample temperature can have varied with time due to the presence of the shroud filled with liquid nitrogen. The temperature at the sample is given in TABLE 3.

The effect of the two ageing tests on the irradiated sample (A) is definitely to enhance the number of "breakdown events". These events can be put in evidence, at 20 keV only, as small pulses in the leakage current record.

FIGURES 37a,b,c, are records of the leakage and secondary currents for an electron beam at 20 keV and 0.5 nA cm^{-2} : FIGURE 37a is related to the initial characteristics of both samples A and C; FIGURE 37b is related to the characteristics of the irradiated sample (sample A) after completion of both irradiations; FIGURES 37 c gives the characteristics of the non irradiated specimen (sample C) in the same conditions.
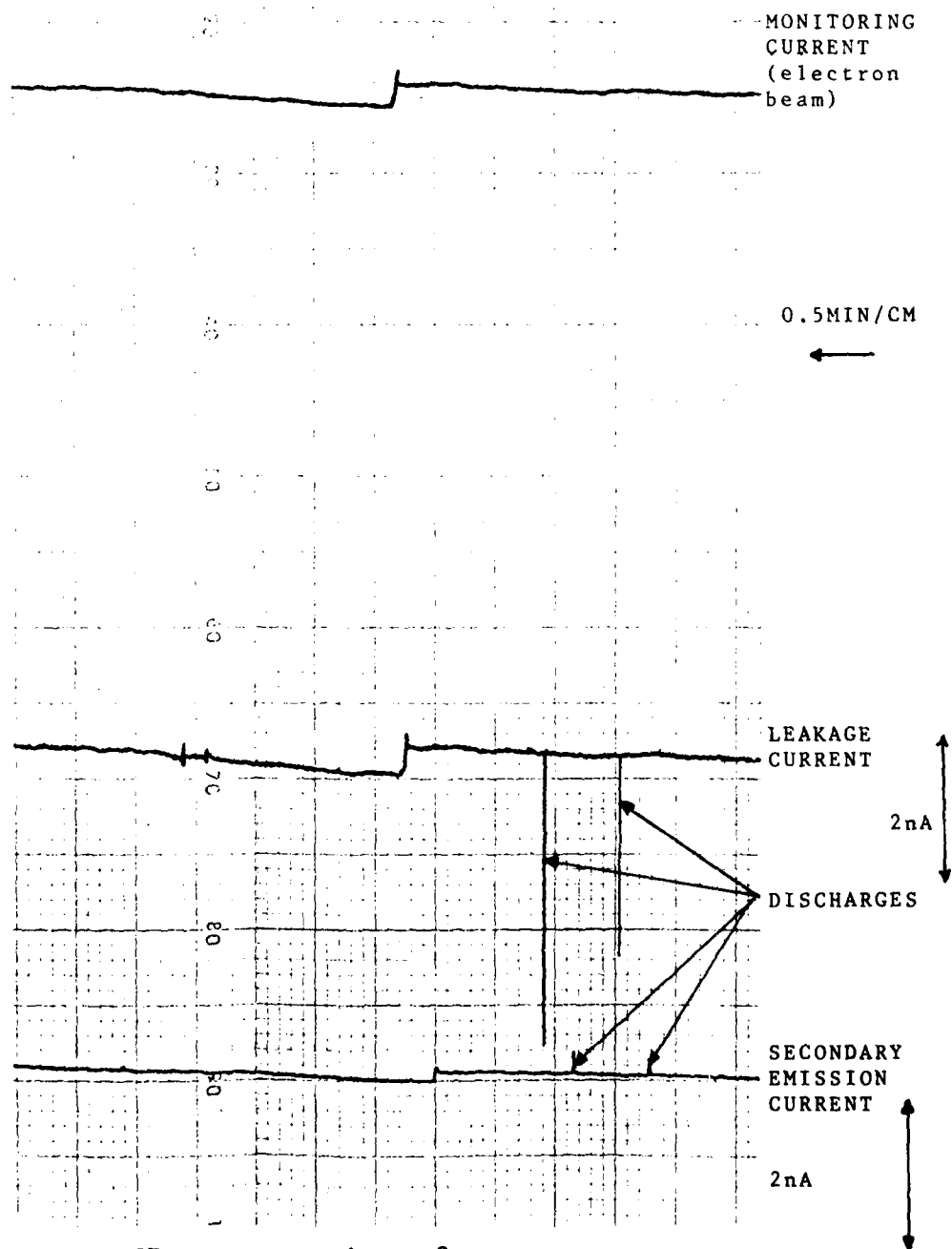
FIGURE 37A - SAMPLES A AND C. CHARACTERIZATION BEFORE
TEST 20 KEV 0.5 NA CM^{-2}

70
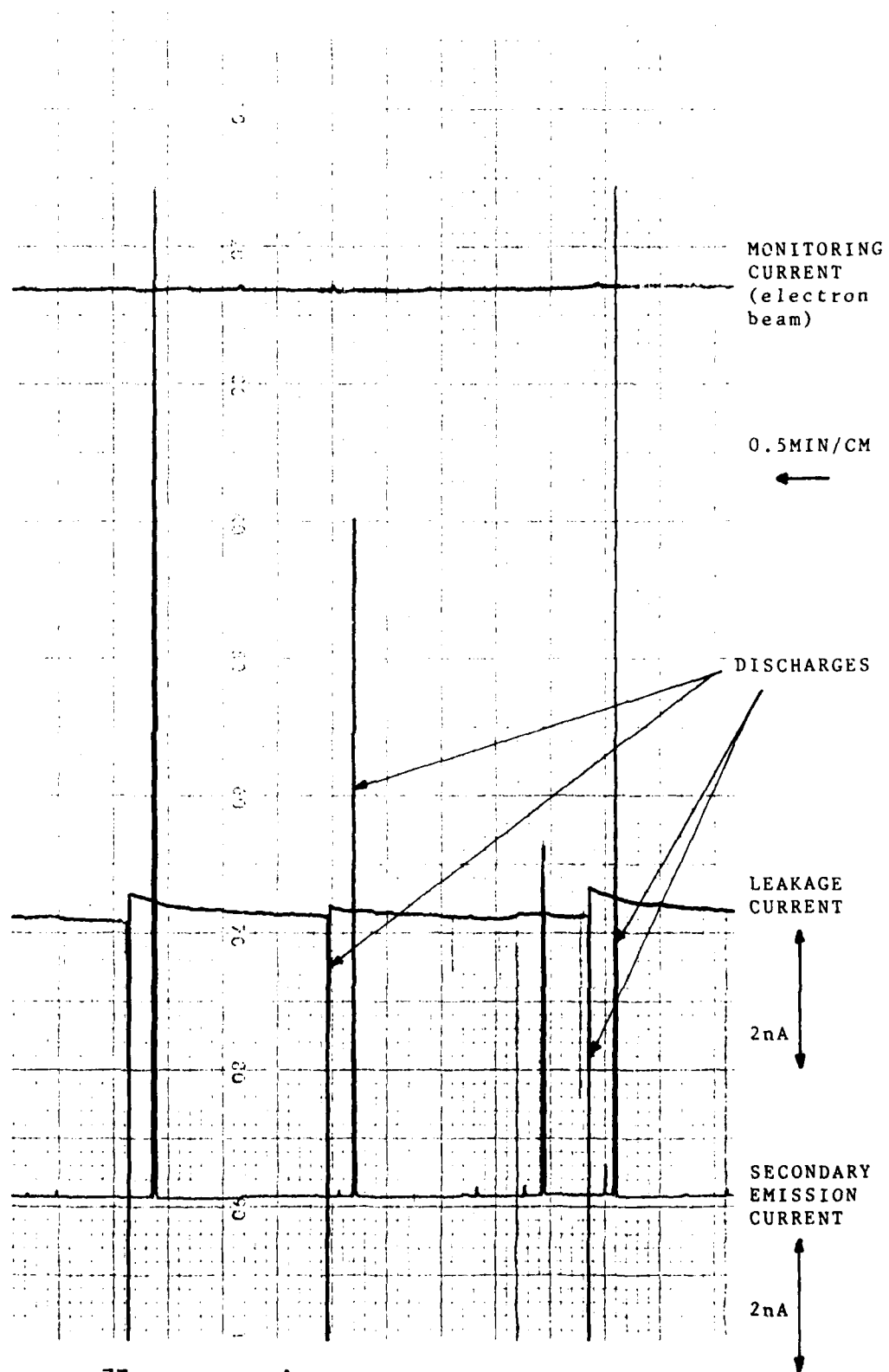
FIGURE 37B - SAMPLE A. CHARACTERIZATION AFTER TEST
20 KEV 0.5 NA CM^{-2}

71

MONITORING
CURRENT
(electron
beam)

0.5MIN/CM

⟵

DISCHARGES

LEAKAGE
CURRENT

2nA

SECONDARY
EMISSION
CURRENT

2nA
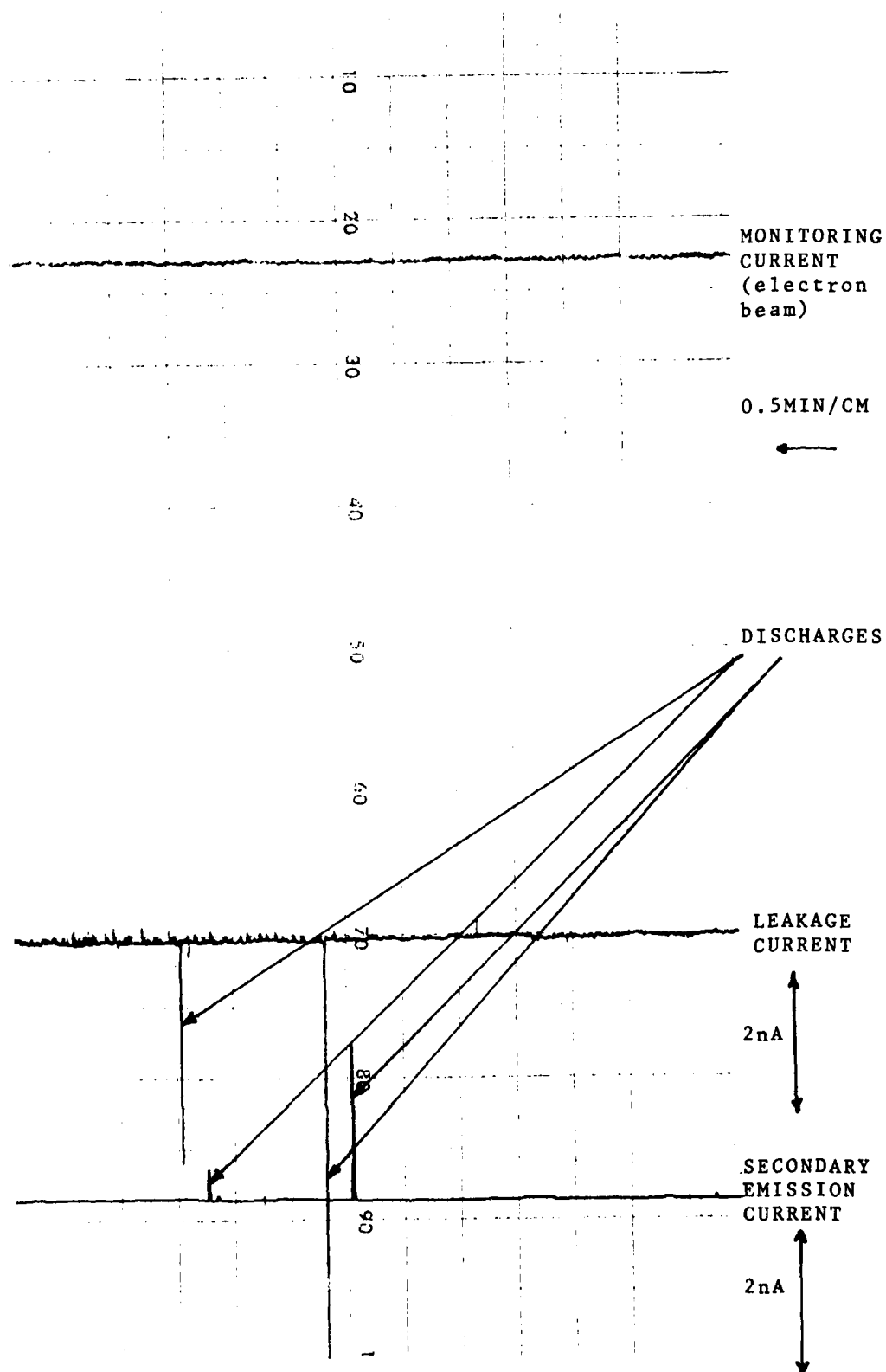
FIGURE 37c - SAMPLE C, CHARACTERIZATION AFTER TEST
20 KEV 0.5 NA CM^{-2}

72

MONITORING
CURRENT
(electron beam)

10CM/HOUR

6nA

SECONDARY
EMISSION CURRENT

LEAKAGE CURRENT

20nA
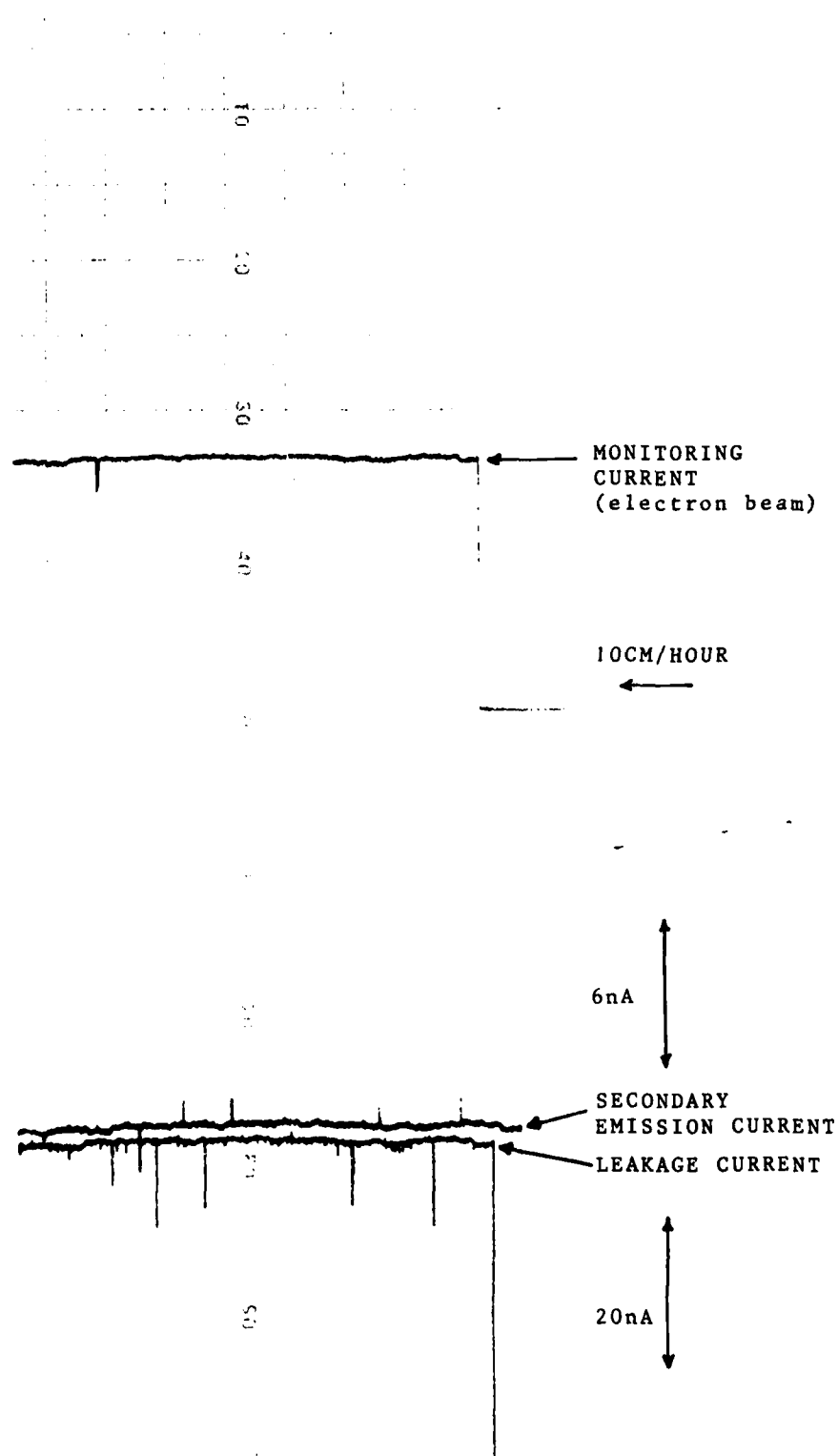
FIGURE 38A – SAMPLE A – RECORD OF CURRENTS AT END OF
THE IRRADIATION WITH THE CRYOGENIC SHROUD

73
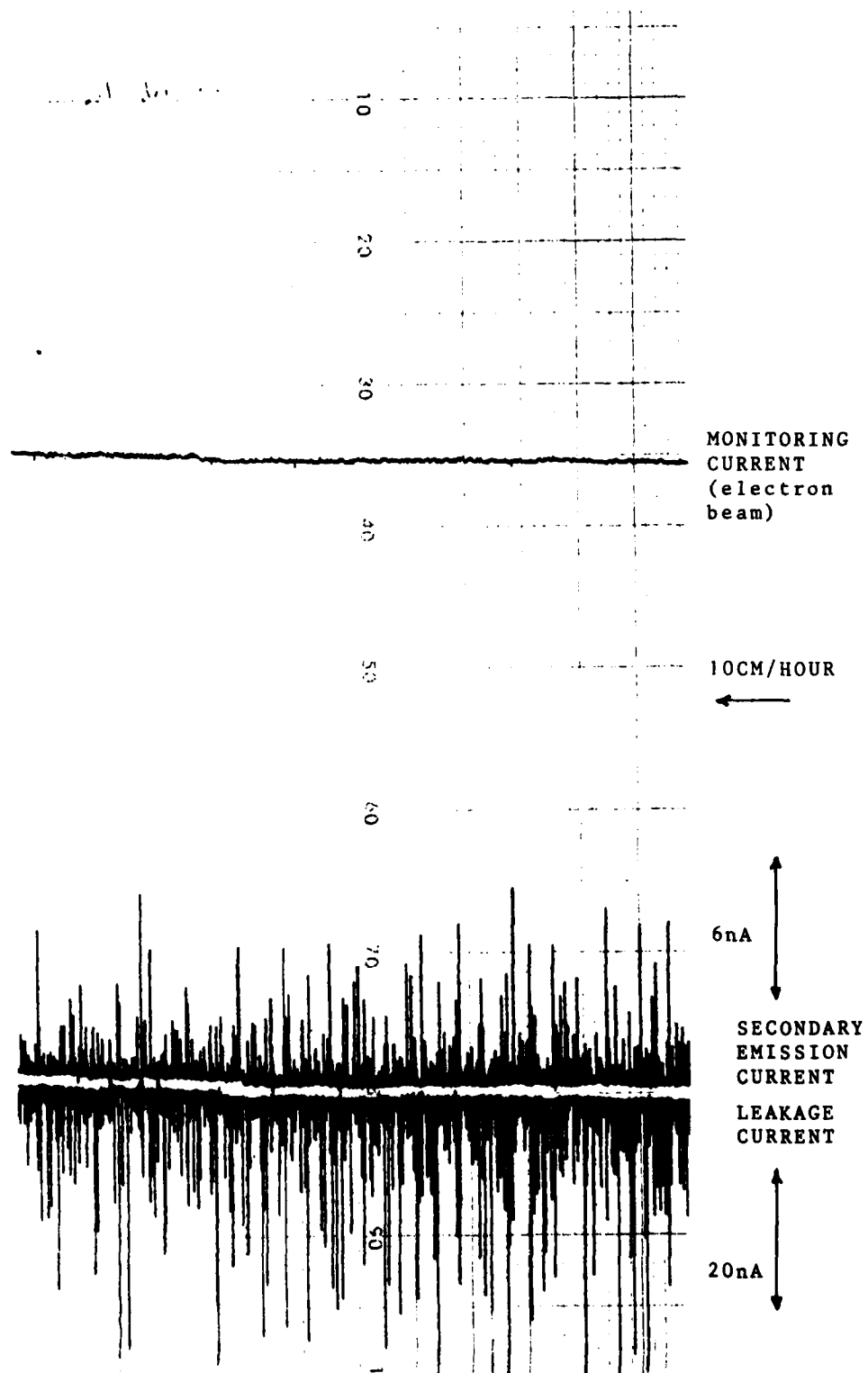
FIGURE 38B - SAMPLE A. RECORD OF CURRENTS AT BEGINNING
OF THE IRRADIATION TEST WITHOUT CRYOGENIC
SHROUD   74

MONITORING
CURRENT
(electron beam)

10cm/hour

6nA

secondary
emission current

leakage current

20nA
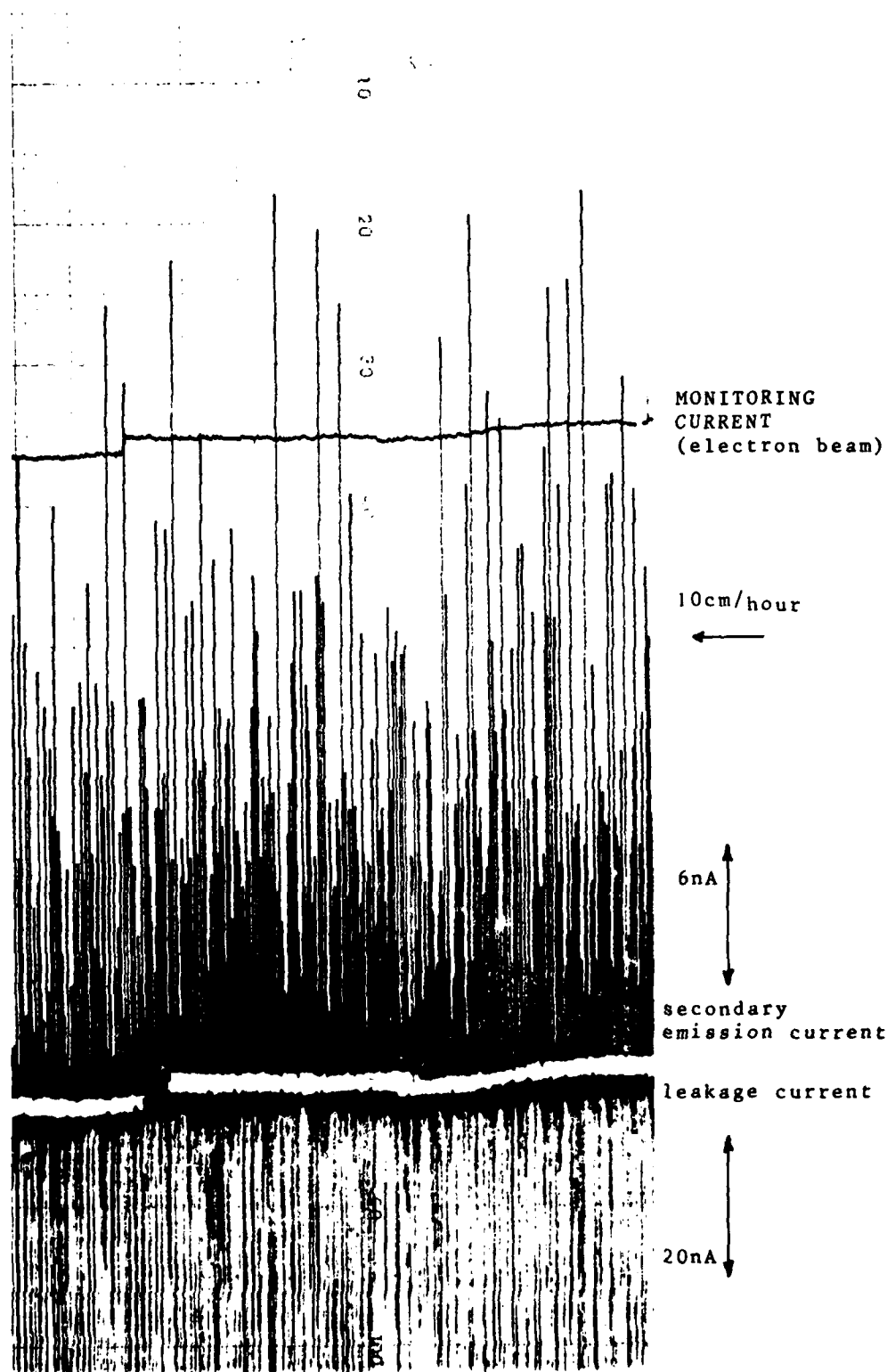
FIGURE 38c - SAMPLE A. RECORD OF CURRENTS AT END OF THE
IRRADIATION WITHOUT CRYOGENIC SHROUD

75

3.3.4 Discussion

It is obvious that both samples (not irradiated or irradiated for 32 hours at 20 keV/3nA cm^{-2}) exhibit large charges in their surface potential at the end of both test periods (that is to say with and without shroud filled with liquid nitrogen).

The increase in potential of the sample C that has been exposed only to vacuum (without being irradiated) is definitely not equal to zero, even for the period of time when the cryogenic shroud has been operating at liquid nitrogen temperature : this observation suggests that a contamination of sample A has actually occured even in the "clean" vacuum conditions.

Anyway the sample that has been simultaneously exposed to vacuum and irradiated by 20 keV electrons at 3nA cm^{-2} for 32 hours shows a far larger change in its electrostatic performance than the one shown by the sample that has been only exposed to vacuum.

The fact that a contamination has actually occured in vacuum conditions that had been expected to be very clean, prevents one from coming to a definite answer concerning the relative importance of the contamination effect and the ageing effect.

However the silica fabrics and the composites appear to be very sensitive to a combined contamination plus irradiation effect. There is a large increase in the surface potentials in terms of time. This leads to a far greater probability of arcing events, as it was experienced in the laboratory conditions : we have recorded an extremely high rate of "breakdowns" at the end of the 32 hours irradiation of the sample A as compared with the number of events recorded at beginning of this irradiation : see FIGURES 37a & 37b. Some discharge pulses are also recorded for sample C (FIGURE 37c),which has not been irradiated (except for the initial characterization period) but the pulses are far

less numerous than for the irradiated sample A. Moreover, sample A
(FIGURE 37b) exhibits some very large variations in the leakage
current : of significance is this latter behaviour since it is
similar to the behaviour we have called "A" and described in
Section 3-5-2 of Ref 3. It suggests very large variations in the
sample surface potential. Sample C exhibits also some small dis-
charge pulses as already mentioned, but no large variation with
time of the level of the leakage current I_c is noticed.

The influence of the irradiation test on sample A is parti-
cularly illustrated in the records obtained during the ageing test
itself: FIGURES 38a,38b & 38c are records of the leakage, secon-
dary and monitoring currents during ageing of sample A.

FIGURE 38a is related to irradiation under the above mentio-
ned "clean conditions" and is taken at the end of the test, while
FIGURES 38b and 38c are related to the ageing under the ordinary
vacuum conditions or "unclean vacuum". FIGURE 38b is taken at the
beginning of this latter test and FIGURE 38c at its end. (The test
is corresponding to a 16 hours irradiation at 20 keV, 3nA cm^{-2})

The influence of the contamination naturally produced by
the chamber, its pumps and accessories when the cryogenic shroud
is released at the end of the "clean ageing test" is shown by com-
parison of FIGURES 38 a and 38b.

The comparison between 38b and 38c illustrates the importance
of the irradiation (or the combined irradiation/contamination) effect:
the discharge rate is very substantially increased at the end of
the test. From the point of view of the discharge rate, the test
indicates that there is a combined ageing and contamination problem
since the enhancement of the discharge rate observed in the unclean

ageing test was not observed in the clean ageing test (in this latter case the rate was constant during the 16 hours irradiation).

3 - 4   CONCLUSION

Silica fabrics and composites made of silica fabrics, FEP and aluminum have been prime candidates for use on board geosynchronous satellites, owing to their unique properties that lead to very moderate increases in surface potential during substorm. But these materials are very sensitive to contamination, or contamination plus irradiation effects: surface potentials are increasing with time in normal laboratory experiments, as confirmed by the results given in this section as well as those given at section 2 (FIGURES 23, 24, 25). The same tendency can be expected in space: the good initial electrostatic behaviour will be probably progressively degraded as a function of the number of orbits with a greater probability of arcing events, if a great care is not taken in preventing from contamination.

4. Evaluation of conductive flexible second surface mirrors with a conductive adhesive grounding system.

4 - 1   INTRODUCTION

This report presents the results of a programme of prequalification
tests performed on conductively coated second surface mirrors (SSM)
with a grounding technique consisting of an aluminium strap bonded
to the conductive layer by means of a conductive adhesive.
The SSM are based on the polymer FEP teflon with a silver or aluminium
layer vacuum deposited on one side. The opposite space exposed side
is covered with a layer of conductive Indium-oxide or Indium-tin-oxide
(ITO) to prevent electrostatic charging of spacecraft by plasma currents
in geosynchronous orbit.

4 - 2   BASIC MATERIALS

4.2.1   Aluminised FEP teflon with ITO conductive layer

- Aluminised FEP teflon

  2 mil FEP teflon produced by Dupont with a 1000 $\overset{o}{A}$ layer of vacuum
  deposited aluminium by Sheldahl, USA.

- ITO layer

  250 - 300 $\overset{o}{A}$ ITO vapour deposited by Sheldahl, USA.

Complete material procured from Sheldahl under the commercial code
G409520. The material was perforated by Perforating Industries Inc., USA.

4.2.2   Silvered FEP teflon with ITO conductive layer

- Silvered FEP teflon

  5 mil FEP teflon produced by Dupont with a 1000 $\overset{o}{A}$ layer of vacuum
  deposited Inconel and vacuum deposited silver by Sheldahl, USA.

- ITO layer

  200 $\overset{o}{A}$ ITO RF sputtered by General Electric. USA.

Complete material procured from General Electric under the batch code
5/3/80-8. The material was not perforated.

4.2.3   RTV 566 Adhesive with conductive loading

- Adhesive

  RTV 566 silicone rubber produced by General Electric.

79

- Primer

  DC 1200 primer produced by Dow Corning, USA.

- Conductive powder

  Cho-Bond 1029B produced by Chomerics, USA.

4.2.4 DC 93500 Adhesive with conductive loading

- Adhesive

  DC 93500 silicone rubber produced by Dow Corning, USA.

- Primer

  DC 1200 primer produced by Dow Corning, USA.

- Conductive powder

  Cho-Bond 1029B produced by Chomerics

  or

  XRP-1 grade silver powder procured from Drijfhout (NL)

4 - 3   SSM INITIAL ELECTRICAL AND OPTICAL PROPERTIES

4.3.1 Test procedure

A sample of 2 x 2 cm has been cut out of each type of sheet material. The solar absorptance (α_S) and normal emittance (ε_N) of the samples have been measured according to ESA specification PSS-16/QRM-09T The surface resistivity (ρ_S) has been measured with a probe consisting of two 1 cm wide copper electrodes at 1 cm distance of each other in combination with a Hewlett Packard digital multimeter 3465B. A weight of 200 g was applied to the probe to maintain a standard pressure. The materials were also visually examined for cosmetic appearance.

4.3.2 Accuracy of the measurements

Solar absorptance (α_S)

Reproducibility $\quad \Delta\alpha_S = \pm\ 0.005$

Max. absolute error $\Delta\alpha_S = \pm\ 0.02$

Normal emittance (ε_N)

Reproducibility $\quad \Delta\varepsilon_N = \pm\ 0.005$

Max. absolute error $\Delta\varepsilon_N = \pm\ 0.02$

Ref. 7 F. LEVADOU - Specification for the measurement of the thermo-optical properties of thermal control materials at ESTEC ESA/PSS-16/QRM-09T (issue 1) Feb. 1977

Surface resistivity[*] (ρ_s)

Accuracy $\Delta\rho_s = \pm\ 0.1\ \Omega$

[*] This measurement should be considered as a relative comparison between the materials, rather than an absolute measurement.

4.3.3   Test results

- Sheldahl SSM   : α_S = 0.178

           ε_N = 0.637

           ρ_s = 6-19 MΩ

- General Electric SSM : α_S = 0.122

           ε_N = 0.795

           ρ_s = 30-40 KΩ

Visual inspection of the Sheldahl material indicated many crazes and scratches, both in the ITO and aluminium layers. Inquiry with the manufacturer proved that perforation took place after metallizing which caused the degraded cosmetic appearance.

Visual appearance of the General Electric material is good, no excessive scratching or spots have been identified.

4 - 4   DEFINITION OF THE GROUNDING SYSTEM

4.4.1   Purpose of the investigation

The basic grounding system is an aluminium strap 8 mm wide and 30 μm thick which is bonded to the top ITO layer of the conductive SSM by means of a conductive adhesive. A cross-section of a grounding point is shown in figure 39.

30 μm ALUMINIUM FOIL CONDUCTIVE ADHESIVE

INDIUM OXIDE LAYER

FEP TEFLON

3M 467 ADHESIVE

AL SUBSTRATE

METAL LAYER
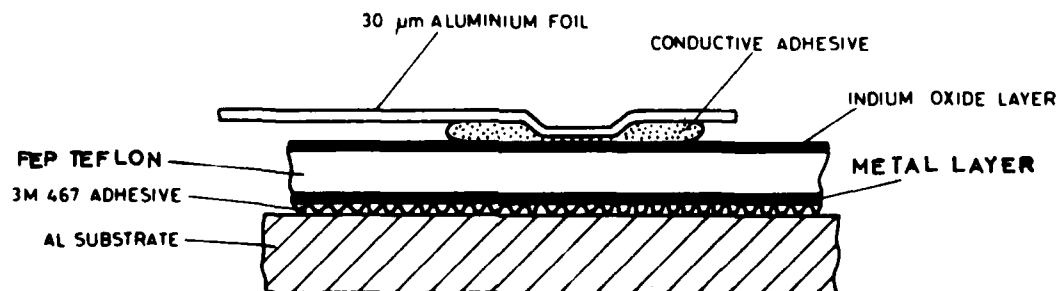
FIGURE 39 - CROSS SECTION OF GROUNDING POINTS

The purpose of this preliminary investigation was to identify if a conductive adhesive bond could be applied to the FEP teflon based conductive SSM. Furthermore to identify the optimum temperature and pressure conditions for the special heat probe used to manufacture the

81

grounding points. For a description of the heat probe refer to appendix. The two conductive adhesives identified in sections 4.2.3 & 4.2.4 were investigated in combination with the Sheldahl material. The General Electric material was not used, because this material had not yet been procured in this preliminary phase.

72 grounding straps were made using various probe temperatures and probe loadings.

4.4.2 Sample preparation

4.4.2.1 Substrate preparation

50 x 20 mm pieces of Sheldahl SSM were bonded with 3M 467 transfer tape to 1 mm thick aluminium plate of the same dimensions.

4.4.2.2 Aluminium foil tabs

$30 \mu m$ aluminium foil tabs of dimensions 70 mm x 8 mm were prepared.

4.4.2.3 Priming

The substrates and foil tabs were carefully degreased by wiping with a Freon TF soaked Kimwipe. Dow Corning DC 1200 was applied to the end of each tab to a distance of 20 mm from one end. Primer was applied to each end and in the middle of the conductive SSM substrate.

4.4.2.4 Conductive adhesive preparation

Conductive RTV 566 The adhesive was prepared as follows:

RTV 566 A   - 100 parts by weight

Cho-Bond 1029B - 250 parts by weight

were mixed thoroughly and to the mixture was added:

RTV 566 B   - 0.15 parts by weight

After further mixing the adhesive was degassed under vacuum.

Conductive DC 93500 The adhesive was prepared as follows:

DC 93500 A + B - 100 parts by weight

Cho-Bond 1029B - 600 parts by weight

were mixed thoroughly and degassed under vacuum.
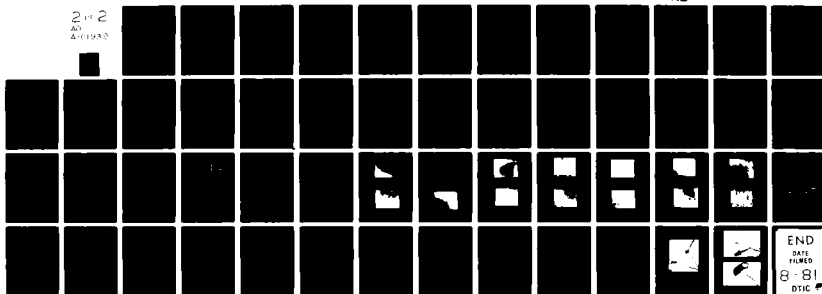
4.4.2.5 <u>Joint formation</u>

A small amount of adhesive was placed on the primed area of the conductive SSM. The primed aluminium foil was placed over it, and the heated tool, having already been set to the required load and temperature, was applied for the required time and then the joint left to cure fully overnight.

Table 4 shows the full work schedule. In total 72 joints were made on 24 substrates, 3 to each substrate. 15 Samples (AM 1-15) were prepared with conductive RTV 566. 9 Samples were prepared with conductive DC 93500. Loads of 100 to 300 g were applied at temperatures of 50, 100 and 150°C. The duration of the probe application was 2 minutes. The samples were left a further 16-24 hours to cure completely.

4.4.3 **Electrical resistance measurement**

4.4.3.1 <u>Electrical contact resistance</u> (R_c)

The three contact principle is used to obtain the contact resistance of the centre electrode. All three electrodes are aluminium straps bonded with conductive adhesive as described in section 4.4.1

Figure 40 shows the sample configuration and the applied electrical circuit.
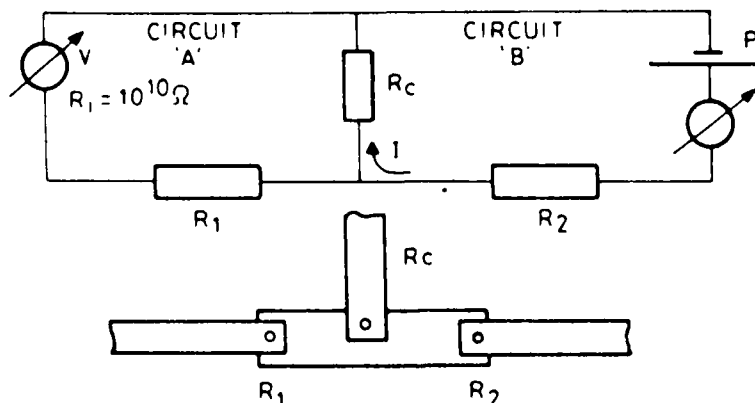
FIGURE 40 - CONTACT RESISTANCE MEASUREMENT

The symbols used in figure 40 have the following meanings:

P = power supply

A = Keithly model 602 electrometer (applied in ammeter mode)

V = Hewlett Packard multimeter 3465B (applied in voltmeter mode)

TABLE 4 - SAMPLE PREPARATION

	R_c (%) \ probe temp	$50^{\circ}C$	$100^{\circ}C$	$150^{\circ}C$
RTV 566 N = 15	R ≤ 10	2	2	5
	20 > R > 10	2	2	–
	R ≥ 20	1	1	–
	N	5	5	5
DC93500 N = 9	R ≤ 10	1	2	3
	20 > R > 10	2	1	–
	R ≥ 20	–	–	–
	N	3	3	3
Total N = 24	R ≤ 10	?	4	8
	20 > R > 10	4	3	–
	R ≥ 20	1	1	–
	N	8	8	8

R_i = internal resistance of voltmeter = $10^{10}\Omega$

R_1 = contact resistance of left electrode plus resistance of ITO layer between left and centre electrodes

R_2 = contact resistance of right electrode plus resistance of ITO layer between right and centre electrodes

R_c = contact resistance of centre electrode

The power supply and the ammeter are connected to the centre and right electrodes; the right electrode functions only as a current conductor. The voltmeter is connected between the centre and left electrodes. The left electrode functions as a potential electrode. Owing to the internal resistance of the voltmeter, the current passing through circuit "A" will be approximately a factor 1000 smaller than that passing through circuit "B".

Adjusting the power supply in circuit "B" enables the current through the contact resistance to be fixed. Circuit "A" is used to determine the voltage drop over the contact resistance, from which the contact resistance can be deduced.

On the basis of this method, a jig has been developed which ensures that the samples are measured under similar conditions of electrode pressure and sample positioning.

4.4.3.2 Total electrical resistance

After each successive test, the total electrical resistance of each sample was measured according to the electrical circuit as shown in figure 41 The total electrical resistance is defined as the electrical resistance measured between left and right electrodes and includes contact resistance of left and right electrodes as well as the resistance of the intervening ITO layer.

Figure 41 illustrates the test method.

4.4.3.3 Sample conditioning

New test data for conductive SSM (ref. 8) has shown that the conductivity of the ITO layer is very susceptible to humidity: conductivity decreased with increased humidity due to water absorption in the ITO layer. Also long term storage (2 years) in a high humidity environment (65 to 70%) degrades the ITO layer.

It has therefore been decided to store and condition samples in a normal laboratory environment (50% RH) throughout the programme.
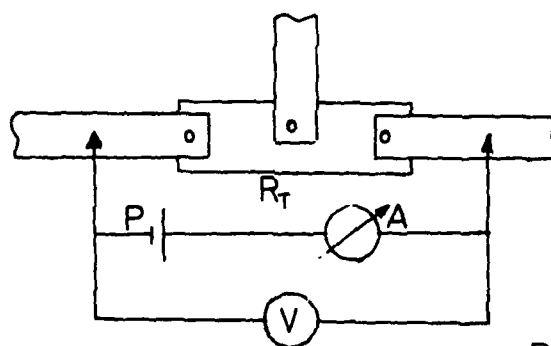
R_T = total electrical
resistance.

FIGURE 41 – TOTAL RESISTANCE MEASUREMENT

4.4.3.4 Test conditions

Samples were measured in a normal laboratory environment for reasons stated in section 4.4.3.3.

4.4.3.5 Applied current

For the measurement of the electrical contact resistance, the applied current was set at 10^{-6}A.

For the total electrical resistance, the applied current was set at 10^{-8}A. This setting was required for the voltmeter, as the potential drop over the resistance should not exceed 2 V otherwise the voltmeter range must be changed and the internal resistance is no longer garanteed at $>10^{10}\Omega$.

4.4.3.6 Electrification time

The electrification time for each measurement was set at 1 minute before the measurement value was read.

4.4.3.7 Accuracy of the measurement

The read-out accuracy of the voltmeter is $\pm$ 0.0001 V

The read-out accuracy of the amperemeter is $\pm$ 1%.

The relative error, due to read-out accuracies in volt- and amperemeter, in resistance measurement is $\pm$ 1%.

4.4.3.8 Reproducibility of the measurements

According to ASTM D 257-1 (ref. 9) resistance measurements of this type do not have a reproducibility of better than 10%.

4.4.4 Test results

The test results are noted in table 5. All contact resistances are within the range of 0.1-3 MΩ. The total resistances are in the range 1-60 MΩ. The contact resistance varies with the surface resistivity of the substrate material, which is due to the fact that the contact always includes a

Ref. 8   LEVADOU F. BOSMA S.J. PAILLOUS A. - *Materials characterization study of conductive flexible second surface mirrors - Presentation 3rd Spacecraft Charging Technology Conference. Colorado Spring. Nov. 1980*

Ref. 9   *Standards methods of test for DC resistance or conductance of insulating materials (D257-46) 1975 Annual book of ASTM standards.*

TABLE 5 - SPECIMEN RESISTANCE

Sample	R_{C_L} (MΩ)	R_{C_R} (MΩ)	R_T (MΩ)	R_{ITO} (MΩ)	R_C/R_{ITO} (%)
AM 1	1.2	1.5	49	46	3
2	2.3	2.0	17	13	18
3	2.5	2.7	16	11	25
4	0.8	1.1	15	13	8
5	1.5	1.3	13	10	15
6	1.3	1.3	10	7	19
7	1.5	1.2	19	16	9
8	0.8	0.9	8	6	15
9	0.7	0.4	16	15	5
10	2.8	1.8	16	11	25
11	1.7	1.1	22	19	9
12	2.7	1.5	32	28	10
13	0.5	0.5	14	13	4
14	0.2	1.3	38	37	4
15	2.8	1.6	55	51	5
AN 1	0.9	0.9	9	7	13
2	1.0	1.1	11	9	12
3	0.7	0.3	8	7	10
4	0.3	0.3	4	3	10
5	0.3	0.4	8	7	6
6	0.7	0.8	6	4.5	17
7	1.4	1.4	18	15	9
8	1.0	1.6	20	17	9
9	1.0	0.8	21	19	5

$$R_{ITO} = R_T - (2R_C)$$

88

barrier layer of the substrate material.

An effort has been made to normalize the results so that substrate resistance is neutralised and the contacts can be evaluated for the variations of probe temperature and pressure.

It has been assumed that left and right electrodes have similar contact resistances as the centre electrode. The surface resistance of the ITO layer (R_{ITO}) is than determined by subtracting $2 \times R_c$ from the total resistance (R_T).

In table 5 two values have been noted for R_c; these were determined by interchanging the two side contacts as potential and current electrodes. The highest of the two values for contact resistance has been converted to a relative value of the substrate resistance ($R_c/R_{ITO} \times 100\%$).

4.4.5 Discussion of test results

In tables 6 and 7 the test results are shown as a function of probe temperature, resp. probe pressure.

It becomes evident from table 6 that the contact resistance improves with probe temperature for both conductively loaded RTV 566 and DC 93500. For 50°C only 3 out of 8 samples have a contact resistance of less than 10% of the ITO resistance.

For 150°C all 8 samples have a contact resistance of less than 10%.

The effect of probe pressure on contact resistance is not very critical although there is some indication that the contact will improve with low probe pressures.

The high probe temperature also improves the curing of the adhesive. Good contacts were achieved with both conductively loaded RTV 566 and conductively loaded DC 93500.

It appears that the contact resistance is dependant of the surface resistivity of the substrate material, which is not surprising as the contact resistance always includes a barrier layer of the substrate material.

A nominal value for contacts on the ITO coated FEP teflon is 10% of the surface resistivity of the ITO. This is in good agreement with the results for ITO coated Kapton (Ref. 3, Section 2-2)

The contact resistance on ITO/Kapton was 20-400 Ω.

The surface resistance of the ITO was 2-3 KΩ, indicating that the contacts are again approximately 10% of the ITO resistance.

TABLE 6 : CONTACT RESISTANCE VERSUS PROBE

TEMPERATURE

Material	Probe pressure (g)	Probe temperature		
		50°C sample no.	100°C sample no.	150°C sample no.
RTV 566 + Cho-bond 1029 B	100	AM 1	AM 6	AM 11
	150	2	7	12
	200	3	8	13
	250	4	9	14
	300	5	10	15
DC93500 + Cho-bond 1029 B	100	AN 1	AN 4	AN 7
	200	2	5	8
	300	3	6	9

TABLE 7 – CONTACT RESISTANCE VERSUS PROBE

PRESSURE

	probe pressure R_c (%)	100 (g)	150 (g)	200 (g)	250 (g)	300 (g)
RTV 566 N= 15	R ≤ 10	2	2	1	3	1
	20 > R > 10	1	1	1	–	1
	R ≥ 20	–	–	1	–	1
	N	3	3	3	3	3
DC93500 N = 9	R ≤ 10	2		2		2
	20 > R > 10	1		1		1
	R ≥ 20	–		–		
	N	3		3		3
Total N = 24	R ≤ 10	4		3		3
	20 > R > 10	2		2		2
	R ≥ 20			1		1
	N	6		6		6

4.4.6 Conclusions

The basic grounding system described in section 441 is feasible on conductive FEP teflon based SSM.

Contact resistances are in the 0.1-1 MΩ range for grounding straps on the Sheldahl SSM which has a relatively high surface resistivity of 6-19 MΩ. For conductive SSM with a lower resistivity the contact resistance should definitely improve.

The optimum probe parameters:

probe temperature : 150°C

probe pressure : 100-200 g

probe application : 2 minutes

In principle contacts are possible with both conductively loaded RTV 566 or DC 93500.

Although the joints based on DC 93500 showed good promise, in that they were easily cured and exhibited low contact resistance, an outgassing test according to ESA specification PSS-09/QRM-02T proved that CVCM data is borderline: (Ref. 10)

TML %   0.46

RML %   0.45

CVCM%   0.09

The reason could be that accelerator and catalyst in the Cho-Bond 1029B are left unpolymerised and are thus free to outgas.

Further tests using DC 93500 with silver powder grade XRPI proved unsuccessful. The adhesive failed to cure under the heated tool and also after a further 7 days at room temperature.

The adhesive can be cured at 80°C but this is of course impractical for grounding of large blanket etc. It was decided to abandon a grounding system based on DC 93500. In view of these results the following prequalification programmes were initiated.

- 41 samples of General Electric conductive SSM with conductive RTV 566 grounding points.
- 41 samples of Sheldahl conductive SSM with conductive RTV 566 grounding points.

Ref. 10 - Zwaal A. - A screening test method employing a thermal vacuum for the selection of materials to be used in space - ESA PSS 09/QRM-02T

4 - 5   PREQUALIFICATION OF THE CONDUCTIVE SSM/
CONDUCTIVE ADHESIVE BOND SYSTEMS

4.5.1   Purpose of the programme

A study programme was defined in order to check the stability of
both systems (defined in section 4.6) under humidity, chemical spray
and thermal cycling.

4.5.2   Preparation of the samples

4.5.2.1   Substrate preparation

Two series of 41 rectangular samples of aluminium alloy (20 x 50 x 1 mm)
were abraded with Scotch-Brite and degreased in Freon TF vapour. For the
first series the Sheldahl SSM and for the second series the General
Electric SSM was cut to the same dimensions and bonded to the aluminium
substrate with 3M 467 transfer tape.

4.5.2.2   Aluminium straps

Aluminium straps 30 μm thick and measuring 8 mm x 80 mm were prepared.
Each sample was provided with three grounding straps (see figure 4).

ALUMINIUM FOIL STRAPS.
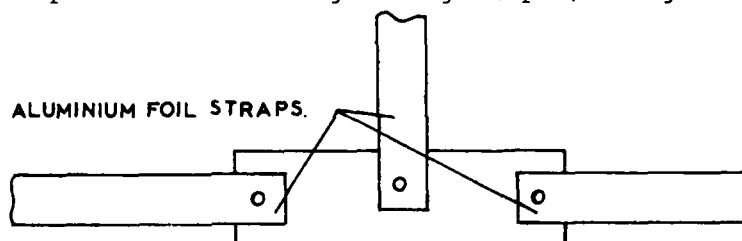
Figure 42 - SAMPLE DESCRIPTION

4.5.2.3   Priming

The straps were degreased by being wiped with a Kimwipe soaked in
Freon TF. Dow Corning DC 1200 primer was applied to the end of each strap
to a distance of 20 mm from one end. Primer was applied to each end of
the conductive SSM substrate as well as in the middle of the samples.

4.5.2.4   Preparation of conductive adhesive

The adhesive was prepared in the following manner:

RTV 566 A   - 100 parts by weight

Cho-Bond 1029B - 250 parts by weight

were mixed throroughly and to the mixture was added:

RTV 566 B   - 0.15 parts by weight

After further mixing, the adhesive was degassed under vacuum.
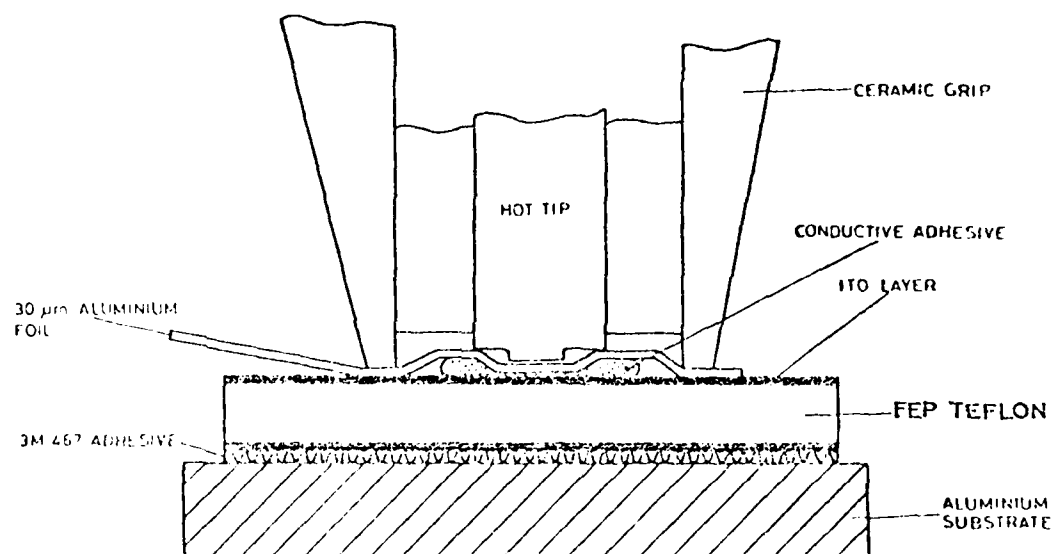
FIGURE 43 - CROSS-SECTIONAL VIEW OF A JOINT DURING
FORMATION

4.5.2.5. <u>Joint formation</u>

A small amount of the conductive adhesive was applied to the primed area of the ITO/SSM, the primed aluminium foil was placed over it and the heated tool was applied over the joint. The tool was applied to the joint for a cure time of 2 minutes, with a hot tip temperature of 150°C and a load of 200 g (see figure 43) ,as determined in section 4.4 In total, three joints were made on each of the substrates.

4 - 6   TEST SEQUENCE

The samples were submitted to the following prequalification tests:

Chemical spray test;

Heat and humidity test;

Thermal cycling test.

After each succesive test, the samples were stored for 48 hours in a normal laboratory environment (18-25°C, 50-60% RH) and were then tested under these conditions.

The test parameters are:

Electrical contact resistance

Visual inspection

Adhesion test

Table 8 illustrates the sequence of tests and the manner in which the samples were divided to determine the influence of any one test. For example, samples 17 and 20 were submitted to chemical spray testing only, while samples 33 and 38 underwent the entire programme of tests. This method makes it possible to determine whether one particular test or a combination of tests is detrimental to the material under evaluation. In addition to being submitted to the standard prequalification programme, the material also underwent several preliminary tests to determine it's basic characteristics.

Note: The electrical resistance measurements were performed according to the method described in section 4.4.3 During the test programme it became evident that this method was not effective for the Sheldahl perforated SSM. Due to the high increase in resistivity of the ITO layer after humidity and thermal cycling tests, the applied current did not follow the path:grounding point - ITO layer - grounding point - (fig. 44a) but the path grounding point -

TABLE 8 - PREQUALIFICATION TEST SCHEDULE

| R | 1 | 2 | 3 | 4 | 5 | 6 | 7 | 8 | 9 | 10 | 11 | 12 | 13 | 14 | 15 | 16 | 17 | 18 | 19 | 20 | 21 | 22 | 23 | 24 | 25 | 26 | 27 | 28 | 29 | 30 | 31 | 32 | 33 | 34 | 35 | 36 | 37 | 38 | 39 | 40 |

VISUAL INSPECTION
IN-AIR RESISTANCE
PEEL TESTING
RESISTANCE/APPLIED CURRENT
LONG TERM STORAGE

CHEMICAL SPRAY
VISUAL INSPECTION
IN-AIR RESISTANCE
PEEL TESTING

HEAT AND HUMIDITY
VISUAL INSPECTION
IN-AIR RESISTANCE
PEEL TESTING

THERMAL CYCLING
VISUAL INSPECTION
IN-AIR RESISTANCE
PEEL TESTING

VISUAL INSPECTION
IN-AIR RESISTANCE
PEEL TESTING

VISUAL INSPECTION
IN-AIR INSPECTION
PEEL TESTING

VISUAL INSPECTION
IN-AIR RESISTANCE
PEEL TESTING

3 months

6 months

1 year

96

(a)   (b)

FIGURE 44 - ELECTRICAL PATH IN A PERFORATED ITO/SSM

It is clear that the ITO layer is by-passed and that the results are no longer valid.

All Sheldahl samples were measured at the end of the programme by applying a probe, consisting of two 10 mm copper electrodes with 10 mm electrode separation, directly onto the ITO surface of the samples and measuring the electrical surface resistivity of the ITO layer. A weight of 200 g was applied to the probe to maintain a standard pressure. Furthermore the probe was situated in such a manner that neither electrode was in contact with the perforation.

Of course only the final combined effect of all tests could be measured on the samples that underwent the entire programme of tests. It was not possible to determine the evolution of one particular sample throughout all tests, rather this evolution was determined from the various groups of samples that had been through one particular test.

4 - 7   PRELIMINARY TESTS

4.7.1   Visual inspection

Throughout the test programme visual inspection was performed with a "zoom" type microscope at 30x magnification. Special attention was given to the ITO layer surrounding the grounding point. The initial inspection revealed no degradation.

4.7.2   Total resistance versus applied current test

The purpose of this test is to determine whether an increase in the electrical current load through the sample configuration would create more current parths in the grounding points and ITO layer and subsequently result in a lower electrical resistance.

TABLE 9

Surface resistivity measurements of ITO layer of Sheldahl 2 mil aluminised SSM

SAMPLE	ITO surface resistivity (Ω)			
	initial value in-air	after chemical spray	after heat and humidity	after thermal cycling
1	11.10×10^7			
2	4.81×10^7			
3	3.36×10^7			
4	1.97×10^7			
5	0.86×10^7			
6	3.21×10^7			
7	0.66×10^7			
8	1.36×10^7			
9	0.99×10^7			
10	3.44×10^7			
11	2.35×10^7			
12	1.77×10^7			
13	1.78×10^7			
14	3.09×10^7			
15	4.64×10^7			
16		12.81×10^7		
17		5.46×10^7		
18		6.18×10^7		
19		23.51×10^7		
20		8.75×10^7		
21			33.21×10^7	
22			36.59×10^7	
23			31.40×10^7	
24			32.38×10^7	
25			34.18×10^7	
26				59.32×10^9
27				18.32×10^9
28				64.32×10^9
29				61.32×10^9
30				48.49×10^9
31				58.77×10^9
32				68.91×10^9
33				58.82×10^9
34				44.31×10^9
35				60.21×10^9
36				62.34×10^9
37				58.59×10^9
38				57.54×10^9
39				62.42×10^9
40				55.32×10^9
R				8.12×10^7

According to the method described in section 4.4.3 the applied current was set at the initial level and remained at this level for 30 seconds, after which the voltage drop over the total resistance was noted. The current was then increased to the next step and the same procedure followed. The current values were (A):

0.5×10^{-7} 0.5×10^{-6} 0.5×10^{-5} 0.5×10^{-4} 0.5×10^{-3}
1.0×10^{-7} 1.0×10^{-6} 1.0×10^{-5} 1.0×10^{-4} 1.0×10^{-3}

This sequence was then reversed. In some cases the upper current limit was not reached because the required voltage exceeded 150 V, which is the limit of the power supply.

Figure 45 shows the typical results of two Sheldahl samples. There is a decrease in resistance with increasing current, however, when the sequence is reversed the sample achieves more or less its initial value.

Figure 46 illustrates that this phenomenon is also apparent for the General Electric SSM

For both materials there is no permanent improvement of total resistance.

4.7.3   Initial in-air resistance measurements

4.7.3.1   Sheldahl SSM (table 9)

The initial surface resistivity of the ITO layer of the samples was 5 to 100 MΩ (table 9), which is of the same order of magnitude as the results for the try-out samples (table 5).

Because of the reasons stated in section 4.6 no results are noted for the total and contact resistances of the the Sheldahl samples.

4.7.3.2   General Eelectric SSM (tables 10 & 11)

The initial contact resistance of most of the samples showed a value between 1 and 100 kΩ. Four samples had values higher than 100 kΩ and one sample showed a value of several Ohms. The initial total resistance of most of the samples varied between 0.1 and 10 MΩ. Five samples had values higher than 10 MΩ All samples were relatively stable during the measurements.

4 - 8   CHEMICAL SPRAY TEST

4.8.1   Test method

The samples were sprayed with iso-propyl-alcohol at room temperature for one minute.
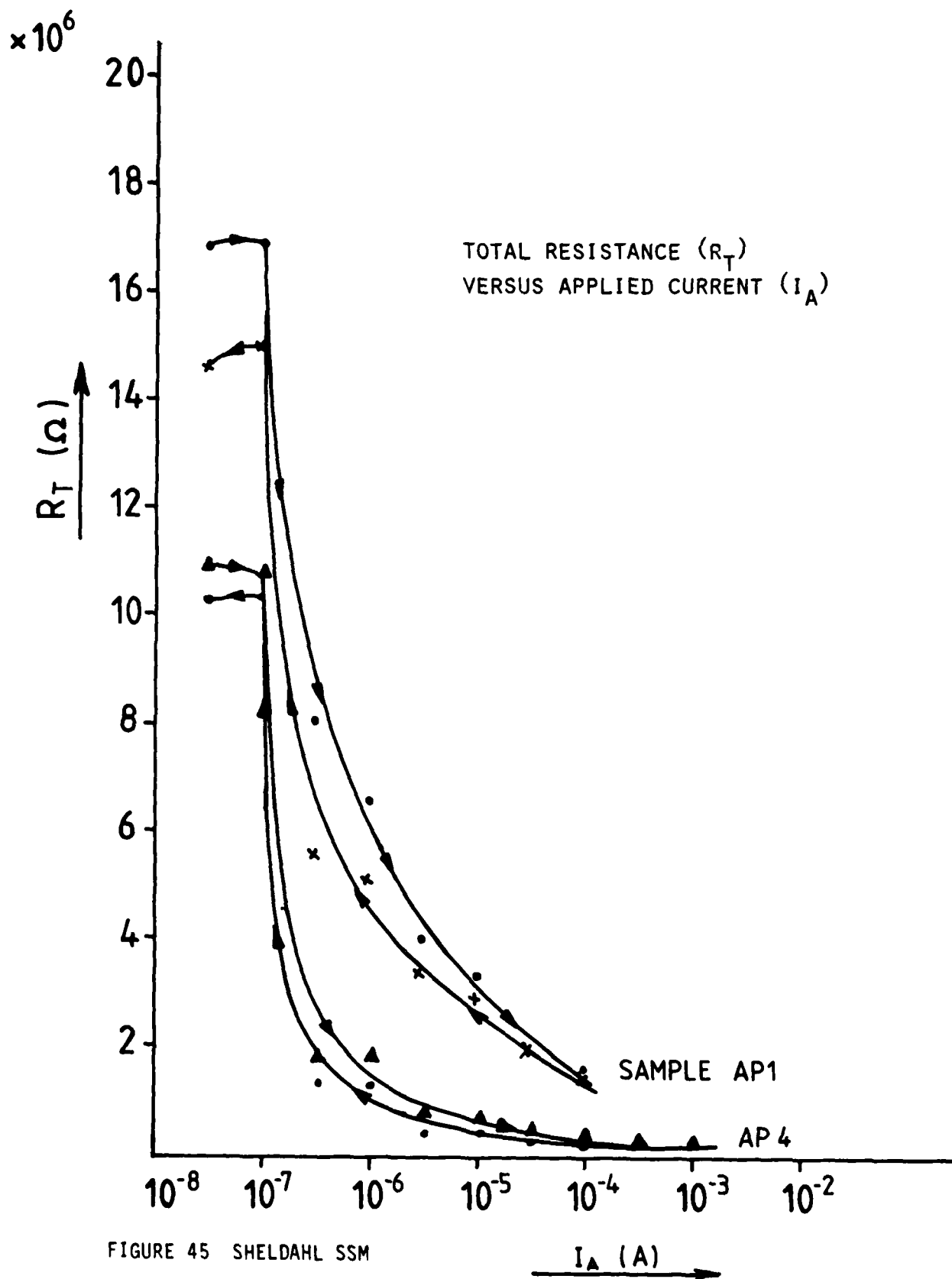
FIGURE 45 SHELDAHL SSM

100
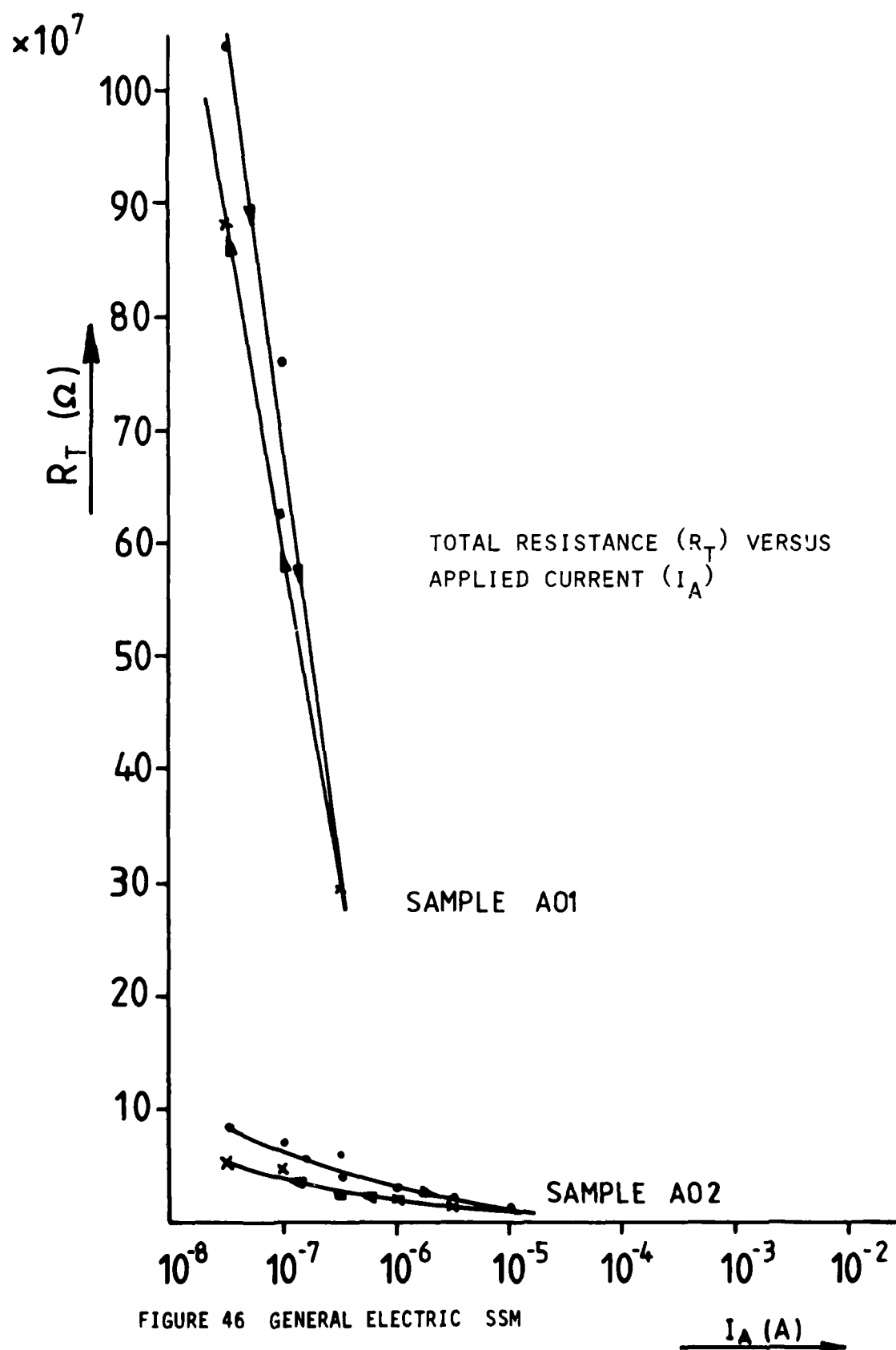
FIGURE 46 GENERAL ELECTRIC SSM

TOTAL RESISTANCE (R_T) VERSUS
APPLIED CURRENT (I_A)

SAMPLE A01

SAMPLE A02

TABLE 10

Total resistance measurements of General Electric conductive SSM

SAMPLE	Total resistance (Ω)			
	initial value in air	after chemical spray	after heat and humidity	after thermal cycling
1	0.86×10^6			
2	0.54×10^6			
3	1.67×10^6			
4	0.76×10^6			
5	0.36×10^6			
6	0.51×10^6			
7	0.47×10^6			
8	1.08×10^6			
9	1.70×10^6			
10	2.39×10^6			
11	6.42×10^6			
12	2.85×10^6			
13	1.33×10^6			
14	0.31×10^6			
15	4.55×10^6			
16	1.11×10^6	2.35×10^6		
17	0.61×10^6	2.24×10^6		
18	0.63×10^6	1.17×10^7		
19	0.29×10^6	0.92×10^6		
20	1.27×10^6	2.00×10^6		
21	2.62×10^6		18.81×10^6	
22	28.91×10^6		5.22×10^{10}	
23	0.92×10^6		4.83×10^{10}	
24	4.55×10^6		11.13×10^{10}	
25	1.69×10^6		4.74×10^7	
26	0.53×10^6			8.03×10^7
27	0.85×10^6			1.28×10^8
28	0.39×10^6			8.00×10^9
29	0.90×10^6			8.50×10^9
30	15.21×10^6			1.33×10^9
31	0.26×10^6	0.55×10^6	5.88×10^8	7.47×10^7
32	0.36×10^6	0.65×10^6	5.86×10^7	$>' 10^{11}$
33	0.81×10^6	1.35×10^6	5.71×10^7	9.37×10^9
34	2.16×10^6	3.56×10^6	8.53×10^7	7.43×10^9
35	12.81×10^6	8.87×10^6	4.62×10^{10}	8.48×10^9
36	16.46×10^6	7.21×10^8	5.12×10^{10}	7.95×10^9
37	0.61×10^6	1.83×10^6	8.60×10^8	3.64×10^7
38	0.79×10^6	1.33×10^6	7.22×10^7	7.65×10^9
39	0.61×10^6	1.17×10^6	6.43×10^7	8.69×10^9
40	12.83×10^6	3.97×10^6	7.24×10^9	9.07×10^9
R	1.28×10^6	5.18×10^6	8.19×10^6	9.34×10^6

TABLE 11

Contact resistance measurements of General Electric conductive SSM

S A M P L E	Contact resistance (Ω)			
	initial value in air	after chemical spray	after heat and humidity	after thermal cycling
1	25.0×10^3			
2	7.8×10^3			
3	12.1×10^3			
4	10.3×10^3			
5	13.2×10^3			
6	15.5×10^3			
7	8.0×10^3			
8	38.4×10^3			
9	17.0×10^3			
10	46.4×10^3			
11	47.7×10^4			
12	33.0×10^3			
13	13.2×10^3			
14	20.5×10^3			
15	15.3×10^4			
16	4.5×10^3	8.0×10^3		
17	8.9×10^3	5.3×10^3		
18	8.0×10^3	2.2×10^3		
19	7.4×10^3	5.0×10^3		
20	15.0×10^3	17.6×10^3		
21	13.6×10^4		5.7×10^6	
22	64.3×10^3		n.p.	
23	14.8×10^3		n.p.	
24	5.4×10^3		n.p.	
25	11.5×10^3		2.8×10^3	
26	10.3×10^3			7.0×10^4
27	3.7×10^3			1.3×10^6 ↑
28	2.2×10^3			8.8×10^5 ↑
29	1.7×10^3			n.p.
30	29.3×10^4			n.p.
31	0.2×10^3	0.8×10^3	5.4×10^5	1.5×10^5
32	2.9×10^3	5.5×10^3	5.6×10^5	n.p.
33	8.6×10^3	31.0×10^3	1.6×10^5	n.p.
34	20.9×10^3	25.5×10^3	4.3×10^5	5.9×10^6
35	7.3×10^3	3.3×10^4	n.p.	n.p.
36	33.2×10^3	12.4×10^4	n.p.	n.p.
37	3.8×10^3	1.6×10^3	2.8×10^5	1.6×10^3
38	2.2×10^1	0.5×10^3	1.1×10^6	1.0×10^6
39	1.4×10^3	32.9×10^3	1.7×10^6	n.p.
40	19.0×10^3	32.4×10^3	1.5×10^6	n.p.
R	17.8×10^3	30.2×10^3	24.0×10^3	14.3×10^3

4.3.2   Test results

4.8.2.1 Sheldahl SSM

(a) Electrical surface resistivity measurements (table 9 figure 47).
    The average initial value of ρ_s for samples 1 to 15 is $3.0 \times 10^7 \Omega$,
    compared to an average value $11.3 \times 10^7 \Omega$ for samples 16 to 20 after
    chemical spray. Apparently this is only a slight increase of surface
    resistivity due to the chemical spray test.

(b) Visual inspection
    No degradation of the surface was traceable to chemical spray.

General Electric SSM

(a) Electrical resistance measurements (tables 10 & 11 figures 48 & 49).
    Table 12 gives the average resistance values for the sample groups
    and also indicates the number of samples which show an increase or a
    decrease compared to their initial value.

TABLE 12 - GESSM : ELECTRICAL RESISTANCE

Parameter	Test	Sample no.	Average value (Ω)	Decrease	Increase
Contact res.	Initial	16-20, 31-40	9.4×10^3	n.a.	n.a.
Contact res.	Chemical	16-20, 31-40	19.7×10^3	6	9
Total res.	Initial	16-20, 31-40	3.4×10^6	n.a.	n.a.
Total res.	Chemical	16-20, 31-40	2.6×10^6	3	12

In general it appears that there is no significant change of the
electrical properties after chemical spray. There is a slight tendency to
increase resistance but the reference sample also showed an increase
in resistance during the time period of this test.

(b) Visual inspection
    No degradation of the surface was traceable to chemical spray.

4 - 9   HEAT AND HUMIDITY TEST

4.9.1   Test method

The samples were kept in the humidity chamber for seven days and were
submitted to a temperature of $50^\circ C$ and a relative humidity of 95%.

104

4.9.2 Test results

4.9.2.1 Sheldahl SSM

(a) Electrical surface resisitivity measurements (Table 9, Fig. 47)

The average value of sample 21 to 25 after heat and humidity is 33.5×10^7 Ω, compared to the average initial value of 2.0×10^7 Ω there is an increase by a factor 10.

(b) Visual inspection.

No degradation of the surface was traceable to the heat and humidity test.

4.9.2.2 General Electric SSM

(a) Electrical resistance measurements (tables 10 & 11, figures 48 & 49)

TABLE 13   ELECTRICAL RESISTANCE OF THE GE SSM AFTER HEAT AND HUMIDITY TEST

Parameter	Test	Sample no.	Average Value (Ω)	Decrease	Increase
Total res.	Initial	21-25	7.7×10^6	n.a.	n.a.
Total res.	Heat	21-25	4.2×10^{10}	-	5
Total res.	Initial	31-40	4.8×10^6	n.a.	n.a.
Total res.	Heat	31-40	1.1×10^{10}	-	10

The contact resistance could not be determined in all cases because the ITO resistance is so high that the limits of the measuring equipment applied in the three electrode arrangement are exceeded. In those cases where contact resistance was measured, the values had increased to the 10^5 to $10^6\Omega$ region.

The total resistance of all samples increased after the heat and humidity test. Of the samples 21-25 that had been through this test only, 3 out of 5 jumped to $10^{10}\Omega$. Of the samples 31-40, that had been through all previous tests, 7 out of 10 had values in the 10^7 to $10^8\Omega$ region. The others were in the $10^{10}\Omega$ region.

These $10^{10}\Omega$ values dominate the average values noted in table 13, so that the average is not representative of the sample group.
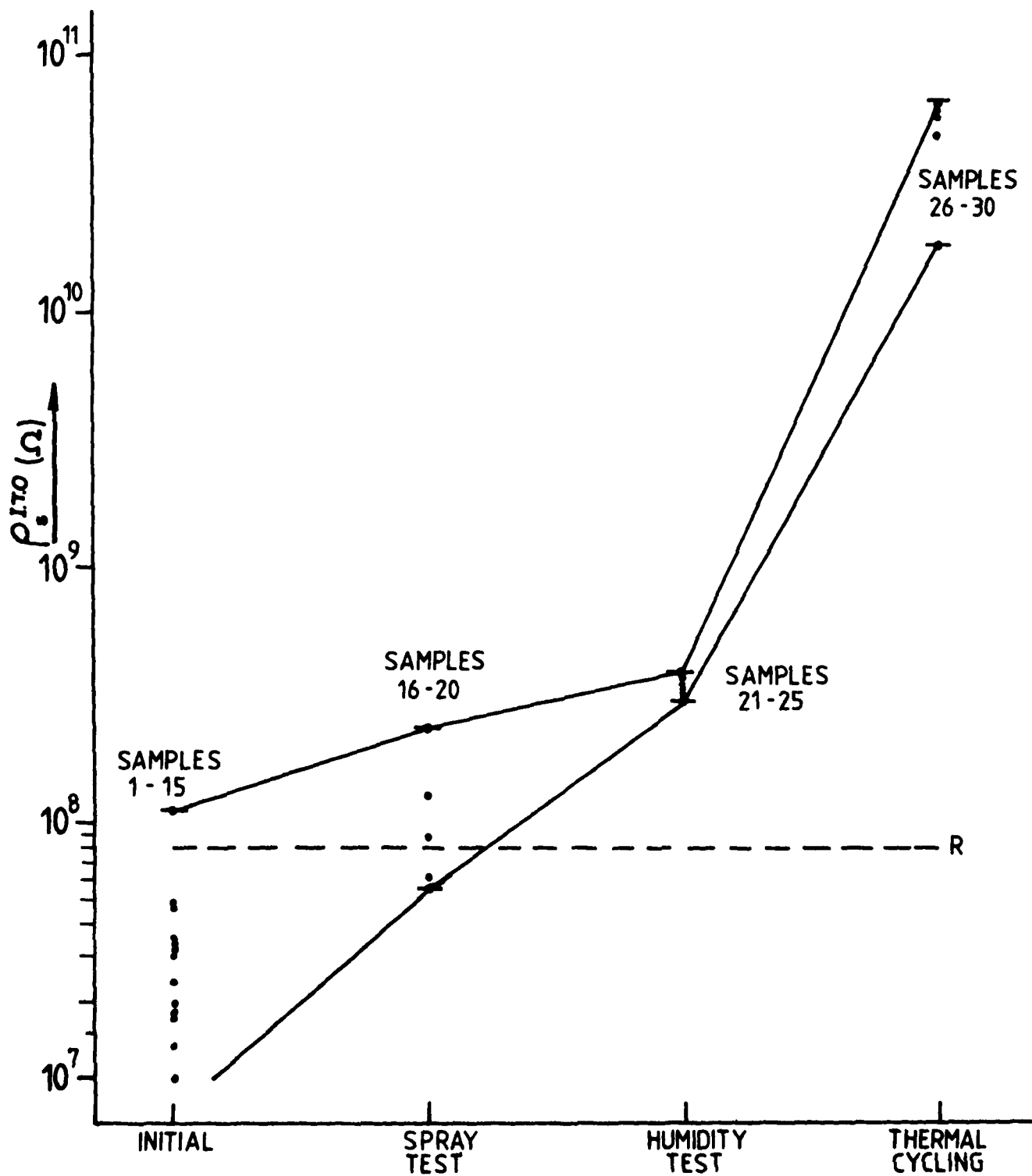
FIGURE 47   SURFACE RESISTIVITY MEASUREMENT OF ITO LAYER OF SHELDAHL 2 MIL
ALUMINISED SSM.
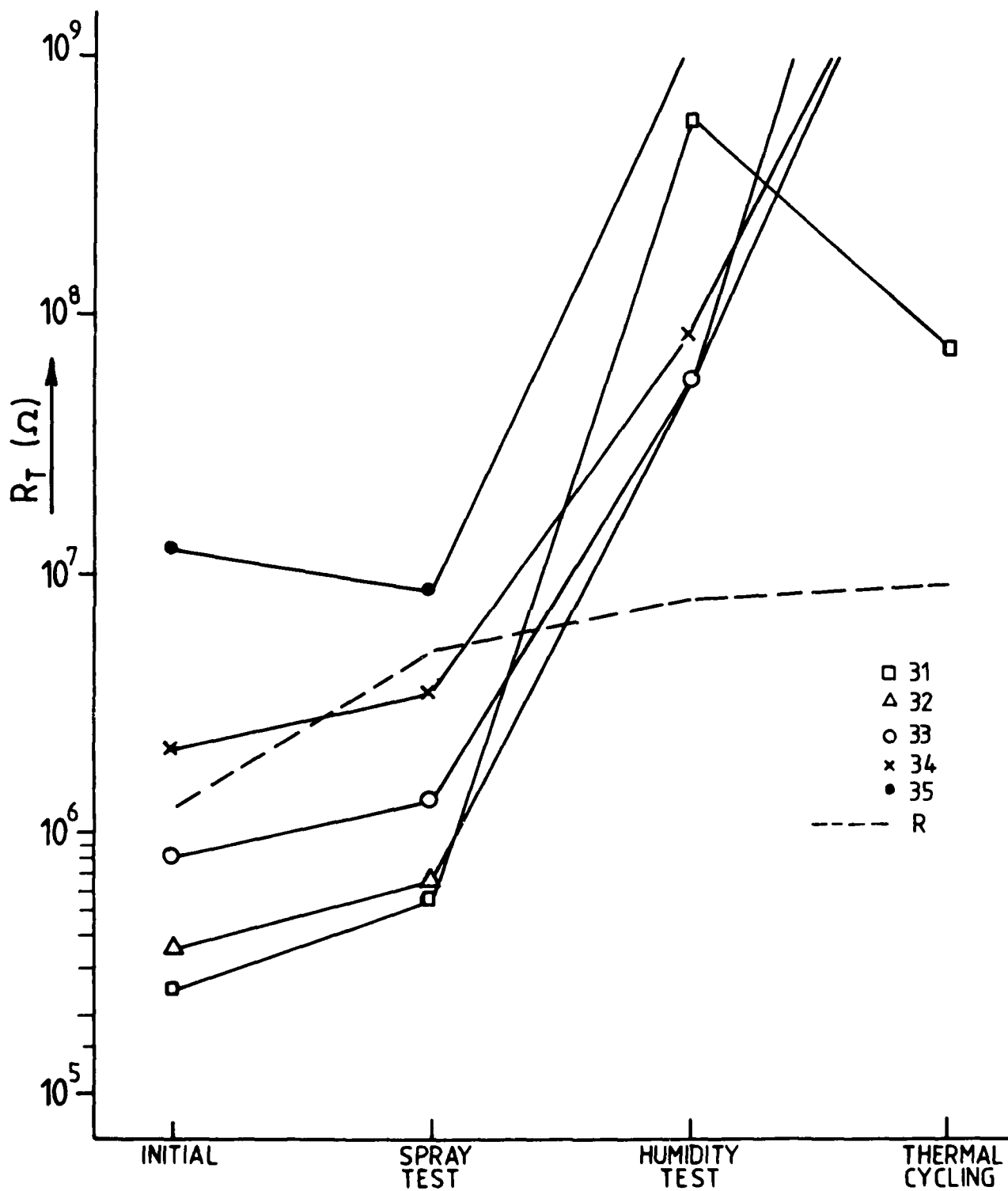
FIGURE 48   TOTAL RESISTANCE MEASUREMENTS OF GENERAL ELECTRIC SSM

107
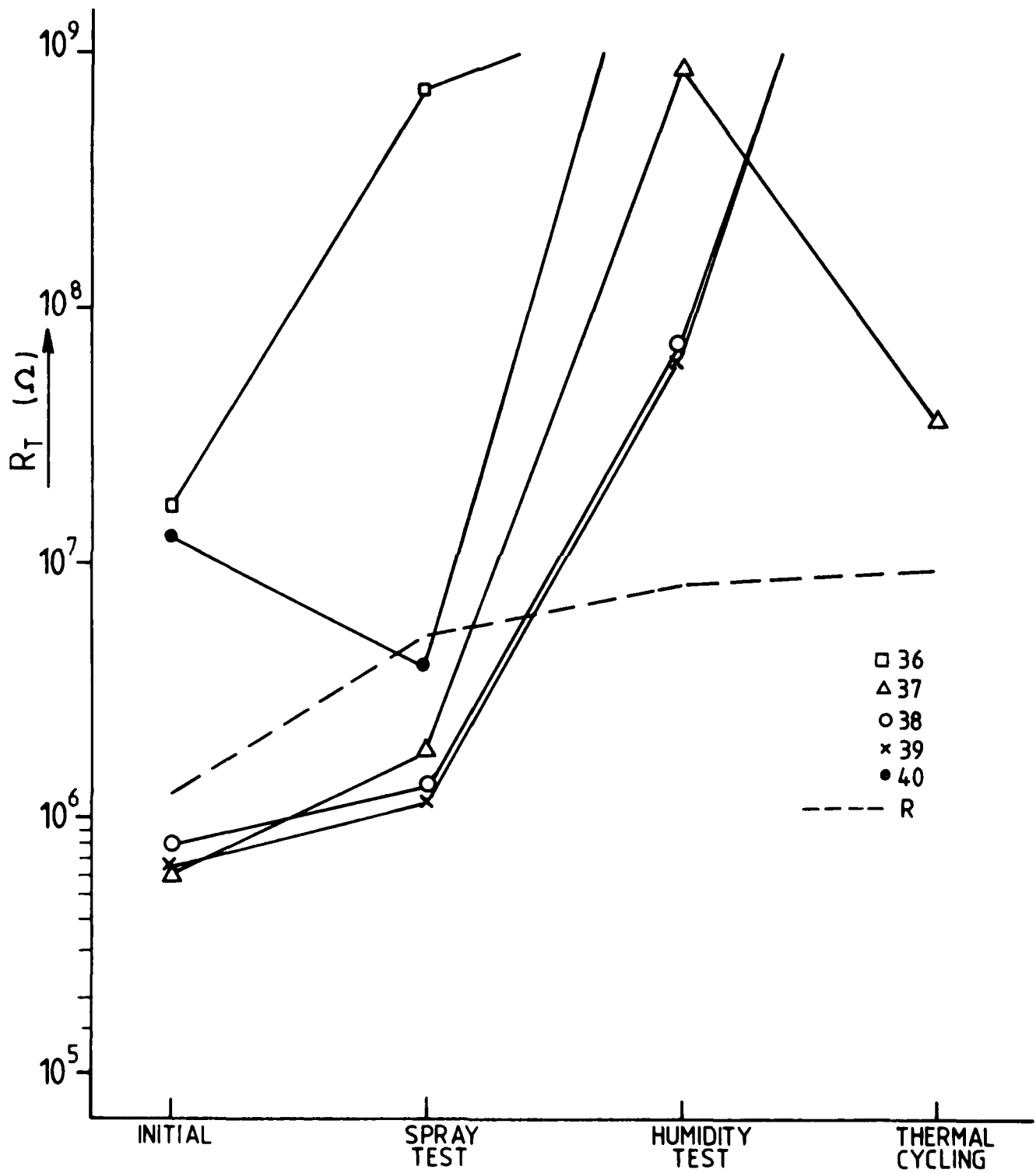
FIGURE 49   TOTAL RESISTANCE MEASUREMENT OF GENERAL ELECTRIC SSM

108

(b) Visual inspection

No degradation of the surface was traceable to the heat and humidity test.

4 - 10   THERMAL CYCLING TEST

4.10.1   Test method

The test was performed in accordance with specification ESA PSS-11/QRM-04T (ref. 11).The samples were submitted to 100 cycles between $+100^\circ C \pm 5^\circ C$ and $-150^\circ C \pm 5^\circ C$ at a change rate of $10^\circ C \pm 2^\circ C$ per minute, with dwell times of 5 minutes $\pm$ 5 minutes under vacuum.

4.10.2   Test results

4.10.2.1   Sheldahl SSM

(a) Electrical surface resistivity measurements (table 9, figure 47).
The average value of samples 26-30 after thermal cycling is 50×10^9 Ω compared to the average initial value of 3.0×10^7 Ω there is an increase by a factor 10^3.
The samples 31 to 40 that had been through all tests showed an average value of 59×10^9 Ω, which is again near the maximum limit of detectability and indicates a serious deterioration of the samples after thermal cycling.

(b) Visual inspection.
All samples have an overall "milky" appearance (photograph 7). In the case of the samples which had been through all previous tests, this degradation was not apparent before thermal cycling. This test appears to be the most significant contributor to the increase in resistance.

4.10.2.2   General Electric SSM

(a) Electrical resistance measurements (tables 10&11, figures 48&49).

TABLE 14   G.E.SSM : ELECTRICAL RESISTANCE AFTER THERMAL CYCLING

Parameter	Test	Sample no.	Average Value ( )	Decrease	Increase
Total res.	Initial	26-30	3.6×10^6	n.a.	n.a.
Total res.	Cycling	26-30	3.6×10^9	-	5
Total res.	Initial	31-40	4.8×10^6	n.a.	n.a.
Total res.	Cycling	31-40	6.5×10^{9}*	-	15

*Average does not include value of sample 32. The contract resistance

Ref. 11 DUNN B. ESA PSS 11/QRM 04 T

TABLE 15

Test results for shear and peel tests

Sample number	Shear test		90°peel test	
	Break load (g)	Failure position	Pull-off load (g)	Failure position
General 5	1380	in Al foil	260	in adhesive
Electric 6	1380	"	320	"
7	1350	"	310	"
16	1260	"	270	"
17	1330	"	290	"
18	1400	"	295	"
21	1440	"	170	"
22	1470	"	240	"
23	1340	"	210	"
26	1490	"	315	"
27	1480	"	285	"
28	1470	"	200	"
31	1400	"	295	"
32	720	"	250	"
33	1460	"	260	"
Sheldahl 5	1500	in Al foil	290	in adhesive
6	1100	"	275	"
7	1490	"	295	"
16	1570	"	320	"
17	1630	"	310	"
18	1310	"	320	"
21	1360	"	320	"
22	1470	"	325	"
23	1570	"	345	"
26	1470	"	330	"
27	1600	"	280	"
28	1160	"	330	"
31	710	"	305	"
32	1520	"	310	"
33	1470	"	255	"

measurement proved to be non-feasible in most cases because of the reasons already stated in section 4922 In those cases where contact resistance was measured, the values had increased to the 10^5 and 10^6 region.

The total resistance of the samples 26-30, that had been through thermal cycling only, jumped to values in the 10^8 to $10^9 \Omega$ region. Of the samples 31 to 40, that had been through all previous tests, 4 out of 10 samples showed a slight decrease, compared to the values after the humidity test. The others showed further increase in total resistance.

(b) Visual inspection.

A majority of the samples showed localised areas of severe degradation (photograph 14), which turned out to be numerous microcracks in the silver layer.

All samples showed these microcracks over the total sample area but the cracks were on a larger scale.

The reason for these localised areas is most likely the lifting of the SSM from the aluminium substrate due to bubbling of the entrapped air in the intermediate adhesive. The thermal contact during the cycling is definitely not ideal due to the "lifting" effect and could explain the local degradation and why some samples did not show a further increase in electrical resistance.

4 - 11   ADHESION TEST

4.11.1   Test method

The tests were performed with an Instron tensile test machine at a cross head speed of 0.2 cm/min.

The two opposite grounding straps of each sample were submitted to a shear test and the central strap to a 90° peel test.

Visual inspection of the samples was made after each test in order to determine the position of the failure.

Figure 50 shows the test configuration for (a) shear test and (b) 90° peel test.

4.11.2   Test results

Table 15 lists the results for both systems. As a result of the shear test the aluminium strap of one of the grounding points of each sample tore. This indicates that the bond strength of the aluminium-strap/conductive glue/ITO layer system is greater than the strength of the aluminium strap itself.

111

KEY

▨ ALUMINIUM
■ SSM
▧ ITO (INDIUM TIN OXIDE)
■ RTV 566-CHO-BOND 1029B
□ ALUMINIUM FOIL

a)   b)
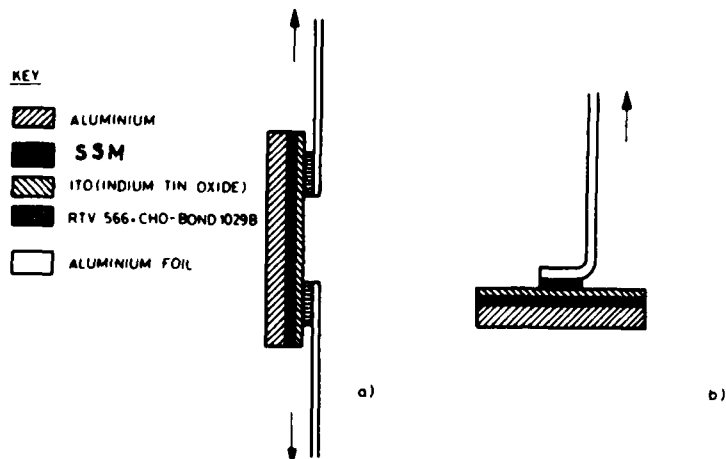
FIGURE 50 - SCHEMATIC SHOWING TEST CONFIGURATION FOR (A)
SHEAR TEST AND (B) 90° PEEL TEST

As a result of the 90° peel test, the aluminium strap was separated from
the conductive adhesive. The greater part of the conductive adhesive
remained bonded to the ITO layer, but a sufficient layer was removed with
the strap to indicate that the bonding strength of the glue to the aluminium
is adequate. No major variations of the adhesion characteristics were
identified for a sample after a particular test or the combination of all
tests, which implies that the mechanical reliability of the bond is high.
The adhesive strength of all test samples is considered to be satisfactory
and is comparable with the results for a similar grounding technique on
ITO coated Kapton (ref. 3).

4 - 12   OPTICAL MICROSCOPE EXAMINATION

4.12.1   Test method

A Reichert projection microscope was applied in the interferometer mode
using the Nomarski technique. This technique makes the cracks easier to
see, but - because the light is polarised - the vertical defects are far
more strongly emphasized than the horizontal ones. The magnification used
was x300.

112

4.12.2 Examination results: Sheldahl SSM

4.12.2.1 Pre-test results

The ITO layer, in particular surrounding the grounding points, was carefully examined. No major cracks could be observed in any of the samples (photograph 1).
The aluminium layer was scratched (photograph 2) as had been observed when the material was received (section 3.3).

4.12.2.2 Chemical spray test

No major degradation could be observed either in the ITO layer (photograph 3) or in the aluminium layer.

4.12.2.3 Heat and humidity test

No major degradation could be observed either in the ITO layer (photograph 4) or in the aluminium layer.

4.12.2.4 Thermal cycling test

Numerous microcracks could be observed in the ITO layer of the samples that had been through thermal cycling only (photograph 5) as well as of the samples that had been through all previous tests (photograph 6).
The teflon has a "milky" appearance after thermal cycling which caused an increase of solar absorptance. Photograph 7 compares samples that have been through different tests. The sample that was submitted to thermal cycling shows visual degradation.

4.12.3 Examination results: General Electric SSM

4.12.3.1 Pre-test results

The ITO layer, in particular surrounding the grounding points was carefully examined. No major cracks could be observed in any of the samples (photograph 8).
The silver layer showed no defects, except in the neighbourhood of the grounding spots where concentric cracks were identified (photograph 9).

4.12.3.2 Chemical spray test

No variation could be observed either in the ITO layer or in the silver layer.

4.12.3.3 Heat and humidity test

No variation could be observed either in the ITO layer or in the silver layer.

113

4.12.3.4 Thermal cycling test

Numerous microcracks could be observed in both the ITO layer (photograph 10) and the silver layer (photograph 11).

A majority of the samples showed localised areas of severe degradation. These areas showed excessive microcracking of both ITO and silver layers (photographs 12 and 13). The degradation was similar for samples that had been through all previous tests as well as samples that had been through thermal cycling only.

Photograph 14 compares samples that have been through different tests. The areas of excessive degradation are easily identified on the sample that was submitted to thermal cycling.

4 - 13 LONG TERM STORAGE

4.13.1 Test method

Samples 8 to 15 are being subjected to long term storage in a normal laboratory environment (18-25°C, 50-60% RH). Samples 8 and 9 are to be adhesion tested after 3 months, samples 10 and 11 after 6 months and samples 12 and 13 after 1 year.

4.13.2 Test results

No results are available as the test is still in progress.

4 - 14 ELECTROSTATIC BEHAVIOUR IN A SIMULATED SUBSTORM ENVIRONMENT

4.14.1 Purpose of the experiments

The purpose of this test was to determine the electrostatic behaviour in a simulated substorm environment for a component (ITO coated SSM with its interconnects) before and after a prequalification program.

4.14.2 Samples used in the test

Two specimens of the same material sample were prepared at the same time. A sketch of the specimen is given in Figure 51.

Photograph 1
Sheldahl SSM, pre-test. Sample 1: ITO surface, no degradation

Photograph 2
Sheldahl SSM, pre-test. Sample 1: aluminium surface, scratches.

115

Photograph 3
Sheldahl SSM, after chemical spray test. Sample 20: ITO surface, no degradation.

Photograph 4
Sheldahl SSM, after humidity test. Sample 23: ITO surface , no degradation.

116
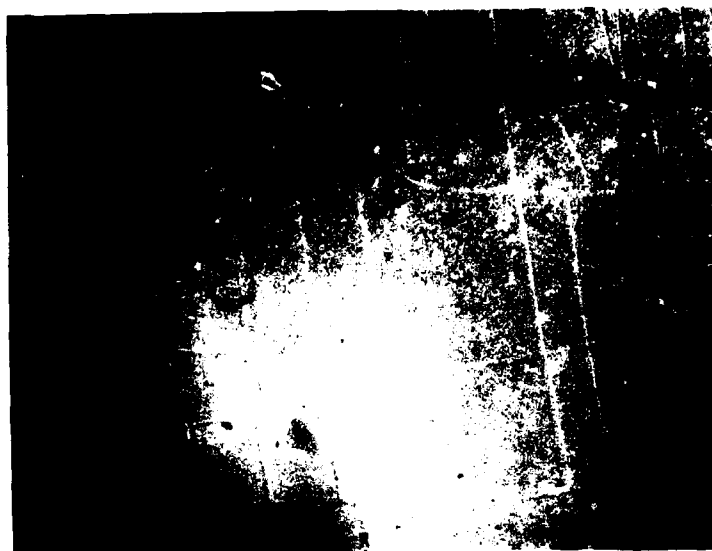
Photograph 5
Sheldahl SSM, after thermal cycling. Sample 26: ITO surface, microcracks.
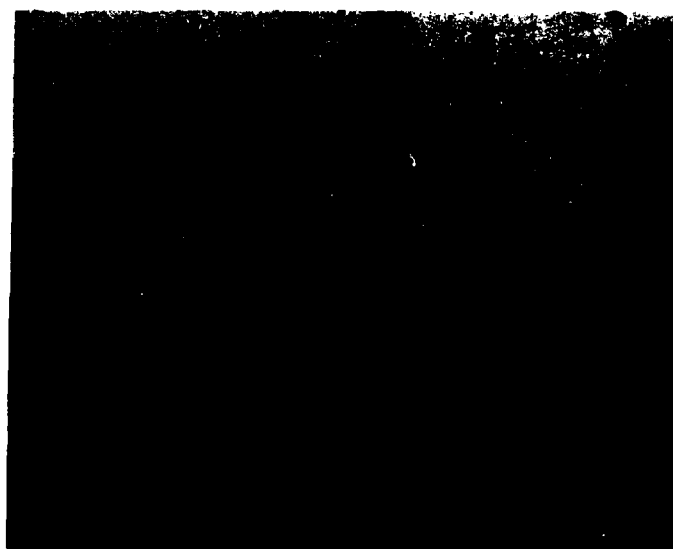
Photograph 6
Sheldahl SSM, after combined tests. Sample 38: ITO surface, microcracks.
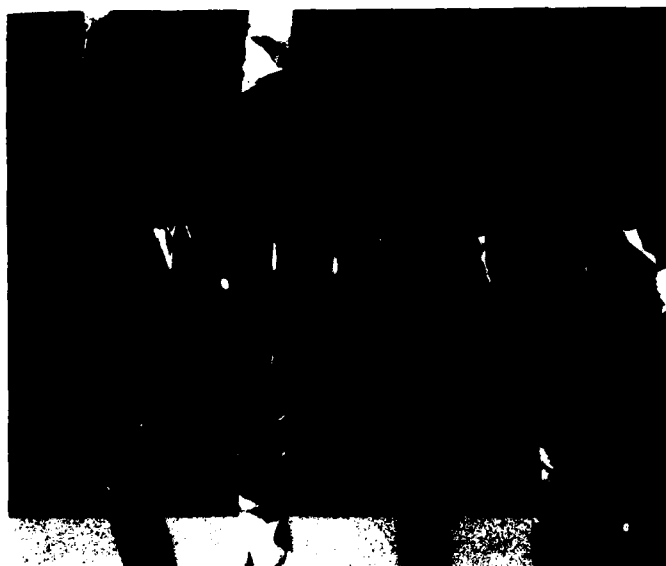
pre-test   chem. spray   humidity   thermal cycling

Photograph 7
Sheldahl SSM. Comparison of samples.
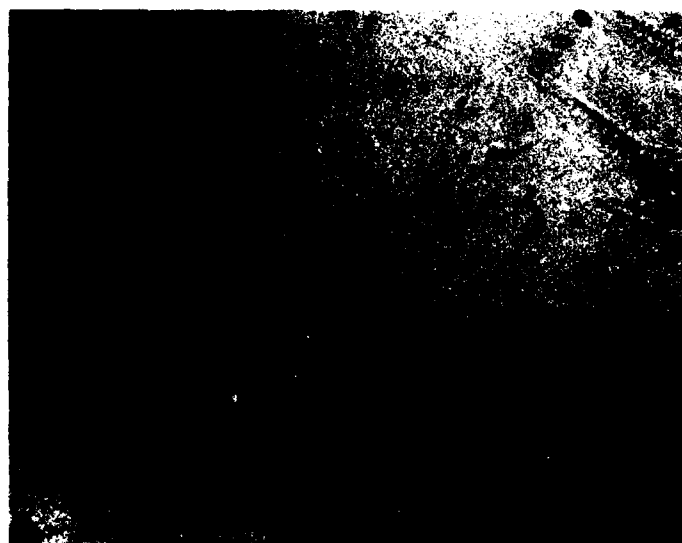
Photograh 8
G.E. SSM, pre-test. Sample 1: ITO surface near grounding point,
no degradation.

Photograph 9
G.E. SSM, pre-test. Sample 2: silver surface, microcracks near
grounding point

Photograph 10
G.E. SSM, after thermal cycling. Sample 40: ITO surface, microcracks
in the centre of the sample.

119

Photograph 11
G.E. SSM, after thermal cycling. Sample 40: silver surface, microcracks
in the centre of the sample.

Photograph 12
G.E. SSM, after thermal cycling. Sample 40: ITO surface, microcracks
near grounding point.

Photograph 13
G.E. SSM, after thermal cycling. Sample 40: silver surface, microcracks near grounding point.

Photograph 14
G.E. SSM, Comparison of test samples.

FIGURE 51 - SAMPLE DESCRIPTION

Each specimen carries four aluminum strips (8 mm wide, 30 µm thick) that were fixed on the ITO coated side of the SSM with the conductive adhesive, following the procedure described at section 4.1.5-2.

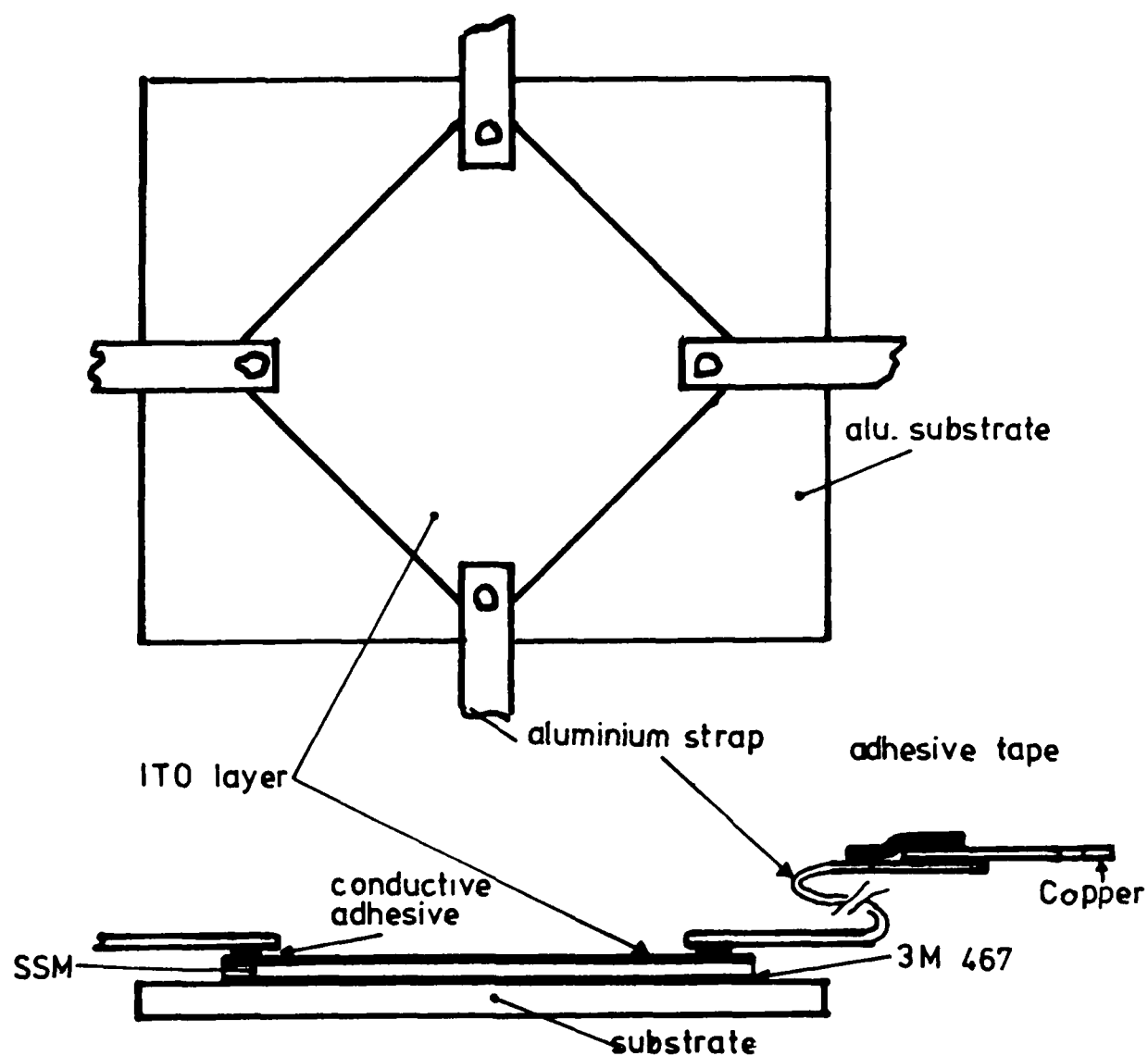One of these specimens (specimen A) was stored in normal laboratory conditions for about 7 months.

The other one (specimen B) was used in the prequalification program described Section 4-6 and went through the chemical spray, heat and humidity, and thermal cycling steps.

Both specimen were exposed in identical conditions to a simulated substorm environment in order to evaluate their performance.

The basic materials that were used in this test are described at Section 4-2.

4.14.3   Test facility

The CEDRE facility was used in its configuration MELEZE that allows the secondary emission to be measured (for more details see Section 3-2 of Ref. 3). The samples were irradiated in a high vacuum (3 10^{-6} Torr) obtained by a turbomolecular pumping unit. The electron beam was delivered by an electron gun giving energies in the range 4 keV to 25 keV. The uniformity of irradiation (better than 10 percent) was obtained at the sample level by means of a scattering foil made of aluminum 1.5 micrometer thick.

The sample under investigation is fixed onto an aluminum plate grounded through a nanoammeter (Keithley 616 electrometer). Each of the four aluminum straps can be connected with a feed-through to an ammeter. The secondary emission of the sample is measured with the collecting hemicylinder.

The surface potential is measured with a capacitive potential probe that faces the samples and that is moved in a direction parallel to them. This measure is performed about 20 seconds after the stopping of irradiations. The sample holder must be rotated in order to allow the potential measurements.

Only a 6 cm diameter surface was irradiated in the
central part of both samples. This 6 cm diameter was deli-
mited by means of a grounded mask (Figure 52). It was not
possible to prevent the electron irradiation of a part of
the aluminum connections (about 4 cm^2).

4.14.4   Test procedure

The procedure that has been followed is given in TABLE 18.
Three electrical currents are continously recorded under
electron irradiation. I_{sec} is the collected secondary emis-
sion. I_{surf} is the total current that is collected on the
four aluminum strips. $I_L + I_C$ is the current that is collec-
ted on the sample holder (see FIGURE 52).

4.14.5   Results

4.14.5.1 ITO layer deposited by SHELDAHL

TABLE 17 summarizes the results obtained at steady state
with this material   under the simulated substorm environ-
ment.
No charge build up under electron beam can be evidenced
when the specimen that has not been submitted to the prequa-
lification programme is irradiated with low energy electron.

The specimen that has been exposed to the prequalification
programme does charge under electron beam : its potential
is about 300 volts for all beam energies. The current collec-
ted by the surface electrodes is also less than in the case
of the sample not exposed to the qualification programme.
No discharge of the specimens has been observed ; however
the leakage current record is slightly more "noisy" in the
case of the specimen that has been exposed to the prequalifi-
cation programme .

4.14.5.2 ITO layer deposited by GENERAL ELECTRIC

TABLE 18 summarizes the results.

124
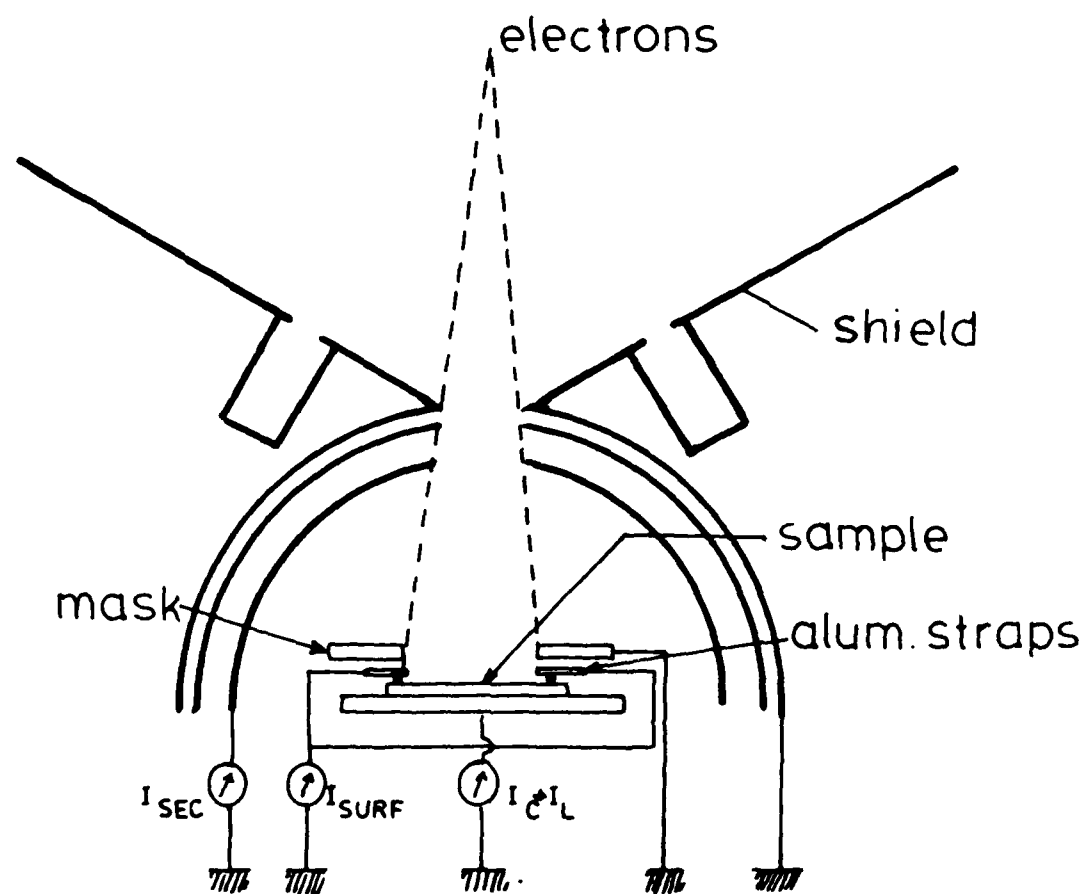
FIGURE   52

SCHEMATIC VIEW OF THE SAMPLE SETTING FOR
ELECTRON IRRADIATION

125

TABLE 16 PROCEDURE FOR THE ELECTROSTATIC TEST

with continuous recording of . leakage current
                             . secondary emission
                             . surface current
and final measurement of the surface potential

0.5 MIN   1 MINUTE   2 MINUTES   5 MINUTES   10 MINUTES

5 keV 1.25 nA cm^{-2}

10 keV 0.7 nA cm^{-2}

15 keV 0.5 nA cm^{-2}
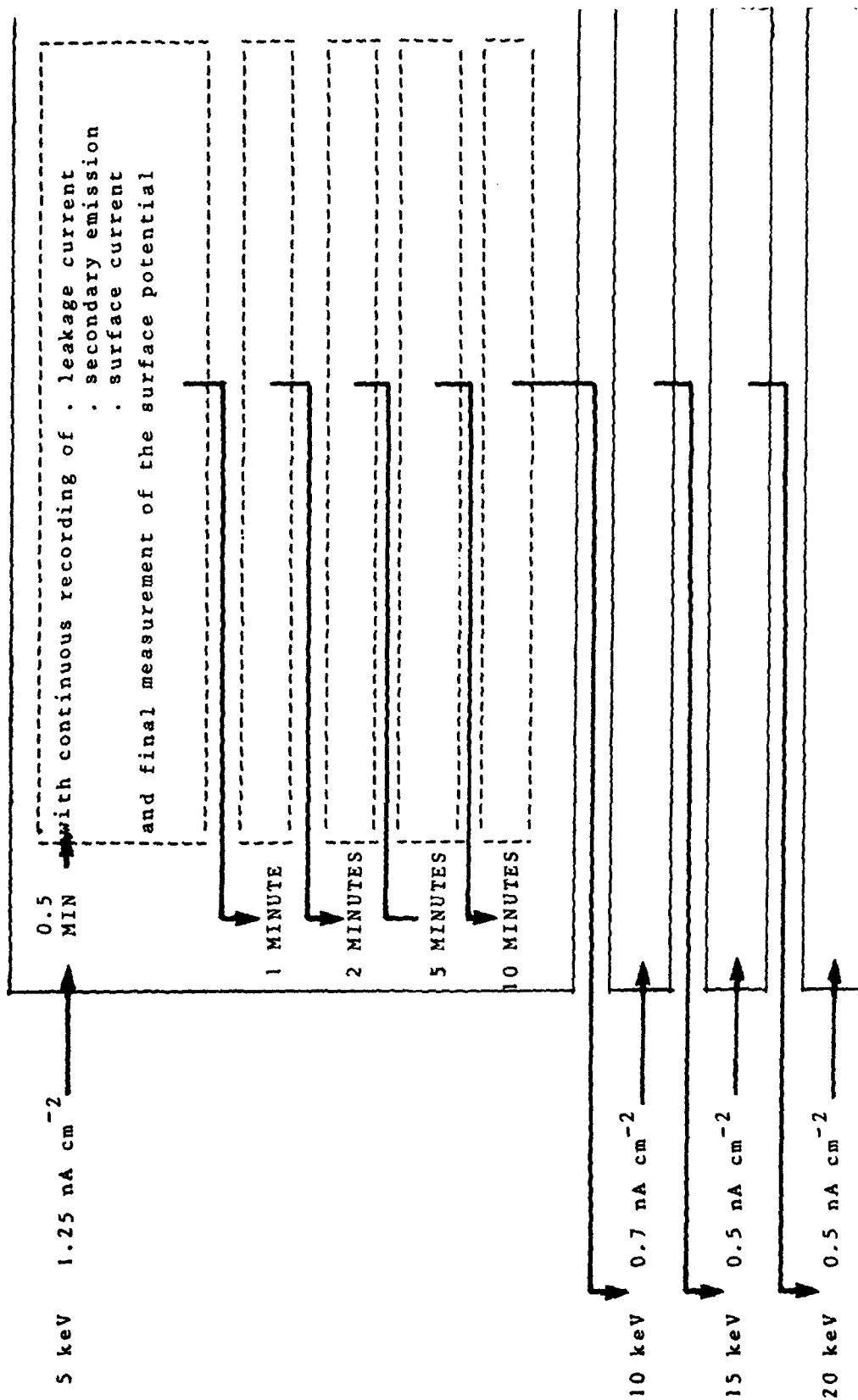
20 keV 0.5 nA cm^{-2}

TABLE 17 Electrostatic behavior of the Sheldahl ITO/SSM

		BEAM ENERGY / INTENSITY			
		5 keV 1.25nA cm^{-2}	10 keV 0.7nA cm^{-2}	15 keV 0.5nA cm^{-2}	20 keV 0.5nA cm^{-2}
BEFORE PREQUALIFICATION PROGRAMME	V (volts)	<10	<10	<10	<10
	$I_C + I_L$ (nA)	1	0.5	0.3	0.3
	I_{SURF} (nA)	17	12	9.3	9.5
	I_{SEC} (nA)	7	2.5	1.3	1.1
	DISCHARGE	no	no	no	no
AFTER PREQUALIFICATION PROGRAMME	V (volts)	300	315	300	320
	$I_C + I_L$ (nA)	1.6	0.5	0.3	0.2
	I_{SURF} (nA)	13,5	11	9	9.3
	I_{SEC} (nA)	10,5	3.2	1.7	1.4
	DISCHARGE	no	no	no	no

TABLE 18 Electrostatic behavior of the General Electric ITO/SSM

		5 keV 1.25nA cm^{-2}	10 keV 0.7nA cm^{-2}	15 keV 0.5nA cm^{-2}	20 keV 0.5nA cm^{-2}
BEFORE PREQUALIFICATION PROGRAMME	V (volts)	<10	<10	<10	<10
	$I_C + I_L$ (nA)	1.0	0.4	0.2	0.2
	I_{SURF} (nA)	8	9.8	9.0	9.2
	I_{SEC} (nA)	14	3.8	1.7	1.3
	DISCHARGES	no	no	no	no
AFTER PREQUALIFICATION PROGRAMME	V (volts)	<10	<10	<10	<10
	$I_C + I_L$ (nA)	1.45	0.5	0.2	0.3
	I_{SURF} (nA)	6.5	8.7	9	8.6
	I_{SEC} (nA)	15	4.7	2.4	1.7
	DISCHARGES	no	no	no	no

No charge build up and no discharges have been evidenced for both specimen. The current I_{surf} is only slightly decreased for the specimen that have been exposed to the prequalification programme. Thus the electrostatic behaviour of this material has not been degraded by the prequalification test.

4 - 15 PREQUALIFICATION TEST : CONCLUSIONS

- There is no detectable effect of chemical spray.
- Humidity has a direct influence on the conductivity of the indium-tin oxide layer. All test samples show considerable increases in resistivity after humidity exposure.
- Thermal cycling proved to be detrimental to teflon-based SSM with conductive ITO layers, either vapour deposited (Sheldahl SSM) or sputtered (General Electric SSM). The ITO layer shows numerous microcracks that are believed to be caused by local stresses originating from the differences in thermal expansion for teflon and ITO.

- For some of the General Electric samples, that had been through humidity testing before being submitted to thermal cycling, there was a slight improvement in resistivity. This was caused by lifting of the SSM from the aluminum substrate due to adhesive outgassing under the vaccum conditions of thermal cycling.

  The ITO layer, that improved due to outgassing of the water absorbed during the humidity exposure, was not extensively cracked because of the bad thermal contact in these particular cases and thus showed a slight net improvement of resistivity compared to the values after humidity.

- The Sheldahl SSM had a "milky" appearance after thermal cycling.
- The General Electric SSM had localised areas of excessive ITO degradation and also microcracking of the silver reflector.

The cracks in the silver reflector are liable to cause losses in optical properties due to corrosion during long term contact with chemical agents (as existing in an adhesive).

- A moderate charge build up on the surface of the SHELDAHL ITO/SSM is observed after the prequalification programme, under low energy electron irradiation.

- The adhesion of the bonding technique to the ITO layer of both types of teflon SSM was very satisfactory and did not degrade due to any of the prequalification tests.

4 - 16 DISCUSSION

Since the initial prequalification tests on ITO coated aluminised Kapton (ref. 3), there has been an extensive test programme conducted by ESTEC and DERTS (Toulouse, France) for various projects to characterise materials with conductive layers based on Indium oxide or Indium-tin-oxide (ref. 8). This continuous flow of data has increased the knowledge of these types of conductive layers.

It is now evident that some of the test results of the ITO coated Kapton (ref. 3) have been misinterpretated. The final overall conclusions for the Kapton material are still valid, however, the storage of the samples during 48 hours in a relative humidity of 65-70% after each successive test was a wrong decision. The effects of the storage in this relatively high humidity environment washed out the results of the individual prequalification tests on the Kapton material. This explains why a large variation was found for the total resistance of the teflon based materials after humidity testing while the Kapton material showed hardly any variation.

Also no recovery effects were noted for the Kapton material after thermal cycling, due to the storage in the high humidity before performing the electrical measurements. Recent tests on ITO coated Kapton (ref. 8) do show a recovery effect of the ITO layer after thermal cycling.

The Kapton samples in the first prequalification programme also demonstrated a shift to lower resistance values when submitted to high current loads.

This was not the case with the teflon based samples (section 4.7.2.) again this discrepancy is believed to be caused by desorption of water from the Kapton samples during the electrification.

The resistance measurements in vacuum were not performed in the frame of this prequalification programme, but results have been published for the same material batches in ref. 3. The vacuum exposure improved the conductivity of the ITO layer for all the materials tested.

5. GENERAL CONCLUSION

Concerning the silica fabrics and related composites, it can be stated as a general conclusion:

. it has been verified that the silica fabric/FEP/Alu composites can sustain intense and long irradiations with low energy electrons, without showing any degradation of their aluminum rear face nor of the quartz fabrics themselves.

. The secondary emission conductivity that had been proposed by EAGLES and BELANGER in order to explain the charge dissipation mechanism of silica fabrics under low energy electron irradiation, has been substantiated by the clear dependence on electrical field of the conductivity across the samples.

. The surface potential that has been measured on composites has been proved to be dependent on the flux rate. The surface potential increases when the flux rate is lowered. However this effect is only noticeable for flux rates lower than 0.1 nA cm^{-2}. Actually this fact has no technological involvement that could lead to reject the composite use in substorm conditions, because the fluxes in geosynchronous orbits are higher than this value. On the other hand, the presence of low energy electrons (energies lower than 5 keV) acting together with medium energy electrons does decrease the potential value.

. The surface potentials measured for composite samples are dependent on the sample history. They are increasing with the time of exposure to vacuum and/or irradiation.

. The contamination study we have performed has shown that a contaminant layer increases the surface potential of a composite under a low energy electron irradiation because the secondary emission is lowered (such a decrease in the secondary emission has also been measured for a conductive SSM with an ITO layer that had been deliberately contaminated). Long term irradiations with particles and UV radiation enhance the contaminant build-up on the sample. Thence, in space the good electrostatic behaviour of the quartz fabrics will be progressively degraded as a function of the number of orbits with a greater probability of discharges, if a great care is not exercised in preventing from contamination.

Concerning the ITO layers on SSM, Teflon based conductive SSM proved to be extremely vulnerable to thermal cycling: both sputtered (General Electric type) and vacuum deposited (Sheldahl type) ITO layers showed numerous microcracks. In the case of the General Electric SSM, the silver reflector was also cracked. Thermal cycling caused the SHELDAHL to go "milky", while the General Electric SSM showed localised areas of extreme microcracking. Indium based conductive layers are very vulnerable to water absorption. Short term humidity effects will recover during vacuum exposure, however, previous tests (ref. 8) show that long term humidity exposure causes permanent damage. The ESA developed grounding technique based on conductively loaded RTV 566 proved to be applicable to both types of teflon based material and was stable during the prequalification tests. The degradation of the samples was due to failure in the ITO layer rather than in the bonding technique. The teflon based SSM with a conductive ITO layer evaluated during this programme did not fulfil strict electrostatic charging requirements and based on this criterion it failed the prequalification programme.

APPENDIX

1. THE PROBE

The tool is a Weller WECP-Temtronik soldering station with the iron modified (Fig. C1). Photograph C1 shows the tool in the stowed position and in Photograph C2 the hand grip and hot end can be seen. Photograph C3 shows the heated face in detail
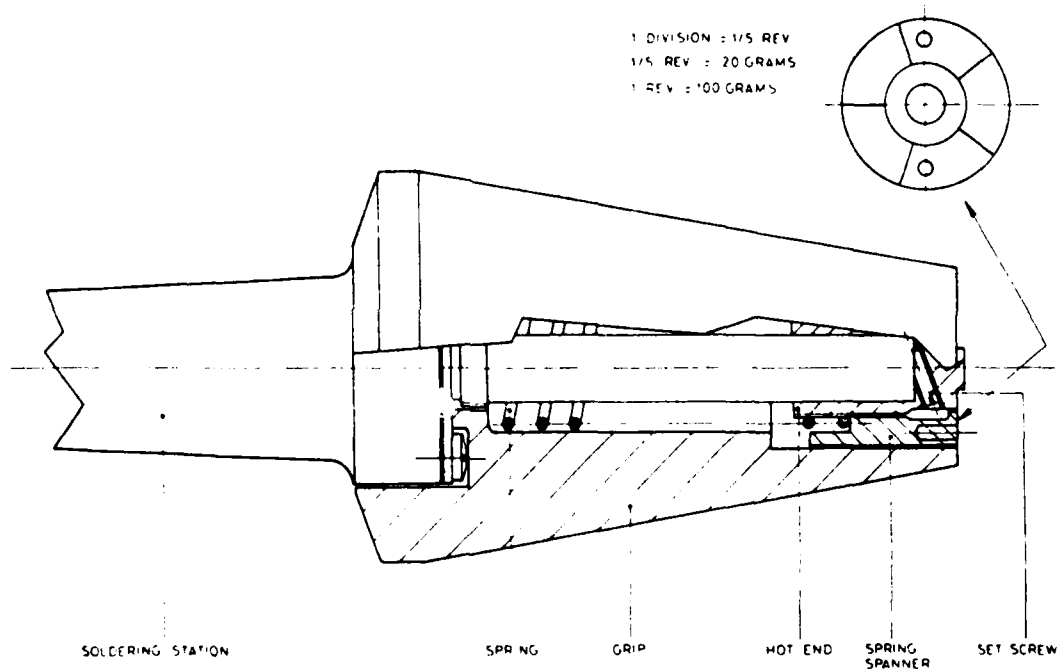

Figure C1. Pressure-controlled heat probe for curing conductive adhesives.

The face of the hot end has a raised area 0.7 mm in height which, when pressed down to the level of the ceramic grip, produces a load of 100 g. The stainless-steel spring spanner has five divisions. One division is equivalent to 20 g and one full revolution is equivalent to 100 g. The load is increased or decreased by rotating the spanner.

The probe is held by the ceramic grip and the hot end is applied to the desired place.

133
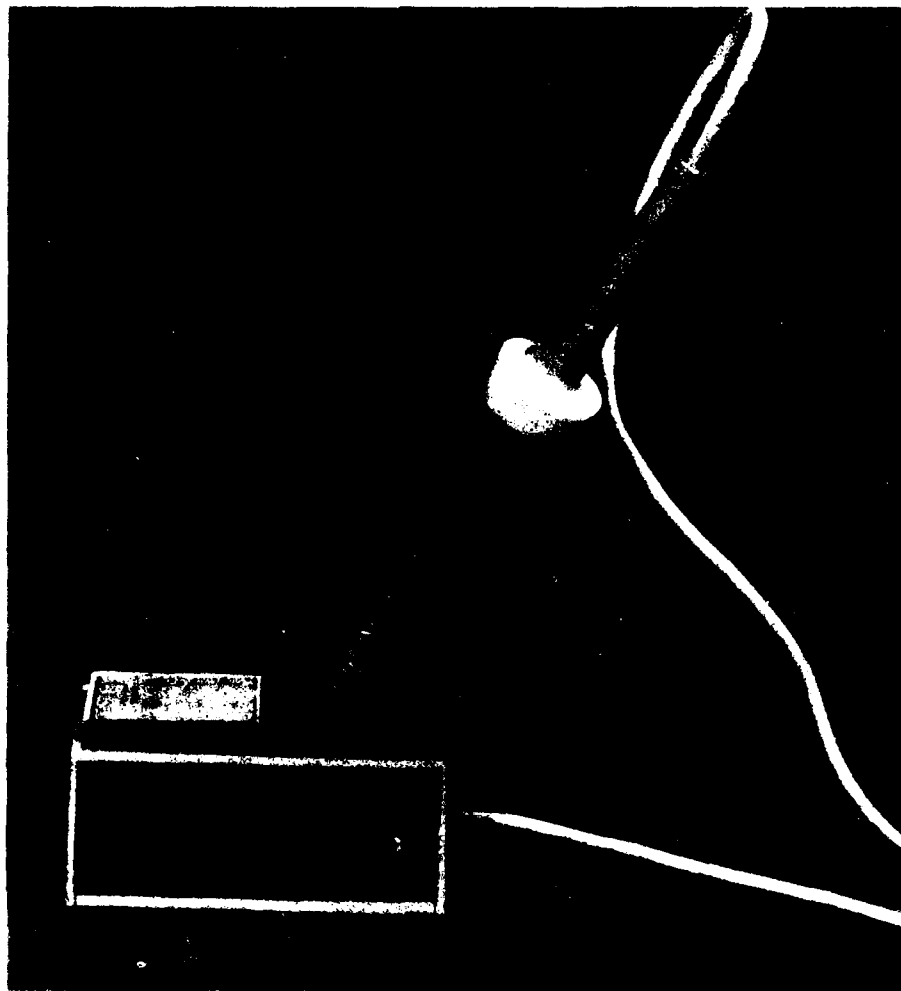
PHOTOGRAPH C1   View showing tool stowed in probe holder
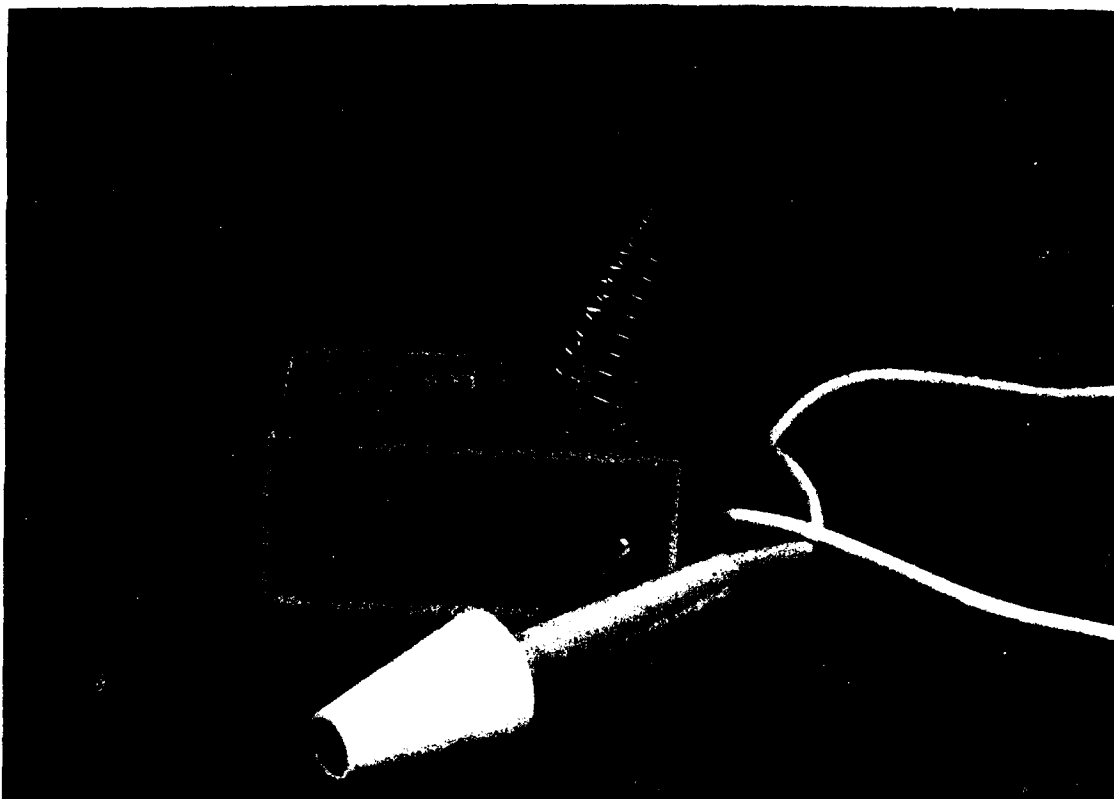
PHOTOGRAPH C2 View showing the ceramic hand grip and the copper hot end. The temprature control dial can be seen on the console behind.

PHOTOGRAPH C3 View showing the copper hot end and the adjustable spring spanner.

135

DAT
ILM